

Pontifícia Universidade Católica do Rio Grande do Sul
Curso de Pós-Graduação em Biologia Celular e Molecular

Juleane Lunardi

**A enzima histidinol desidrogenase de *Mycobacterium tuberculosis*
como alvo macromolecular para o planejamento de novos candidatos a
fármacos para o tratamento da tuberculose**

Porto Alegre
2015

Juleane Lunardi

**A enzima histidinol desidrogenase de *Mycobacterium tuberculosis*
como alvo macromolecular para o planejamento de novos candidatos a
fármacos para o tratamento da tuberculose**

Tese apresentada como requisito para a
obtenção do grau de Doutor pelo
Programa de Pós-Graduação em Biologia
Celular e Molecular da Faculdade de
Biociências da Pontifícia Universidade
Católica do Rio Grande do Sul

Orientador: Pablo Machado

Porto Alegre
2015

Juleane Lunardi

Tese apresentada como requisito
para a obtenção do grau de Doutor
pelo Programa de Pós-Graduação
em Biologia Celular e Molecular da
Faculdade de Biociências da
Pontifícia Universidade Católica do
Rio Grande do Sul

Aprovada em: _____ de _____ de _____.

BANCA EXAMINADORA:

Dr. Diogo Onofre Gomes de Souza (UFRGS)

Dr. Jeverson Frazzon (UFRGS)

Dr^a. Nadja Schroder (PUCRS)

Porto Alegre
2015

AGRADECIMENTOS

Ao Prof. Diógenes Santiago Santos, agradeço por ter acreditado em meu potencial e me proporcionado a oportunidade de integrar seu grupo de pesquisas, por fazer parte de toda a minha formação, da graduação ao doutorado, por possibilitar a minha formação acadêmica e profissional e pelo exemplo científico a ser seguido. Ao Prof. Luiz Augusto Basso, por todo conhecimento compartilhado com muita paciência, pelas correções e sugestões que foram essenciais para a realização deste trabalho.

Agradeço ao Prof. Pablo Machado pela orientação, ensinamentos e palavras de incentivo. Ao Dr. Leonardo Martinelli pelas horas de discussão de artigos e resultados, pelo auxílio no planejamento experimental e pela troca de conhecimento que foram de extrema importância para este trabalho.

Aos meus amigos e colegas do CPBMF, principalmente, a Anne D. Villela e Mariane Rotta. À Kênia Pissinate e Alessandra S. Raupp, agradeço pela ajuda e por terem “vestido a camisa do trabalho”. Agradeço, especialmente, a Ale por compartilhar comigo as notícias boas e as ruins, me ouvindo e me aconselhando.

Agradeço a todos os meus colegas da empresa Quatro G P&D Ana Christina Dias, Maria Gleci A. Ferreira, Helen C. de Paula pela ajuda e dedicação. Gostaria de agradecer também a Dra. Gaby Renard pelos conselhos, ensinamentos e amizade e a Dra. Jocelei Maria Chies por não me deixar desistir nos momentos mais difíceis, Muito Obrigada.

Agradeço aos amigos Daiana Renck, Diana C. Rostirolla, Natasha Kuniechick, Rafael Munareto e Ardala Breda, por todo apoio, carinho, conselhos, por estarem sempre presentes (mesmo que a distância) nos momentos felizes e nos momentos difíceis, por todas as risadas compartilhadas e pela amizade a mim dedicada que me ajudaram tanto a prosseguir. Agradeço também, ao amigo e colega José Eduardo S. Nunes por toda a ajuda, incentivo e, principalmente, pela amizade.

Um agradecimento especial aos meus familiares Jultir, Lecir e Fabrício pelo carinho, companheirismo, conforto, compreensão pela minha ausência e meu humor em alguns momentos e, principalmente, pelo amor incondicional que foi essencial para esta conquista.

“The most important kind of freedom is to be what you really are. You trade in your reality for a role.

You trade in your sense for an act. You give up your ability to feel, and in exchange, put on a mask.”

James Douglas Morrison

“O que vale não é o quanto se vive, mas como se vive.”

Martin Luther King

RESUMO

Dentre as doenças infecciosas que acompanham o homem ao longo da história, a tuberculose (TB), atualmente, é a segunda responsável pelo maior número de mortes no mundo. As últimas estimativas da Organização Mundial da Saúde apontam 9 milhões de novos casos de TB em 2013 e 1,5 milhões de mortes. O surgimento de novas linhagens de *M. tuberculosis* resistentes aos fármacos utilizados no tratamento está se tornando um problema sério e crescente, uma vez que o tratamento de pacientes infectados com cepas de tuberculose resistente à múltiplos fármacos e extensivamente resistente à fármacos é muito mais difícil e oneroso. Isso remete a discussões sobre a drástica situação de casos de TB virtualmente incuráveis e aponta para a urgente necessidade de introduzir novos e eficazes medicamentos anti-TB no mercado. A pesquisa para o desenvolvimento de novos agentes antimicobacterianos torna-se necessária, bem como a identificação de novos alvos para futuros medicamentos. A via de biossíntese de histidina compreende dez etapas enzimáticas catalisadas por oito enzimas. Esta via está presente nos organismos procarióticos, organismos eucarióticos inferiores e em plantas, mas está ausente em animais, corroborando com os princípios de toxicidade seletiva. Estudos de mutagênese demonstraram que os genes desta via são essenciais para a sobrevivência do *M. tuberculosis*. A enzima histidinol desidrogenase, codificada pelo gene *hisD*, catalisa a última etapa da biossíntese de histidina, convertendo L-histidinol para L-histidina. A essencialidade do gene *hisD* em mutantes de *M. tuberculosis*, com o referido gene nocauteado, já está descrita na literatura. Este trabalho trata sobre o aprofundamento dos estudos cinéticos, utilizando ensaios para determinação de parâmetros termodinâmicos, fluorimetria e ensaios em estado pré-estacionário. A caracterização da reação catalisada pela enzima HisD micobacteriana é uma etapa importante para o desenvolvimento de novos fármacos de ação específica que permitam o melhor controle da tuberculose. Os dados de caracterização cinética da enzima foram utilizados como ponto de partida para o planejamento, seleção e teste de inibidores seletivos contra a HisD de *M. tuberculosis*. Uma série de onze hidrazonas derivadas da L-histidina foi sintetizada, foram identificados quatro compostos com perfil de inibição competitiva pelo substrato L-histidinol. As interações destes compostos com a enzima foram analisadas por docagem molecular para melhor compreensão do mecanismo inibitório. Os resultados deste trabalho colaboraram ainda para uma melhor compreensão do metabolismo da biossíntese de histidina em micobactérias. Além disso, os dados dos estudos de inibição com os compostos aqui sintetizados servem como ponto de partida para o desenvolvimento de novas moléculas visando a otimização da inibição da enzima e a da inibição do crescimento do *M. tuberculosis*.

Palavras-chave: Biossíntese de histidina. *Mycobacterium tuberculosis*. Histidinol desidrogenase. Desenho de fármacos.

ABSTRACT

Among the infectious diseases that humans have been dealing with throughout history, tuberculosis (TB) is currently the second responsible for most of the deaths worldwide. The latest estimates of WHO showed that 9 millions of new cases of TB occurred in 2013 and 1.5 million of deaths. The emergence of new drug resistant *M. tuberculosis* strains is becoming a serious increasing problem as the treatment of infected patients with multi drug-resistant TB and extensively drug-resistant TB strains is much more difficult and costly. This brings discussions about the drastic situation of virtually untreatable TB cases and shows the urgent need to introduce new and effective anti-TB drugs. The research for the development of new antimycobacterial agents becomes a necessity, as well as the identification of new targets for future drugs. The histidine biosynthetic pathway is comprised of ten enzyme steps catalyzed by eight enzymes. This pathway is present in prokaryotic organisms, lower eukaryotic organisms and plants, but is absent in animals, which is in accordance with the principles of selective toxicity. Mutagenesis studies have shown that the genes of this pathway are essential for the survival of *M. tuberculosis*. The histidinol dehydrogenase enzyme, encoded by *hisD*, performs the last two steps in the biosynthesis of histidine, converting L-histidinol to L-histidine. The essentiality of the *hisD* gene in *M. tuberculosis* mutants with referred gene knockout is already described in the literature. This work describes kinetic studies using thermodynamic parameters, fluorescence spectroscopy, and pre-stationary states to better understand the enzymatic mechanism of MtHisD. Characterization of the reaction catalyzed by mycobacterial HisD is important to structure-based drug development. The data from enzyme's kinetic characterization were the starting point for HisD specific inhibitors planning, selection, and testing. A series of eleven hydrazones derived from L-histidine was synthesized, from which four compounds were identified as showing a competitive inhibition profile for L-histidinol substrate. The interactions of these compounds with the enzyme were analyzed by molecular docking to understand the inhibitory mechanism. Results from this work are believed to enhance the understanding of mycobacterial histidine metabolism. Moreover, data from inhibition studies with the synthesized compounds, serve as the starting point for the development of new molecules to enhance the enzyme inhibition and to inhibit the *M. tuberculosis* growth.

Keywords: Histidine biosynthesis. *Mycobacterium tuberculosis*. Histidinol dehydrogenase. Drug design.

LISTA DE ILUSTRAÇÕES

Figura 1 Quadro global da tuberculose.....	15
Figura 2. Via de biossíntese de histidina.....	22
Figura 3. Reação catalisada pela enzima histidinol desidrogenase.	24
Figura 4. Modelagem Molecular da MtHisD baseada na estrutura tridimensional da <i>EcHisD</i>	26

LISTA DE ABREVIATURAS, SIGLAS E SÍMBOLOS

AICAR: 5'-fosforibosil-4-carboxamida-5-aminoimidazol, do inglês *5'-phosphoribosyl-4-carboxamide-5-aminoimidazole*

AIDS: síndrome da imunodeficiência humana adquirida do inglês *acquired human immunodeficiency syndrome*

ATP: adenosina 5'-trifosfato

DARQs: diarilquinolinas

DOTS: Tratamento Diretamente Supervisionado de Curta Duração, do inglês *Directly Observed Treatment Short course*

FDA: do inglês *Food and Drug Administration*

HisB: imidazol glicerol-fosfato desidratase

HisC: histidinol-fosfato aminotransferase

HisD: histidinol desidrogenase

HisE: pirofosforibosil-ATP pirofosfohidrolase

HisG: ATP fosforibosil transferase

HisH/HisF: imidazol glicerol fosfato sintase

HisI: pirofosforibosil AMP ciclohidrolase

HisN: histidinol fosfato fosfatase

HIV: vírus da imunodeficiência humana adquirida, do inglês *human Immunodeficiency virus*

HPase: histidinol fosfato fosfatase

IAP: imidazol acetol fosfato, do inglês *imidazole acetol phosphate*

IC₅₀: quantidade de um inibidor necessária para inibir a atividade de uma enzima pela metade.

IGP: imidazol glicerol fosfato, do inglês *imidazole glycerol phosphate*

IGPD: imidazol glicerol-fosfato desidratase

ITC: calorimetria de titulação isotérmica

k_{cat}: Constante catalítica

K_d: Constante de dissociação

K_i: Constante de inibição

K_M: Constante de Michaelis-Menten

MDR-TB: tuberculose resistente a múltiplos fármacos, do inglês *multi drug-resistant tuberculosis*

MIC: concentração inibitória mínima, do inglês *minimal inhibitory concentration*

MTB: *Mycobacterium tuberculosis*

NAD⁺: nicotinamida adenina dinucleotídeo, forma oxidada

NADH: nicotinamida adenina dinucleotídeo fosfato, forma reduzida

OMS: Organização Mundial da Saúde

PrFar: fosforibosil-forminino-AICAR-fosfato, do inglês *phosphoribosyl-forminino-AICAR-phosphate*

PRPP: 5-fosforibosil-1-pirofosfato, do inglês *5-phosphoribosyl-1-pyrophosphate*

PriA: fosforibosil isomerase A

SKIE: efeitos isotópicos do solvente, do inglês *solvent kinetic isotope effects*

TB: tuberculose

TBL: tuberculose latente

TDR-TB: tuberculose totalmente resistente a fármacos, do inglês *totally drug-resistant tuberculosis*

XDR-TB: tuberculose extensivamente resistente a fármacos, do inglês *extensively drug-resistant tuberculosis*

ΔG[#]: variação da energia livre de Gibbs do estado de transição

ΔG°: variação da energia livre de Gibbs de ligação

ΔH[#]: variação da entalpia do estado de transição

ΔH°: variação da entalpia de ligação

ΔS[#]: variação da entropia do estado de transição

ΔS°: variação da entropia de ligação

SUMÁRIO

CAPÍTULO 1	13
1. INTRODUÇÃO	14
1.1. A <i>Tuberculose</i>	14
1.2. O <i>Mycobacterium tuberculosis</i>	17
1.3. Biossíntese de Histidina	21
1.4. <i>Histidinol Desidrogenase</i>	24
2. JUSTIFICATIVA	28
3. OBJETIVOS	30
3.1. <i>Objetivo Geral</i>	30
3.2. <i>Objetivos Específicos</i>	30
CAPÍTULO 2	32
Manuscrito submetido ao periódico <i>Journal of Biological Chemistry</i> , 2015.	
CAPÍTULO 3	62
Artigo de revisão publicado no periódico <i>Current Topics in Medicinal Chemistry</i> , 2013.	
CAPÍTULO 4	82
CONSIDERAÇÕES FINAIS.....	83
REFERÊNCIAS	88
ANEXOS	97
ANEXO A	98
ANEXO B	100

Capítulo 1

1. Introdução

1.1. A Tuberculose

1.2. O *Mycobacterium tuberculosis*

1.3. Resistência a Múltiplos Fármacos

1.4. Biossíntese de Histidina

1.5. Histidinol desidrogenase

2. Justificativa

3. Objetivos

3.1. Objetivo Geral

3.2. Objetivos Específicos

1. Introdução

1.1. A Tuberculose

Dentre as doenças infecciosas que acompanham o homem ao longo da história, a tuberculose (TB), atualmente, é a primeira responsável pelo maior número de mortes no mundo, perdendo apenas para a AIDS (1). Epidemiologistas estimam que um terço da população mundial esteja infectada pelo bacilo causador da TB, sendo que cerca de 8 a 10 milhões de pessoas desenvolvem a doença e, em torno de 2 milhões morrem anualmente (2-4). As últimas estimativas da Organização Mundial da Saúde (OMS) apontam 9 milhões de novos casos de TB em 2013 e 1,5 milhão de mortes (1).

Apesar dos esforços da OMS para combater a TB, esta continua tendo uma alta incidência no mundo, principalmente em países em desenvolvimento, onde se concentram aproximadamente 95% dos casos (5). Os países que formam o BRICS (Brasil, a Rússia, Índia, China e África do Sul) representam, em conjunto, quase 50% dos casos mundiais de TB (1). Em 1998, o Brasil já ocupava o décimo terceiro lugar entre os 22 países que concentram cerca de 80% dos casos diagnosticados (6), já em 2013, segundo dados da OMS, o Brasil ocupou o décimo sexto lugar (1). Um retrato do quadro global da TB pode ser visto na Figura 1.

A grande incidência de TB ao longo dos anos tem sido justificada por fatores como a reativação de infecções latentes, a migração de estrangeiros oriundos de países com alta prevalência da doença, casos de co-infecção com o vírus da imunodeficiência humana (HIV), o surgimento de cepas de *Mycobacterium tuberculosis* (MTB) resistentes ao tratamento, transmissão da doença por pessoas com TB ativa (7), conglomerados de pessoas em prisões, hospitais e casas de abrigo e a deterioração do sistema de saúde, entre outros. Estes fatores podem favorecer um aumento da transmissão e, consequentemente, do número de infectados pela doença (6-8).

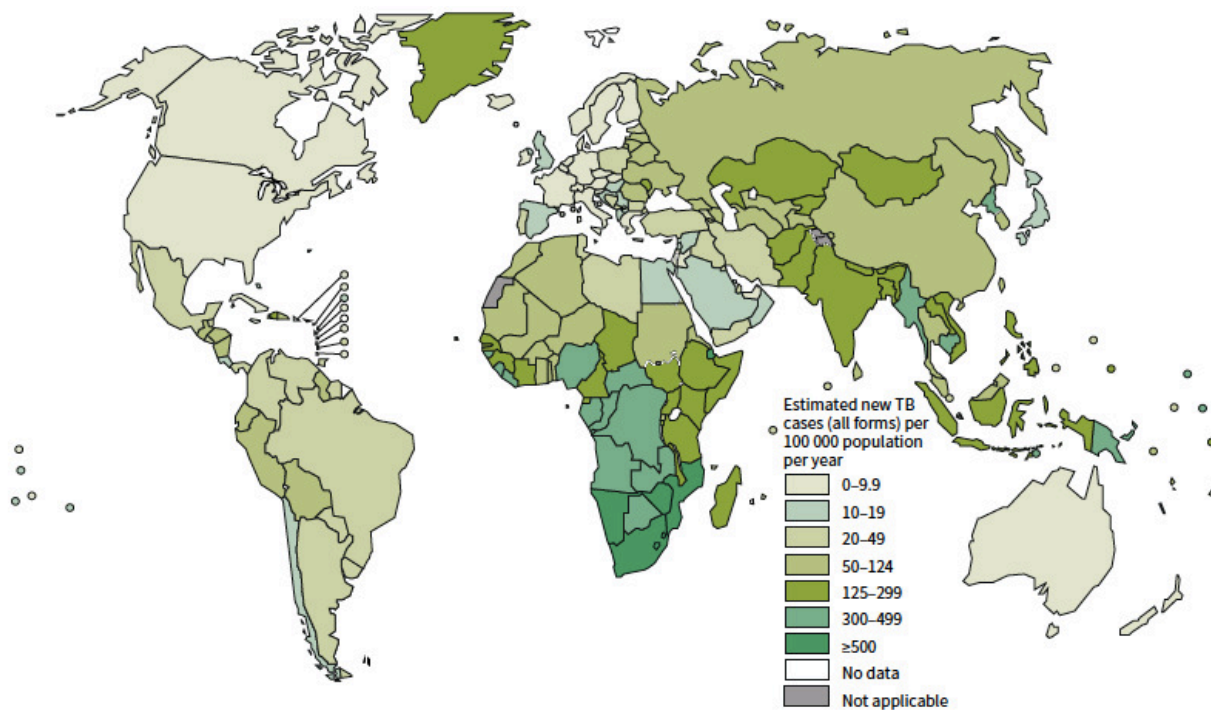


Figura 1 Quadro global da tuberculose: taxas de incidência por país no ano de 2013 (extraído de WHO Report 2014 (1)).

Os índices globais da TB tem diminuído lentamente com o passar dos anos, estima-se que 37 milhões de vidas foram salvas entre 2000 e 2013, através de um diagnóstico e tratamento eficaz (1). Apesar do Tratamento Diretamente Supervisionado de Curta Duração (DOTS) preconizado pela a OMS e proclamado como “um dos principais sucessos na história da saúde pública na década de 90” ser amplamente utilizado, a incidência e mortalidade da doença continuam aumentando em alguns países, exacerbadas pelos altos níveis de co-infecção com o HIV, baixa qualidade dos sistemas de saúde pública e, principalmente, indisponibilidade de novos medicamentos (1).

O controle sustentável da epidemia de TB não pode ser alcançado em um país, sem que se leve em conta a epidemia global. Existem amplas diferenças geográficas na incidência e prevalência da TB. Exemplo disso é o maior número de casos de TB na Índia e China (39% dos casos notificados de TB em 2012), e a mais alta incidência na África Subsaariana (23% dos casos notificados em 2012) (9). Nas Américas, o Brasil somado a outros países fazem com que a América Latina tenha uma das maiores incidência de TB, apesar dos índices decrescentes do Brasil entre os anos de 1990 a

2010. Nos últimos dez anos, o Brasil reduziu em 22,8% a incidência de casos novos de TB e em 20,7% a taxa de mortalidade pela doença. Em 2014, a incidência de TB no Brasil foi de 33,5 casos por 100 mil habitantes, contra 43,4 por 100 mil em 2004. A taxa de mortalidade de 2013 foi de 2,3 óbitos por 100 mil habitantes, abaixo dos 2,9 óbitos por 100 mil habitantes registrados em 2003. O Rio Grande do Sul apresentou uma incidência de 42,4 casos de TB por 100 mil habitantes, sendo o sexto estado da federação com maior incidência da doença. Porto Alegre é a capital com maior incidência de TB, 99,3 casos por 100 mil habitantes (10). Entre os 22 países com maior incidência de TB no ano de 2013, o Brasil se destaca por apresentar o segundo pior resultado no tratamento da TB (72% dos pacientes em tratamento foram curados ou completaram o tratamento), ficando à frente apenas da Rússia (69% dos pacientes em tratamento foram curados ou completaram o tratamento) (1).

A primeira descrição formal da capacidade de infecção da TB foi realizada em 1865, pelo cirurgião militar francês Antoine Villemin. Em 1882, o cientista Robert Koch isolou e cultivou o bacilo causador da TB, que, desde então, passou a ser conhecido por Bacilo de Koch. Vinte e seis anos mais tarde, dois pesquisadores do Instituto Pasteur, Albert Calmette e Camille Guérin, cresceram o bacilo bovino, *Mycobacterium bovis*, e observaram que, ao longo das gerações, o bacilo se tornava não virulento quando administrado em modelos animais, abrindo margem para a sua utilização profilática contra a cepa de MTB causadora da TB em humanos. Posteriormente, criou-se uma vacina, chamada de BCG (bacilo Calmette-Guerin) (11), que é atualmente a mais utilizada em todo mundo (12). No entanto, estudos demonstram que a vacina possui uma eficácia que varia de 0 a 80% em diferentes populações humanas (7).

O tratamento para a TB é de difícil manejo, já que requer um longo período de administração de medicamentos. Os sintomas da doença desaparecem após 2 a 4 semanas de tratamento contínuo, o que leva muitos pacientes à desistência. Os diversos efeitos colaterais e interações medicamentosas apresentados pelos fármacos utilizados, também aumentam as taxas de abandono do tratamento. Assim, se criam condições para a seleção de microrganismos resistentes a medicamentos, uma vez que em

muitos desses pacientes acaba ocorrendo a reativação da doença (12-14). O DOTS, incentivado pela OMS, conta com a participação de agentes de saúde que acompanham o tratamento dos pacientes, monitorando a administração regular de pelo menos três agentes quimioterápicos e a manutenção do tratamento por um período de 6 a 9 meses. O regime de tratamento consiste na administração de rifampicina, pirazinamida, isoniazida e etambutol durante os dois primeiros meses e isoniazida e rifampicina durante mais quatro meses (13, 15, 16). O atraso excessivo, especificamente, no diagnóstico correto da doença e no tratamento, permanece uma falha na estratégia de controle da TB (17). Tais atrasos são críticos, pois se indivíduos infectados permanecem não tratados na comunidade, aumentam a probabilidade de transmissão da doença (17).

1.2. O *Mycobacterium tuberculosis*

Mycobacterium tuberculosis, o principal agente etiológico da TB humana, apresenta crescimento lento, envelope celular complexo, patogenicidade intracelular e homogeneidade genética. É uma bactéria aeróbia facultativa, que infecta e se prolifera no interior de macrófagos (18). O gênero é considerado bacilo álcool-ácido resistente (BAAR) devido à capacidade de reter fucsina básica na parede celular mesmo na presença de álcool e ácido, quando é utilizado o método de Ziehl-Neelsen para sua coloração.

A parede micobacteriana possui características diferenciadas, apresentando uma camada de peptideoglicano composta de ácido *N*-glicolilmurâmico ao invés de ácido *N*-acetilmurâmico. O envelope celular é composto por ácidos graxos incomuns, conhecidos como ácidos micólicos (19). Esta constituição da parede celular confere uma característica impermeável à célula micobacteriana, facilitando sua sobrevivência dentro de macrófagos e aumentando a propensão do MTB a desenvolver resistência, com isso os medicamentos disponíveis no mercado, na maior parte das vezes, acabam sendo apenas parcialmente efetivos (20).

O genoma da linhagem melhor caracterizada, MTB H37Rv, possui 4.411.529 pares de base dispostos em um cromossomo circular, sendo 65,6% composto por bases G+C (18). Esta linhagem tem sido utilizada mundialmente na pesquisa biomédica devido à manutenção de virulência e alta sensibilidade a medicamentos. O bacilo da TB é naturalmente resistente a muitos antibióticos, em parte, devido ao envelope celular hidrofóbico que age como barreira permeável e, em parte, à resistência codificada em seu genoma, que produz enzimas hidrolíticas e modificadoras de fármacos. Fosfolipases C, esterases e lipases podem atuar como fatores de virulência, podendo atacar membranas celulares ou vacuolares (18).

A maioria das infecções por MTB não resultam na doença ativa, em torno de 90% dos casos os indivíduos infectados permanecem assintomáticos, com a chamada TB latente (TBL) (21-24). A TBL pode progredir para uma doença ativa, depois de alguns anos ou, até mesmo, décadas após a infecção inicial, momento no qual o sistema imunológico hospedeiro se encontra debilitado, como nos casos de infecção com HIV, subnutrição, uso de drogas, câncer, diabetes (25), quimioterapia imunossupressora (26) e insuficiência renal crônica (27). A reativação da TB pode representar um grande problema de saúde devido à dificuldade de controle e diagnóstico da TBL (23, 24). O tratamento da TBL consiste no uso de isoniazida, por um período de aproximadamente nove meses, levando à redução do risco de reativação da TBL em 80% dos casos (28-30). A isoniazida está relacionada a sérios efeitos secundários, como hepatotoxicidade, assim há uma significativa limitação no uso deste medicamento, novos fármacos para reforçar o tratamento da TBL são essenciais para o controle da TB (31).

O aparecimento de novas linhagens de MTB resistentes aos fármacos utilizados também está se tornando um problema sério e crescente; o tratamento de pacientes infectados com cepas resistentes a múltiplos fármacos (MDR-TB) (definida como aquela na qual o paciente possui a doença ativa com bacilo resistente a, pelo menos, isoniazida e rifampicina) é mais difícil e oneroso, levando à morte do paciente em 80% dos casos (32). A resistência a múltiplos fármacos desenvolvida pelo MTB representa uma preocupação mundial, predominando em países pobres e em

desenvolvimento, onde os programas de controle da doença são extremamente ineficientes. O aumento nos casos de resistência se deve principalmente à administração inadequada dos medicamentos.

A quimioterapia contra a TB se desenvolveu ao final da década de 40, com a utilização de estreptomicina (33), seguida por ácido *p*-amino-salicílico (pouco utilizado atualmente). A isoniazida e a rifampicina foram introduzidas ao final da década de 60 e a pirazinamida, já conhecida no final da década de 50, foi introduzida no tratamento contra TB cerca de uma década depois.

A aquisição de resistência do MTB a múltiplos fármacos deve-se a diferentes eventos de mutação cromossômica. Durante a exposição bacteriana aos medicamentos, ocorre uma pressão seletiva a favor de mutantes resistentes. Mecanismos moleculares de resistência em MTB a agentes antimicobacterianos têm sido evidenciados nos últimos anos; para cada um dos medicamentos utilizados, há pelo menos um gene envolvido, no qual mutações específicas estão correlacionadas com o surgimento de um fenótipo resistente (34-36).

Pacientes com MDR-TB devem ser tratados com uma combinação de medicamentos de segunda linha que, além de representarem um custo maior, possuem mais efeitos tóxicos e são menos efetivos que os medicamentos de primeira linha (37). Em países industrializados, o tratamento habitual custa em torno de 2 mil dólares por paciente, mas alcança 250 mil dólares para pacientes com MDR-TB (38).

Em 2006 a OMS reportou a identificação de cepas extensivamente resistentes (XDR-TB), as quais, além de resistência à rifampicina e isoniazida, são também resistentes a três ou mais medicamentos de segunda linha (aminoglicosídeos, polipeptídeos, fluoroquinolonas, tiamidas, cicloserina e ácido *p*-aminosalicílico) (39-41). Em 2009, foram reportadas cepas de MTB resistentes a todos os medicamentos de primeira linha e a todos os medicamentos de segunda linha testados, sendo classificadas como cepas totalmente resistentes a fármacos (TDR-TB) (42). Estas cepas apresentam ainda morfologia distinta da MDR-TB e XDR-TB, com espessamento significativo da camada de ácidos micólicos no seu envelope celular (43). Assim, a obtenção de novas estruturas químicas capazes de atuarem como fármacos para o tratamento da TB têm sido preponderante para o combate a

esta enfermidade, que foi declarada pela OMS uma emergência global em 1993 (1, 9, 32).

Casos de co-infecção de HIV e MDR-TB alcançam taxas de mortalidade próximas a 100%, sendo definida como a infecção oportunista mais maligna associada à AIDS (8). Cerca de 300 mil novos casos de MDR-TB são diagnosticados a cada ano, sendo que de 4 a 20 % destes são classificados como XDR-TB. A XDR-TB está sendo relatada em todo o mundo, inclusive nos Estados Unidos, onde a TB estava sendo considerada sob controle. A ocorrência já difundida de XDR-TB traz discussões sobre a drástica situação de casos de TB virtualmente incuráveis e aponta para a urgente necessidade de introduzir novos e eficazes fármacos anti-TB (39).

Dessa forma, a identificação de novos alvos moleculares e o desenvolvimento de novos agentes antimicobacterianos se fazem necessários. A otimização de vacinas, de forma a torná-las mais imunogênicas em humanos, também deve ser considerada para o desenvolvimento de uma estratégia profilática eficaz, visando reduzir significativamente o número de casos de TB.

Recentemente, estudos com diarilquinolinas (DARQs), uma nova classe de inibidores da ATP sintase de MTB (44-46) levou o U. S. Food and Drug Administration (FDA) a aprovar o SIRTUROTM (bedaquilina), uma DARQ anti-TB, utilizada em associação com outros medicamentos para o tratamento de adultos com MDR-TB pulmonar (47). Este medicamento é de extrema importância como uma nova opção de tratamento para a TB, sendo o único fármaco anti-TB desenvolvido nos últimos 40 anos. Ainda assim, a possibilidade de rápido aparecimento de novas cepas resistentes e também os efeitos adversos da bedaquilina, como arritmia cardíaca (48), reforçam a necessidade do desenvolvimento de novos medicamentos para o tratamento da TB. Estes fármacos devem ser efetivos contra as linhagens MDR-TB e XDR-TB, ser capazes de eliminar a forma latente do bacilo, diminuir os custos e o tempo de tratamento e não apresentar interações com os medicamentos anti-HIV (49).

1.3. Biossíntese de Histidina

Estratégias baseadas no desenho de novos fármacos dependem da identificação de rotas bioquímicas específicas ao MTB e muitas delas já foram caracterizadas em nível genético. A identificação de genes envolvidos na codificação das enzimas que compõem estas vias metabólicas e a utilização destes por meio de técnicas de DNA recombinante propicia uma caracterização estrutural e funcional mais detalhada de potenciais alvos moleculares, para o desenvolvimento de inibidores de ação seletiva. O desenho de fármacos a partir de alvos moleculares já estabelecidos é baseado no conhecimento do modo de ação e da estrutura molecular do sítio ativo, no caso de enzimas, ao qual, um determinado fármaco, o inibidor, liga-se. Inibidores enzimáticos correspondem a aproximadamente 25 % do mercado de fármacos dos Estados Unidos (50).

A via de biossíntese de histidina comprehende dez etapas enzimáticas, que incluem reações complexas e não triviais, catalisadas por oitos enzimas (51). A via está presente nos organismos procarióticos, organismos eucarióticos inferiores e em plantas, mas está ausente em mamíferos. Em função disto, as enzimas que compõe esta via biossintética geram grande interesse como potenciais alvos para a ação de novos medicamentos antimicrobianos e herbicidas (51-53). Os organismos que apresentam esta via são capazes de converter a partir de fosforribosil pirofosfato (PRPP) e ATP até L-histidina (L-His), produto final da via (Figura 2).

A HisG (ATP fosforribosil transferase) catalisa a primeira reação da biossíntese de L-His, a conversão de fosforribosil pirofosfato (PRPP) e ATP em fosforribosil-ATP. Esta enzima também realiza uma função regulatória, através de um mecanismo de *feedback* negativo por inibição alostérica do produto final da rota (51).

HisE (pirofosforribosil-ATP pirofosfotidrolase) e HisI (pirofosforribosil AMP ciclohidrolase) são responsáveis pela segunda e terceira reações da via, respectivamente. Em MTB dois genes codificam separadamente HisE (*hisE*) e HisI (*hisI*), essa organização varia entre diferentes organismos (54-63). Porém, a completa caracterização funcional destes genes de MTB ainda não foi reportada na literatura (64).

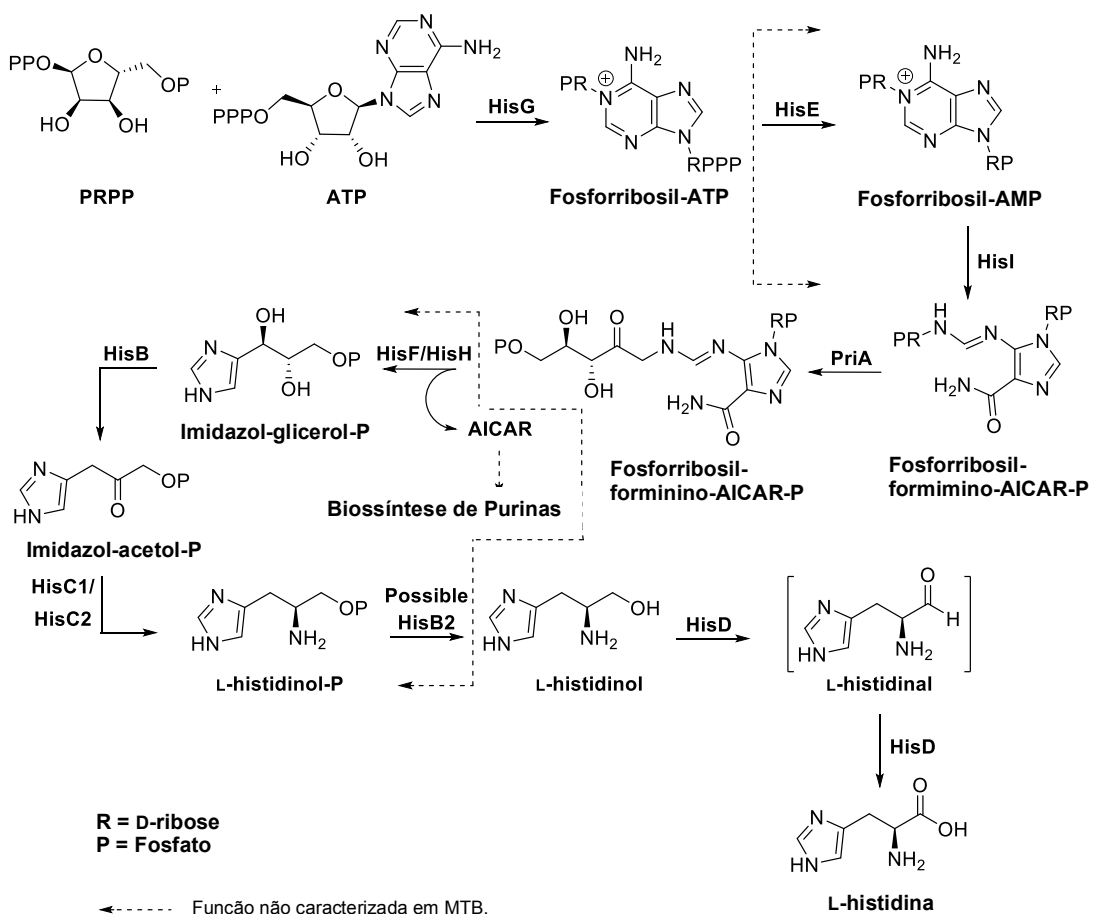


Figura 2. Via de biossíntese de histidina. Partindo dos precursores ATP e PRPP, em dez etapas catalisadas por enzimas ocorre a produção de histidina. *Adaptado de Lunardi et al. (64).*

A quarta etapa da biossíntese de histidina é a reação catalisada pela PriA (fosforribosil isomerase A), enzima bifuncional, que atua nas vias biossintéticas da histidina e do triptofano no MTB (55, 56). Este fato faz da PriA um alvo interessante para o desenvolvimento de novos fármacos anti-TB.

As enzimas HisH e HisF (imidazol glicerol fosfato sintase) estão relacionadas com a quinta etapa da via de biossíntese de histidina. No Domínio Bacteria, os produtos dos genes *hisH* e *hisF* são descritos por formar um complexo dimérico estável com atividades de amidotranferase e ciclase, respectivamente (51, 67, 68). No Domínio Eukarya e em algumas δ-Proteobacteira, ambas as atividades são promovidas por um único produto *HIS7* (63, 69, 70). O produto dos genes *hisF* e *hisH*, assim como os de *hisE* e *hisI*, não tem sua caracterização funcional descrita em MTB (64). Nesta etapa

da via ocorre a conversão do fosforribosil-forminino-AICAR-fosfato (PrFar) para imidazol glicerol-fosfato (IGP), com a concomitante liberação de 5-fosforribosil-4-carboxamide-5-aminoimidazol (AICAR), esse subproduto é utilizado na via *de novo* de purinas pelo ciclo do AICAR (51).

A três reações subsequentes à reação de formação do IGP, também não estão devidamente caracterizadas em MTB (64). A enzima HisB (imidazol glicerol fosfato desidratase (IGPD)) já foi caracterizada em fungos (71, 72), plantas (73), Archea e algumas Eubacterias como sendo monofuncional, enquanto outras Eubacterias possuem uma enzima bifuncional, que além da atividade de IGPD, possuem atividade de histidinol fosfato fosfatase (HPase). A atividade de IGPD está relacionada com a sexta reação da via, que converte IGP em imidazol-acetol-fosfato (IAP), e de HPase com a oitava reação, que converte L-histidinol-fosfato (L-Hol-P) em L-histidinol (L-Hol), precursor da L-His (74, 75). Alguns estudos bioquímicos e genéticos sugerem que estas atividades, IGPD e HPase, podem ser independentes uma da outra e estarem situadas em domínios separados da enzima (C-terminal atividade de IGPD e N-terminal atividade de HPase) (70). Não há dados de um gene *hisB*, que codifica a enzima, bifuncional em MTB, sendo IGPD a única atividade descrita para o produto deste gene (70, 76). Algumas evidências sugerem que a atividade de HPase pode ser codificada pelo gene *hisN* (parólogo ao gene *gmhB*) e a atividade de IGPD pelo gene *hisB* (70, 77). Alguns trabalhos estudam a hipótese de que a proteína GmhB (HisB2) pode estar envolvida na oitava reação da rota de biossíntese da L-His em MTB (64).

A sétima etapa da via de biossíntese de histidina também não está completamente descrita para MTB. Os genes *hisC1* e *hisC2* codificam duas possíveis histidinol-fosfato aminotransferases, que podem, em princípio, catalisar a conversão de IAP para L-Hol-P. A atividade e a funcionalidade de ambos os produtos destes genes de MTB ainda precisam ser demonstradas. O alinhamento da sequência de aminoácidos da *MtHisC1* e da *MtHisC2* mostraram uma identidade de 29% (78). Estudos cinéticos com a HisC de *Bacillus subtilis* (*BcHisC*) mostraram que a reação de transaminação na síntese de tirosina e fenilalanina pode ser catalizada pela histidinol-fosfato aminotransferase (79, 80). Essa ligação, com a biossíntese de aminoácidos

aromáticos, é mais um indício das interações da via de biossíntese da L-His com outras rotas biossintéticas de extrema relevância, assim como já descrito para as etapas catalisadas pelas enzimas PriA, HisF e HisH.

As duas últimas reações da biossíntese da L-His são catalisadas pela enzima HisD (histidinol desidrogenase), que realiza a conversão de L-Hol a L-His com a formação do intermediário L-histidinal (L-Hal) (81-85). Esta enzima é o objetivo de estudo deste trabalho e será melhor descrita a seguir.

Estudos de mutagênese demonstraram que os genes da via de biossíntese de histidina são essenciais para a sobrevivência do MTB; organismos auxotróficos para histidina não resistem à restrição deste aminoácido (86, 87). Ainda mais específico foi o estudo que demonstrou a essencialidade do gene *hisD* em mutantes de MTB com o referido gene nocauteado, produzidos por recombinação homóloga (88). A importância de algumas enzimas desta via para o desenvolvimento de fármacos para a tuberculose, também foi ressaltada por Aguero (89), que incluiu no banco de dados DTR Targets as enzimas HisG, HisB, and HisD.

1.4. Histidinol Desidrogenase

A enzima histidinol desidrogenase (E.C.1.1.1.23), codificada pelo gene *hisD*, catalisa as duas últimas etapas da biossíntese de histidina, convertendo L-histidinol para L-histidina, passando por L-histidinal como intermediário (Figura 3) (70, 82).

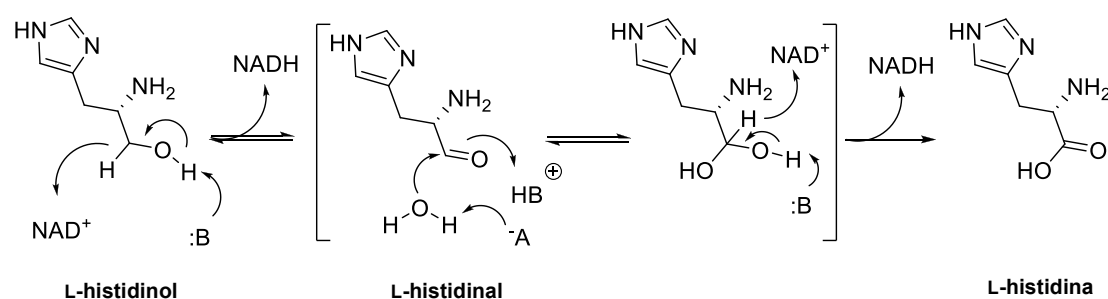


Figura 3. Reação catalisada pela enzima histidinol desidrogenase. Adaptado de Lunardi et al. (64).

A importância desta enzima para a virulência já foi demonstrada para algumas bactérias patogênicas como *Brucella suis* (90), *Salmonella typhimurium* (91) e *Burkholderia pseudomallei* (92). Estudos com a HisD de *Salmonella typhimurium* (*StHisD*) mostraram que duas reações sucessivas são catalisadas no mesmo sítio ativo de cada subunidade da enzima, contendo um átomo de Zn⁺² e um sítio ligante de NAD⁺ cada. A dependência da enzima pelo metal foi caracterizada, mas não foi demonstrada uma função catalítica deste (93). A formação do dímero (estado oligomérico da *StHisD* em solução) requer o metal, já a sua remoção causa a dissociação das subunidades diméricas (93). Assim, o íon zinco não está diretamente envolvido na catálise, mas interage com grupos de aminoácidos do L-Hol que podem influenciar o correto posicionamento do substrato no sítio ativo da enzima (85).

No MTB, o gene *hisD* tem sido descrito como essencial para sobrevivência e virulência (86, 87, 94). Além disso, a enzima está entre os 50 melhores alvos para desenvolvimento de medicamentos contra tuberculose pelo banco de dados TDR Targets (89). A partir da elucidação de todas estas informações e da identificação da ORF Rv1599 em MTB H37Rv como o provável gene codificante para histidinol desidrogenase micobacteriana (438 aminoácidos, 45.346,10 Da) (18), podemos afirmar que esta enzima representa um potencial candidato a alvo para o desenvolvimento de novos fármacos contra a tuberculose.

A histidinol desidrogenase de *Mycobacterium tuberculosis* (*MtHisD*) é uma metaloenzima dependente de zinco e é encontrada na forma de um homodímero em solução (95). Enzimas contendo metais tem uma elevada importância, pois estão envolvidas diretamente em processos biossintéticos essenciais (96). A caracterização cinética da *MtHisD* foi determinada por um estudo do nosso grupo de pesquisas realizado por Nunes e colaboradores (95). A *MtHisD* segue um mecanismo cinético Bi-Uni-Uni-Bi Ping-Pong, no qual o L-Hol liga primeiramente na enzima e o NAD⁺ é incapaz de se ligar na enzima livre. Uma modelagem molecular foi realizada e a estrutura da *MtHisD* (Figura 4) foi baseado na estrutura tridimensional da HisD de *E. coli* (*EcHisD*) (85), o monômero da *MtHisD* possui quatro domínios e o dímero é

formado pelas subunidade A e B. Os dois sítios ativos estão localizados no limite da interface dos dois homodímeros, os resíduos de aminoácidos de ambas as subunidades (domínios 1, 2 e 4) interagem através de ligações de hidrogênio com o L-Hol e com o zinco, o NAD⁺ interage com resíduos do domínio 1 (95). Para determinar os resíduos envolvidos na catálise e na ligação dos substratos, além da modelagem foram realizados estudos de perfil de pH, que mostraram os aminoácidos His336 e His376 do domínio 2 e o Glu423 do domínio 4 envolvidos na ligação do L-Hol. O íon Zn⁺² é coordenado pelos resíduos Gln267, His270, Asp369, His428 e mais dois ligantes do L-Hol. Os aminoácidos que contribuem para a ligação do NAD⁺ incluem Tyr129, Gly132, Asn221, Gln193, Phe58 e Tyr223 (95).

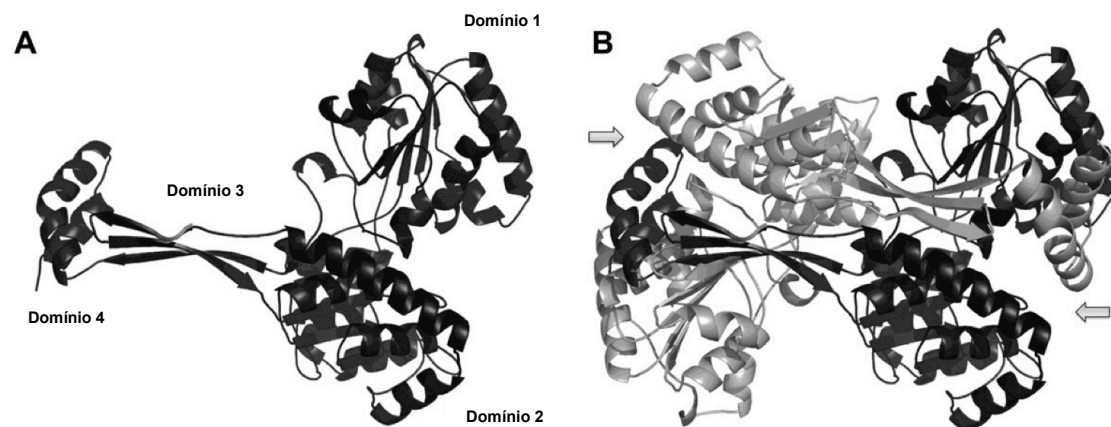


Figura 4. Modelagem Molecular da MtHisD baseada na estrutura tridimensional da *EcHisD*. Em A o monômero da enzima e em B o homodímero formado pelas subunidades A (cinza escuro) e B (cinza claro). As setas indicam as posição dos dois sítios ativos no homodímero. Adaptado de Nunes et al. (95).

Conforme proposto por Barbosa e colaboradores para a enzima de *E. coli* (85) e por Teng e Grubmeyer para *S. typhimurium* (97), o mecanismo de catálise da HisD envolve quatro resíduos básicos na reação (B1-B4). O resíduo His327 (correspondente ao resíduo His336 em MTB) atua em B1, B3 e B4, o resíduo Glu326 (corresponde ao resíduo Glu335 em MTB) atua em B2. B1 abstrai um próton do grupamento hidroxila do L-Hol, assim o resíduo His327 se torna transitoriamente protonado, a molécula de NAD⁺ aceita o hidreto do carbono reativo (carbono ligado ao grupo hidroxila (OH)) que adota uma configuração sp², concluindo a transformação do L-Hol em L-Hal. A

redução para o cofator NADH leva a substituição por uma segunda molécula de NAD⁺ (85). Uma molécula de água próxima é ativada por B2 e realiza um ataque nucleofílico no carbono reativo, concomitante, B3, que está protonado (H:His327), doa seu próton para o oxigênio do aldeído. A configuração do carbono reativo volta a ser sp³ formando L-histidindiol (85). A próxima etapa é uma repetição da primeira, B4 abstrai o próton da hidroxila do L-histidindiol e a segunda molécula de NAD⁺ é reduzida por um hidreto ligado ao carbono reativo, formando a segunda molécula de NADH e L-His, o carbono reativo forma um grupo carboxilato com configuração sp², a His327 é restaurada para o seu estado neutro, pela doação do próton para uma molécula de água próxima (85).

Os primeiros estudos de inibição da HisD utilizaram a enzima de repolho, *E. coli* (98) e *S. typhimurium* (99), os melhores compostos testados contra a HisD obtiveram valores de IC₅₀ entre 20 e 40 µM. Posteriormente, compostos derivados da L-His, contendo uma cadeia aromática que interage com o sítio lipofílico adjacente ao sítio catalítico da HisD de *Brucella suis* (*Bs*HisD), foram estudados por Abdo e colaboradores (100), mostrando valores de IC₅₀ abaixo de 10 µM. Uma segunda série de inibidores da *Bs*HisD, com compostos N-L-histidinil fenilsulfonil hidrazida, foi testada (101), mas exibiram uma capacidade inibitória inferior a série anterior de benzil cetonas derivadas da L-His (100). Uma terceira série de moléculas foi sintetizada, com uma extensão da cadeia aromática por um segundo anel separado por diferentes ligantes (102), obteve valores de IC₅₀ abaixo de 70 µM, além de apresentarem inibição do crescimento de *B. suis* em meio mínimo e redução da sua replicação intramacrofágica (102). Estes estudos de inibição, com proteínas ortólogas, servem como ponto de partida para os estudos de inibição realizados no nosso trabalho com a *Mt*HisD, os quais, como já mencionado, não possuem relatos na literatura (64).

Além dos dados já obtidos por Nunes e colaboradores (95), se fazem necessários mais estudos para aprofundar a caracterização da *Mt*HisD como alvo macromolecular. Isso pode complementar o conhecimento já existente sobre o mecanismo da enzima, o que é muito importante para conseguirmos desenhar compostos inibidores da *Mt*HisD mais específicos e eficientes.

2. Justificativa

A terapia moderna padrão de curta duração para TB está baseada em um regime de quatro fármacos, que são isoniazida, rifampicina, pirazinamida e etambutol por dois meses, seguido por tratamento com uma combinação de isoniazida e rifampicina por quatro meses adicionais. Essa terapia combinada deve ser estritamente seguida para prevenir a resistência a medicamentos, e a observação direta da adesão do paciente é a maneira mais confiável para assegurar um tratamento efetivo e impedir o desenvolvimento de resistência. Mutações no DNA identificadas em cepas de MTB resistentes a fármacos, as quais conduzem ao insucesso da terapia, têm sido revistas (103-105). Fármacos bacteriostáticos de segunda linha como etionamida, cicloserina e ácido *p*-aminosalicílico são reservados para reforçar o tratamento da doença resistente a fármacos ou quando o uso de medicamentos bactericidas são proibidos pela toxicidade (106). O MTB tem sido considerado o patógeno mais bem sucedido no mundo devido à enorme habilidade do bacilo em persistir nos tecidos do hospedeiro, onde medicamentos que são bactericidas *in vitro* necessitam administração prolongada para alcançar efeitos comparáveis (107, 108). O surgimento das cepas MDR-TB e XDR-TB bem como a urgência em combater cepas latentes de TB ressaltam a necessidade do desenvolvimento de novos agentes anti-TB mais efetivos e menos tóxicos a fim de diminuir a duração do atual tratamento, aumentar o tratamento da TB resistente a fármacos e fornecer tratamento efetivo para infecção de tuberculose latente.

A falta de interesse das indústrias farmacêuticas no desenvolvimento de novos fármacos para tratar a doença impele os grupos de pesquisa dos países em desenvolvimento, empresas de menor porte e as agências financiadoras a atuarem neste problema de saúde pública. Além disso, tem sido relatado que existe uma rápida capacidade de crescimento para empreender inovações na saúde em diversos países em desenvolvimento, incluindo o Brasil, que possuem a capacidade tecnológica e recursos humanos, mas relativamente pouca vontade financeira (109). Portanto, sentimos que o desenvolvimento de agentes quimioterápicos, objetivo de um

projeto maior do qual o presente trabalho faz parte, para combater a mortalidade e morbidade causada pelo MTB representa uma importante contribuição socioeconômica. A HisD representa um alvo em potencial, pois, além de ser considerada essencial para a sobrevivência do MTB, ela não está presente em humanos.

Além disso, o projeto apresentado é inovador porque contempla uma abordagem focada na caracterização bioquímica, modelagem molecular e desenvolvimento de compostos químicos ativos contra um alvo validado a partir do MTB e para o qual não há relatos na literatura de compostos inibidores (64).

3. Objetivos

3.1. Objetivo Geral

Este projeto tem como objetivo geral aprofundar o conhecimento do mecanismo enzimático e desenvolver novas moléculas capazes de inibir a enzima histidinol desidrogenase de *Mycobacterium tuberculosis* (*MtHisD*), como etapa na busca por novos fármacos anti-TB.

3.2. Objetivos Específicos

1. Realizar estudos da cinética da reação da enzima em estado pré-estacionário;
2. Realizar estudos de energia de ativação e determinar os parâmetros termodinâmicos do estado de transição da reação;
3. Estudar os efeitos isotópicos de solvente e realizar ensaios de volume excluído (*molecular crowding*);
4. Estudar a atividade inibitória de compostos sintetizados frente à atividade da *MtHisD* e analisar a ligação destes compostos com a enzima por docagem molecular;
5. Determinar a constante de dissociação do composto com maior capacidade inibitória;
6. Determinar os parâmetros termodinâmicos da ligação do composto com maior capacidade inibitória com a enzima livre de MTB;
7. Determinar a concentração inibitória mínima em culturas de *Mycobacterium tuberculosis* (MICs) dos compostos que apresentarem melhor inibição enzimática.

Os demais capítulos desta tese estão organizados da seguinte forma:

No **Capítulo 2** consta o manuscrito do artigo científico submetido ao periódico internacional *Journal of Biological Chemistry*, que é composto pelos

resultados dos objetivos específicos 1-7.

No **Capítulo 3** consta o artigo de revisão publicado no periódico internacional *Current Topics in Medicinal Chemistry* que é composto por uma revisão da bibliografia sobre a via de biossíntese da histidina no *Mycobacterium tuberculosis*.

No **Capítulo 4** são apresentadas as considerações finais e as referências bibliográficas.

É importante ressaltar que o trabalho tema desta tese foi contemplado no edital FAPERGS nº 013/2011- Pesquisador na Empresa, que objetiva a concessão de bolsas para alunos de doutorado, regularmente inscritos em Programas de Pós-Graduação devidamente aprovados pela CAPES e oferecidos por instituições de ensino públicas ou privadas sem fins lucrativos, com sede no Rio Grande do Sul, para executarem projetos de pesquisa em ciência, tecnologia e inovação referente às suas teses, no ambiente das empresas, de pequeno e médio porte, sediadas no Estado do Rio Grande do Sul. Assim, a doutoranda e o projeto aqui apresentado obtiveram auxílio financeiro da Fundação de Amparo à Pesquisa do Estado do Rio Grande do Sul (FAPERGS), do Serviço Brasileiro de Apoio às Micro e Pequenas Empresas do Rio Grande do Sul (SEBRAE/RS) e da empresa Quatro G Pesquisa & Desenvolvimento Ltda.

Capítulo 2

**“*Mycobacterium tuberculosis*
histidinol dehydrogenase:
biochemical characterization and
inhibition studies”**

Manuscrito submetido ao periódico
Journal of Biological Chemistry,
2015.

Mycobacterium tuberculosis histidinol dehydrogenase: biochemical characterization and inhibition studies

Juleane Lunardi^{1,2}, Leonardo Kras Borges Martinelli³, Alessandra da Silva Raupp³, José Eduardo Sacconi Nunes², Diana Carolina Rostirolla³, Luís Fernando Saraiva Macedo Timmers^{1,4}, Anne Drumond Villela³, Kenia Pissinate³, Jones Limberger³, Osmar Norberto de Souza^{1,4}, Diógenes Santiago Santos^{1,2,3}, Luiz Augusto Basso^{1,2,3} and Pablo Machado^{1,3,*}.

¹ Programa de Pós-graduação em Biologia Celular e Molecular, Faculdade de Biociências, Pontifícia Universidade Católica do Rio Grande do Sul (PUCRS), 90619-900, Porto Alegre, Rio Grande do Sul, Brazil

²Quatro G Pesquisa & Desenvolvimento, 90619-900, Porto Alegre, Rio Grande do Sul, Brazil

³Centro de Pesquisas em Biologia Molecular e Funcional (CPBMF), Instituto Nacional de Ciência e Tecnologia em Tuberculose (INCT-TB), Pontifícia Universidade Católica do Rio Grande do Sul, (PUCRS), 90619-900, Porto Alegre, RS, Brazil

⁴Laboratório de Bioinformática, Modelagem e Simulação de Biossistemas (LABIO), Faculdade de Informática, Pontifícia Universidade Católica do Rio Grande do Sul (PUCRS), 90619-900 Porto Alegre, Rio Grande do Sul, Brazil

*Running title: *Study of the HisD mechanism and inhibition*

To whom correspondence should be addressed: Pablo Machado and/or Diógenes Santiago Santos, Centro de Pesquisas em Biologia Molecular e Funcional (CPBMF), PUCRS, 90619-900, Porto Alegre, Rio Grande do Sul, Brazil, Tel/Fax: +55(51) 33203629; E-mail: diogenes@pucrs.br (D.S.Santos); pablo.machado@pucrs.br (P.Machado).

Keywords: *Mycobacterium tuberculosis*, tuberculosis, enzyme inhibitor, histidinol dehydrogenase, molecular target, histidine, drug design.

Background: The *Mycobacterium tuberculosis* histidinol dehydrogenase (*MtHisD*) has been described as essential for survival and mycobacterial virulence.

Results: The 2-naphthyl- and 4-chlorobenzaldehyde-substituted compounds showed values in the submicromolar range.

Conclusion: These compounds may thus be considered lead compounds for further development.

Significance: Understanding of the mode of action and inhibition profile can help further efforts to obtain novel anti-tuberculosis drugs.

ABSTRACT

The *hisD*-encoded histidinol dehydrogenase (HisD) catalyzes the two last chemical reactions of the L-histidine biosynthetic pathway, namely the conversion of L-histidinol (L-Hol) to L-histidinaldehyde (L-Hal) and to L-histidine (L-His). The *hisD* gene product has been shown to be essential for *Mycobacterium tuberculosis* survival *in vitro*. Herein, we describe a series of biochemical studies on recombinant *M. tuberculosis* HisD (*MtHisD*). The synthesis of

hydrazones derived from L-histidine yielded inhibitors in the low micromolar range, one of which is endowed with moderate anti-Mtb activity. The compounds described here are, to the best of our knowledge, the first inhibitors of *MtHisD* activity reported in the literature, and they could become promising candidates for future development.

Tuberculosis (TB) continues to claim thousands of lives annually. According to the World Health Organization (WHO), 9 million new cases of the disease were reported worldwide in 2013 with 1.5 million deaths (1). The elevated adaptive capacity of *Mycobacterium tuberculosis* (Mtb), the main etiological agent of human TB, and inappropriate treatments have fuelled the emergence of multi-drug-resistant (MDR-TB) and extensively drug-resistant (XDR-TB) strains for which available treatments are suboptimal and limited. Moreover, eradication of TB is hampered by asymptomatic infection from dormant or latent forms of mycobacteria, which have placed one-third of the world's population at lifelong risk for TB

development from disease reactivation. To achieve infection control, there is an urgent need to develop drugs with novel mechanisms of action. Since the early 1960s, bedaquiline has been the sole drug presenting a new molecular target licensed for TB treatment. This ATP synthase targeted drug was approved for the treatment of adults with MDR-TB when other therapeutic alternatives are not available (2-4). Although treatment with bedaquiline has been described as a promising strategy against MDR-TB strains, its possible cardiac safety concerns (5) and the rapid emergence of new drug-resistant strains have emphasized the need for continuing efforts to discover new TB drugs.

Within this context, the enzymes of the biosynthetic L-histidine pathway have emerged as attractive targets for the design and development of novel chemical scaffolds, which can hopefully become innovative antimycobacterial compounds (6). This pathway utilizes ten enzymatic reaction steps to convert phosphoribosyl pyrophosphate (PRPP) and ATP to L-histidine. Unlike mammals, the L-histidine pathway is present in prokaryotic organisms, lower eukaryotic organisms, and plants (7-9). Consequently, the L-histidine pathway enzymes have been described as potential targets for the development of new herbicides and antimicrobial compounds endowed with selective toxicity (10, 11). It is important to note that this route shows connections to other biosynthetic pathways such as purine and tryptophan biosynthesis (6, 8, 12), making it an important biochemical hub. The bifunctional histidinol dehydrogenase (EC 1.1.1.23), encoded by the *hisD* gene, is responsible for the two last reactions of this pathway, the NAD⁺- and Zn²⁺-dependent conversion of L-histidinol (L-Hol) to L-histidine (L-His) through an L-histidinaldehyde (L-Hal) intermediate (13-15), leading to the concomitant reduction of 2 NAD⁺ molecules. The importance of L-histidinol dehydrogenase for virulence has been demonstrated in pathogenic bacteria such as *Brucella suis* (16), *Salmonella typhimurium* (17), and *Burkholderia pseudomallei* (18).

In Mtb, the enzyme histidinol dehydrogenase (*MtHisD*) has been reported to be essential for survival and mycobacterial virulence (19-22). Indeed, there is an apparent inability of histidine auxotrophs of Mtb to survive single-amino acid starvation under standard culture conditions (19), and the *hisD* gene has been described as essential for *in vitro* mycobacterial growth (20, 22). Incidentally, *MtHisD* has been classified among

the top 50 targets by the TDR Targets Database (21). This rank takes into account aspects such as the existence of a solved structure or structure model, essentiality in any species, the absence of a human ortholog, and expression during latency or dormancy. Accordingly, we have previously reported kinetic, thermodynamic and structural analyses of *MtHisD* to aid the medicinal chemistry campaigns based on the rational drug design (23). We have proposed that *MtHisD* follows a Bi Uni Uni Bi Ping-Pong mechanism in which L-Hol is the first substrate to bind and that L-His is the last product to dissociate and that the amino-acid side chains of His336 and Glu335 are likely involved in catalysis and/or substrate binding (23). Accordingly, imidazole-containing substrate analogues are likely to bind to free enzyme.

Our initial purpose was to try and maintain the possible polar non-covalent interaction mediated by the imidazole ring of L-Hol with catalytic amino acid residue His336 by synthesizing molecules with structural characteristics obtained from the substrate (L-Hol), intermediate (L-Hal), and product (L-His) of the enzyme-catalyzed chemical reaction. In addition, the designed compounds could explore the hydrophobic pocket near the NAD⁺ in the catalytic site of *MtHisD* in accordance with previously published data from orthologous enzymes (24).

As an improved understanding of the mode of action of *MtHisD* could help further medicinal chemistry efforts, here we present pre-steady kinetics studies, the activation energy of the catalyzed reaction, solvent kinetic isotope effects, proton inventory, and molecular crowding effects. Data on synthesis of hydrazones using L-histidine as a scaffold and their evaluation as *MtHisD* enzyme inhibitors are described. Docking experiments were performed to provide a three-dimensional picture of the interaction mode of selected inhibitors. The inhibitory activity on the growth of Mtb (minimum inhibitory concentration (MIC)) are also shown.

Experimental Procedures

All reagents for enzyme activity measurements and inhibition assays were purchased from Sigma-Aldrich and were used without further purification. All measurements were performed at least in duplicate, and the biochemical data, when necessary, were

analyzed using the program SigmaPlot 10.0 (Systat Software, Inc.).

Enzyme assays. Cloning and overexpression of the *hisD*-encoding gene from *Mycobacterium tuberculosis*, purification, and determination of the true steady-state kinetic constants were performed as previously described (23).

The reaction mixture used to determine the steady-state kinetic parameters for the histidinol substrate consisted of variable concentrations of L-Hol (2-120 μM) and a fixed-saturating concentration of NAD⁺ ($2 \times 10^5 \mu\text{M}$). For the NAD⁺ substrate, variable concentrations of NAD⁺ (700-20000 μM) and a fixed-saturating concentration of L-Hol (200 μM) were used. Both assays were performed using 50 mM PIPES as buffer, pH 7.2 (0.5 mL final volume) at 25 °C, and the change in absorbance at 340 nm was monitored using a spectrophotometer (UV-2550 UV/Visible, Shimadzu). One unit of enzyme activity (U) is defined as the amount of enzyme catalyzing the conversion of 1 μmol of substrate per minute in an optical path of 1 cm. The Michaelis-Menten constant (K_M) and k_{cat} values were calculated from Equation 1 and Equation 2 (25), respectively:

$$v = \frac{V_{\max}[S]}{K_M + [S]} \quad (1)$$

$$k_{\text{cat}} = \frac{V_{\max}}{[E]_t} \quad (2)$$

where v is the steady-state velocity, V_{\max} is the maximal rate, $[S]$ is the substrate concentration, K_M is the Michaelis constant, k_{cat} is the catalytic constant, and $[E]_t$ is total concentration of enzyme.

Pre-steady-state kinetics. The increase in absorbance at 340 nm was monitored at 25 °C using an SX-18MV-R stopped-flow spectrofluorimeter (Applied Photophysics). The mixing chamber concentrations of enzyme and reagents in 50 mM PIPES pH 7.2 buffer were: MtHisD at 10 μM , NAD⁺ at $5 \times 10^4 \mu\text{M}$, and L-Hol at 1000 μM . The reaction time was 100 s. These measurements were performed to determine whether product release is part of the rate-limiting step. The control experiment was performed under the same conditions, but in the absence of enzyme. The data were fitted to Equation 3.

$$A = A_0 e^{-kt} \quad (3)$$

where A is the absorbance at time t , A_0 is the absorbance at time zero, and k is the apparent first-order rate constant for product formation.

Energy of activation (E_a). To determine the energy of activation of the MtHisD-catalyzed chemical reaction, initial velocities were measured in the presence of saturating concentrations of both substrates (L-Hol 200 μM ; NAD⁺ $2 \times 10^5 \mu\text{M}$), at temperatures varying from 15 to 40 °C. The enzyme was incubated for three minutes at all temperatures tested and assayed under standard conditions. The E_a was calculated from the slope (E_a/R) of the Arrhenius plot fitting the data to Equation 4. With this result, we can estimate the thermodynamic activation parameters, such as the enthalpy ($\Delta H^\#$), free Gibbs energy ($\Delta G^\#$) and entropy ($\Delta S^\#$), from the transition state theory (26) (Equation 5, 6, and 7), respectively.

$$\ln k_{\text{cat}} = \ln A - \left(\frac{E_a}{R} \right) \frac{1}{T} \quad (4)$$

$$\Delta H^\# = E_a - RT \quad (5)$$

$$\Delta G^\# = RT \left(\ln \frac{k_B}{h} + \ln T - \ln k_{\text{cat}} \right) \quad (6)$$

$$\Delta S^\# = \frac{\Delta H^\# - \Delta G^\#}{T} \quad (7)$$

where R is the universal gas constant (8.314 J mol⁻¹ K⁻¹), A is the Arrhenius constant, which represents the product of the collision frequency (Z) and a steric factor (p) based on the collision theory of enzyme kinetics (26), T is the temperature in Kelvin ($T = {}^\circ\text{C} + 273.15$), k_B is the Boltzmann constant ($1.3805 \times 10^{-23} \text{ J K}^{-1}$), and h is Planck's constant ($6.6256 \times 10^{-34} \text{ J s}^{-1}$). The error in $\Delta G^\#$ was calculated using Equation 8.

$$(\Delta G)_{\text{err}} = \frac{RT(k_{\text{cat}})_{\text{err}}}{k_{\text{cat}}} \quad (8)$$

Solvent kinetic isotope effects (SKIE) and proton inventory. Solvent kinetic isotope effects were determined by measuring initial velocity in the presence of varying concentrations of one of the substrates (L-Hol 4–200 μM or NAD⁺ 100–

20000 μM) and a fixed-saturating concentration of the other substrate (L-Hol 200 μM or NAD⁺ 2 x 10⁵ μM). Both reactions were carried out in H₂O and in 90 atom% D₂O. Furthermore, the reactions were performed in 50 mM PIPES, pH 7.2, and in 50 mM Tris-HCl, pH 9.0. The data were fitted to Equation 9. The proton inventory was determined using saturating concentrations of both substrates (L-Hol 200 μM and NAD⁺ 2 x 10⁵ μM) at different mole fractions of D₂O (0-90%) in 50 mM PIPES, pH 7.2, or 50 mM Tris-HCl (pH 9.0). The solvent kinetic isotope effect data were fitted to Equation 9 (27); in which *V* is the maximal velocity, *A* is the substrate concentration, *K* is the Michaelis constant for *A*, *E_{V/K}* and *E_V* are the isotope effects -1 on *V/K* and *V*, respectively, and *F_i* is the fraction of deuterium label in the substrate.

$$v = \frac{VA}{K(1 + F_i E_{V/K}) + A(1 + F_i E_V)} \quad (9)$$

The dome-shaped proton inventory data (Fig. 4) at pH 7.2 were fitted to Equation 10, and the linear data (Fig. 4 - inset) at pH 9.0 were fitted to Equation 11 (27), in which ^{D₂O}*k* is equal to the ration *k_n/k_l* and ^{D₂O}*k* is equal to the ration *k₀/k_l*, thus *k_n* is the *k_{cat}* at each atom % D₂O, *k₀* is the *k_{cat}* with H₂O, *n* is the atom % D₂O, ϕ^T and ϕ^R represent transition state and reactant state fractionation factors, respectively. The superscripts T₁ and T₂ represent two different transition states in the reaction mechanism of MtHisD that contribute to solvent isotope effects.

$$n_k = {}^{D_2O}k \frac{(1 - n + n\phi^{T_1})(1 - n + n\phi^{T_2})}{1 - n + n\phi^R} \quad (10)$$

$$n_k = {}^{D_2O}k(1 - n + n\phi^T) \quad (11)$$

Molecular Crowding. The enzyme assay for L-Hol was carried out by varying the concentration of L-Hol (2-120 μM) and using a fixed-saturating concentration of NAD⁺ (2 x 10⁵ μM). For NAD⁺, we used varying concentrations of NAD⁺ (700-20000 μM) and a fixed-saturating concentration of L-Hol (120 μM). The reactions were performed in the absence or in the presence of 100 or 200 g L⁻¹ of the inert polymer Ficoll PM70 (Sigma-Aldrich). The apparent parameters (*K_M*, *k_{cat}*, and specificity constant) in the presence and absence of Ficoll were compared.

Synthesis of hydrazone derivatives 4a-k. A simple three-step strategy was applied for the synthesis of histidinol dehydrogenase inhibitors. In the first step, L-histidine **1** was allowed to react with thionyl chloride in methanol, providing L-histidine methyl ester **2** with 96% yield (Scheme 1). Ester **2** was then reacted with hydrazine hydrate in methanol reflux, leading to hydrazide **3** with 80% yield (28). It is noteworthy that the role of NH₂NH₂·H₂O in this step is both to react with the ester moiety and to neutralize the medium, affording a nucleophilic unprotonated hydrazide. Another aspect that deserves to be mentioned is the labored separation of **3** from excess hydrazine hydrate impurities because this nucleophile was used in a 2.1:1 molar ratio in relation to L-histidine methyl ester **2**. To accomplish this task, we developed an alternative strategy: to react the crude product with 4-fluorobenzaldehyde in ethanol. In this way, the unwanted 4-(fluorobenzylidene)hydrazine precipitated, and pure **3** was obtained as a pale yellow oil.

With the precursor **3** in hand, it was reacted with a number of aldehydes, providing the products **4a-4k** with yields ranging from moderate to good (Scheme 1). All synthesized compounds showed spectroscopic and spectrometric data in accordance with the proposed structures (Support Information).

Inhibition studies. The presence of time-dependent inhibitory activity was examined for the compounds synthesized. For this analysis, 1.5 μM of recombinant MtHisD was pre-incubated with 2 μM of inhibitor, and aliquots were withdrawn to be added at different times (up to 30 min) to the reaction mixture (L-Hol, NAD⁺, 50 mM PIPES pH 7.2 and H₂O, and final concentration of 3% DMSO). The change in initial velocity versus time was monitored, and the percentage of inhibition was calculated.

To perform IC₅₀ determinations, the compounds (dissolved in DMSO) were added at various concentrations, ranging from 0 – 120 μM, to the reaction mixture containing MtHisD. The concentration of the added substrates (L-Hol and NAD⁺) was fixed in *K_M* values (23) in the presence of 3% DMSO (a concentration that did not interfere with the assay conditions). The reactions were carried out in 50 mM PIPES pH 7.2 under standard conditions. The IC₅₀ value, which defines the concentration of inhibitor required to reduce in 50% the initial enzyme

activity, was determined by fitting the data to Equation 12.

$$\frac{v_i}{v_0} = \frac{1}{1 + \left(\frac{[I]}{IC_{50}} \right)} \quad (12)$$

in which v_i and v_0 are, respectively, the reaction velocity in the presence and in the absence of inhibitor (I) (29).

The inhibition constant (K_{is}) towards L-Hol was determined for compounds with IC₅₀ values lower than 2.5 μM. The reaction mixture contained 0.36 μM of the enzyme, varying concentrations of L-Hol (2–120 μM), NAD⁺ at the K_M concentration, and inhibitor at concentrations ranging from 0.5 to 30 μM. The K_{is} values were calculated from data fitting to competitive inhibition equation (Equation 13), and the experimental data and predicted values were plotted as double-reciprocals as described by Lineweaver and Burk (30).

$$v = \frac{V[S]}{K_M \left(1 + \frac{I}{K_{is}} \right) + [S]} \quad (13)$$

where V is the maximal velocity, K_M is the Michaelis–Menten constant, $[S]$ is the substrate concentration, I is the inhibitor concentration, and K_{is} is the equilibrium dissociation constant for the enzyme–inhibitor complex (31).

The equilibrium dissociation constant (K_d) for the lead-like compound **4k** was determined by fluorescence spectroscopy (Shimadzu RF-5301PC spectrofluorophotometer). The excitation wavelength was 280 nm, and emission spectra were collected from 300 to 500 nm. The maximum value of fluorescence intensity at 334 nm was plotted as a function of increasing ligand concentration. The enzyme concentration was 2 μM (in 50 mM PIPES pH 7.2 buffer), and the compound concentration ranged from 0.499 to 4.93 μM. The enzyme and the compound were mixed and incubated for three minutes at assay temperature. Binary complex formation for each inhibitor concentration was measured by fluorescence titration, and the inner filter effect (50 mM PIPES buffer, pH 7.2, and varying concentration of the compounds, 0.499 – 4.93 μM) was subtracted. This experiment was performed at different temperatures (15, 20, 25, and 30°C). The dissociation constant values (K_d)

were obtained from data fitting to Equation 14. The ln K_d values were plotted against the inverse of the temperature values, and the standard enthalpy of binding (ΔH°) and entropy of binding (ΔS°) were calculated from data fitting to the van't Hoff equation (Equation 15). An estimate of the standard Gibbs free energy of binding (ΔG°) can thus be derived from Equation 16.

$$\frac{F_0 - F}{F_0 - F_\infty} = \frac{[L]}{K_d + [L]} \quad (14)$$

$$\ln K_d = \left(\frac{\Delta H^\circ}{R} \right) \frac{1}{T} - \frac{\Delta S^\circ}{R} \quad (15)$$

$$\Delta G^\circ = \Delta H^\circ - T\Delta S^\circ \quad (16)$$

F_0 represents the initial fluorescence, F is the observed fluorescence, F_∞ is the maximum change in fluorescence at saturating ligand (L) concentration, K_d represents the equilibrium dissociation constant for protein:ligand binary complex formation, R is the gas constant (8.314 J mol⁻¹K⁻¹), and T is the temperature in Kelvin.

Molecular docking experiments. These studies were performed to analyze the interaction mode of the selected compounds having K_{is} values for MtHisD inhibition lower than 5 μM. The enzyme and ligand structures were prepared using AutoDockTools 1.5.2, and docking simulations were performed with AutoDock 4.2, allowing flexibility in the ligands (32, 33). The experiments were performed with the homology model structure of MtHisD associated with NAD⁺ (23). Because the MtHisD active site is at the interface of two subunits, we used the dimeric form to perform all docking experiments. For all simulations, the 3D-grid dimension used to define the enzyme active site and to evaluate the scoring function was 60 x 60 x 60, with spacing of 0.375 Å. The Lamarckian Genetic Algorithm (LGA) was employed as the docking algorithm with 50 runs, and the remaining parameters were set to their default values except for number of evaluations, which was set to 2,500,000.

Determination of Minimum Inhibitory Concentration (MIC). The growth inhibitory activity of the compounds was tested against the *Mycobacterium tuberculosis* H37Rv strain and was determined by resazurin microtiter assay (REMA) (34). Isoniazid was used as control. *M.*

tuberculosis was cultivated in Middlebrook 7H9 (Difco) liquid medium supplemented with 10% (v/v) OADC (oleic acid, albumin, dextrose, catalase; Becton Dickinson), and 0.05% (m/V) Tween 80 (Sigma). Initially, it was grown at 37 °C up to an optical density at 600 nm (OD_{600}) between 0.6 and 0.8; then, it was diluted in Middlebrook 7H9 to an OD_{600} of 0.006. One hundred μ L of Mtb inoculum were added to each well on a microplate containing 100 μ L of the tested drug, or only Middlebrook 7H9 (control inoculum) to reach an OD_{600} of 0.003. Final drug concentrations ranged from 0.0078 to 4 μ g mL⁻¹ for isoniazid, and from 0.195 to 100 μ g mL⁻¹ for selected compounds. Plates were incubated for 7–9 days at 37 °C. Sixty microliters of 0.01% resazurin solution were added to each well; plates were re-incubated for additional 2 days. A change in color, from blue to pink, indicated the growth of bacteria, and the MIC was read as the minimum drug concentration that prevented the color change in resazurin solution. MIC values reported here represent an average of three tests carried out independently.

Results and Discussion

MtHisD is a bifunctional four-electron dehydrogenase enzyme that catalyzes two subsequent reactions, the oxidation of L-Hol and the reduction of two NAD⁺ molecules (23), with the formation of two intermediaries (L-Hol and L-histidindiol) (35). L-Hol is very unstable at neutral pH when not bound to HisD (14, 15, 36, 37), making study of the half-reaction difficult. The intermediates do not dissociate from the active site during the overall catalysis (13). Another interesting aspect is that this enzyme has a single active site that carries out oxidations of both the L-Hol substrate and the L-Hol (aldehyde) intermediate (13, 14). These specific features reveal that the understanding of this enzymatic reaction is complicated, but very interesting in kinetic terms. A better understanding of the enzymatic mechanism's steps and the enzyme's interactions is important for the rational design of enzymatic inhibitors.

A pre-steady-state kinetics assay was performed to determine whether release of the product participates as a limiting step of the reaction. Fitting the data to Equation 3 resulted in an apparent first-order rate constant value of 0.0604 ± 0.0002 s⁻¹ (Fig. 1), which describes a single exponential curve. As no burst in NADH formation could be detected (Fig. 1), this result

suggests that product release does not contribute to the rate-limiting step of MtHisD-catalyzed chemical reaction. Grubmeyer and Teng (38) showed that no burst could be detected for HisD from *Salmonella typhimurium* (*StHisD*). These authors concluded that the overall rates of the first and second half-reactions were not dramatically different, and thus both rates contribute to the overall rate limitation.

Experiments to determine the energy of activation of the rate-limiting step for the MtHisD reaction were carried out. This energy represents the minimal amount of energy necessary to initiate the enzyme-catalyzed chemical reaction. The dependence of k_{cat} on temperature at saturating concentrations of L-Hol and NAD⁺ was linear (Fig. 2). The linearity of the Arrhenius plot suggests that there is no change in the rate-limiting step over the temperature range utilized in the assay. These data were fitted to Equation 4, yielding a value of $45 (\pm 2)$ kJ mol⁻¹ K⁻¹, and the thermodynamic activation parameters were evaluated using Equation 5-7, yielding $42.25 (\pm 0.04)$ kJ mol⁻¹; $72.07 (\pm 0.07)$ kJ mol⁻¹; and $-100 (\pm 0.09)$ J mol⁻¹ K⁻¹ for $\Delta H^\#$, $\Delta G^\#$, and $\Delta S^\#$, respectively. The positive value (unfavorable) of $\Delta H^\#$ and the negative value (unfavorable) of $\Delta S^\#$ demonstrate a lack of enthalpy-entropy compensation behavior (39-41). This non-compensatory system and the unfavorable $\Delta S^\#$ may be tentatively ascribed to loss of rotational and translational freedom, leading to a more positive value of $\Delta G^\#$. The positive value (unfavorable) of $\Delta G^\#$ represents the energy barrier to transforming ES in the ground state to the activated enzyme-substrate complex ES[#].

The solvent kinetic isotope effects data (Fig. 3) were fitted to Equation 9, and the values obtained are presented in Table 1. These results show contribution of proton transfer from the solvent to the MtHisD-catalyzed chemical reaction. The fractionation factor (ϕ) is a measure of the stiffness or tightness of binding of a solute site versus the solvent sites. A general rule of thumb is that deuterium accumulates where binding is tighter ($\phi > 1$); and correspondingly, protium accumulates where binding is looser ($\phi < 1$) (27). The fractionation factors of transition state protons contribute reciprocally to the solvent kinetic isotope effect, whereas the contribution of a reactant state proton to the isotope effect is equal to its fractionation factor. The values of V and V/K in the assay at pH 7.2 (Table 1) suggest a modest participation of the

proton solvent in catalysis and for L-Hol binding, whereas there appears to be no proton solvent isotope participation in NAD⁺ binding (Fig. 3A and 3B). At pH 9.0, V and V/K showed normal solvent kinetic isotope effect for catalysis and inverse solvent isotope effect for L-Hol and NAD⁺ binding (Fig. 3 - insets; Table 1). The reactant state for V/K is always free enzyme and free substrate and contribution of reactant state protons to solvent kinetic isotope effect is directly proportional to its fractionation factor. The reactant-state fractionation factors of functional groups that are involved in acid-base nucleophilic catalysis (e.g., carboxylic group of glutamate, N-H bond of histidine, phenolic OH of tyrosine, etc) are usually near unity (27). It is thus tempting to suggest that at pH 9 there is an increase in the fractionation factor for transition state (deuterium accumulates in the transition state), whose reciprocal contribution results in an inverse V/K solvent kinetic isotope effect. Proton inventory experiments allow determination of the number of protons that are transferred during the solvent isotope-sensitive step, and can provide the basis for proposal of a model for the origins of solvent isotope effects on enzyme-catalyzed chemical reactions. The data at pH 7.2 showed a dome-shaped proton inventory (Fig. 4), which can have several mechanistic origins (27). A tentative explanation may be that more than a single proton is transferred and that both normal and inverse solvent contributions were giving rise to the observed SKIE. Incidentally, Grubmeyer and Teng (38) reported a slightly convex downward curve in proton inventories, also suggesting the involvement of more than a single proton in the overall effect on StHisD. Fitting the data at pH 7.2 (Fig. 4) to Equation 10, in which the solvent isotope effect arises from a single offsetting reactant state (inverse SKIE) and two transition states (normal SKIE), appears to describe the experimental results. Although a crest-like curve in proton inventory could also be described by offsetting transition-state and medium contributions, the latter would require additional data to be invoked (e.g., solute stability, equilibrium binding). At any rate, the data interpretation here presented is suboptimal, as the half reactions were not studied separately, and thus, these fractionation factors were not determined. The reaction mechanism for HisD from *E. coli* (35) predicts at least two interactions between the transition states and the neighboring water molecule, which can influence SKIE. First, the water is activated by the

negative charge of Glu326 (Glu335 in MtHisD) and makes a nucleophilic attack on the carbonyl group of L-Hol, forming an L-histidindiol (gem-diol) intermediate. The unprotonated His327 of *E. coli* HisD (corresponding the conserved His336 in MtHisD) abstracts a proton of the hydroxyl group bound to *sp*³ carbon of L-histidindiol intermediate followed by hydride transfer to NAD⁺ and formation of L-His. The protonated His327 of *E. coli* HisD is restored to the neutral state by donation of a proton to the nearby water molecule (35). This proposed mechanism suggests that invoking two or more transition states to explain the proton inventory data here presented is warranted. However, additional studies are needed to clarify the exact fractionation factors that are influencing the SKIE. The proton inventory data at pH 9.0, on the other hand, suggest that a single transition-state proton transfer contributes to the solvent isotope effect (Fig. 4 - inset). Accordingly, the data were fitted to Equation 11. The proton inventory data at pH 9 are consistent with the normal solvent kinetic isotope effect for catalysis (Table 1).

It is known that the rate limiting chemical step can change as the pH changes, and the magnitude of the isotope effects on V and V/K change depending on the contribution of the isotope-sensitive step to overall rate limitation at saturating and limiting reactant concentrations, respectively (42). According to the results here presented, the pH-dependent steps are isotope-sensitive. The difference of SKIE at two pHs can be related to the pK_a values of the residues involved in catalysis and L-Hol binding. The apparent pK value of L-Hol binding to free MtHisD is approximately 8 ± 3 (the value attributed to conserved histidine residues in the active site (23)). Titration profiles for StHisD using L-Hol suggested an aminoacid side chain with pK values of 8.17 and 8.35 that are essential for, respectively, catalysis and L-Hol substrate binding (38). It is likely that the imidazole side chain of His336 in MtHisD is involved in both L-Hol binding and catalytic activity of first and second hydride transfer in the reaction (23). As the physiological pH of the host is approximately 7.2, the results of SKIE and proton inventory at this pH reproduce with more reliability the environment found by Mtb when it infects a human cell. Following this line of reasoning, in an attempt to simulate the host cellular environment and to validate our results obtained

in aqueous medium, crowding assays were performed.

Molecular crowding was carried out using an inert polymer to try to reproduce a cell-like environment with high concentrations of macromolecules. The values of steady-state kinetic parameters (K_M , k_{cat} , and specificity constant) in a solution containing Ficoll at two different concentrations in comparison to these parameters in the absence of Ficoll are presented in Table 2. These results validated our experiments with *MtHisD* in aqueous solvent. Other works have obtained similar results. Molecular crowding experiments with phosphoglycerate kinase, glyceraldehyde-3-phosphate dehydrogenase, and acylphosphatase I enzymes in the presence of crowding agents also showed no influence of crowding agents on the kinetic parameters (43).

Designed compounds **4** were synthesized in three steps with moderate to good yields (29–72%). The best yields were obtained for the reactions of 4-nitro-benzaldehyde (69%) and 4-benzyloxi-benzaldehyde (72%). However, 2-naphthaldehyde and 4-cholorobenzaldehyde converted to hydrazone derivatives with only 34% and 29% yield, respectively (for further information on synthesis of compounds, see the supporting information).

After obtaining the compounds, the next step was to evaluate them as possible inhibitors of the reaction catalyzed by *MtHisD*. Inhibition studies of *S. typhimurium* (46), cabbage, *E. coli* (10), and *B. suis* HisD (24, 28, 45) have been reported in the literature (6). In their first range of inhibitors, Abdo and colleagues (45) proposed benzylic ketones derived from L-His as inhibitors of *Brucella suis* HisD (*BsHisD*) activity. In that report, an increased inhibition capacity of compounds with substitutions at the 4-position of the aromatic moiety was observed. The most effective compounds for inhibition of *BsHisD* from the first library of compounds were 4-bromo and 4-benzyloxy derivates (45). A second series of L-histidinylphenylsulfonyl hydrazides (28) was less active than the one previously described, indicating that the nature and the length of the linker between the histidinyl moiety and the phenyl ring as well as the second lipophilic pocket binding the cofactor NAD⁺ are important factors that can modulate the potency of new potential inhibitors in drug discovery campaigns (24).

Table 3 shows the IC₅₀ values against *MtHisD* activity for eleven compounds synthesized from

L-histidine (Scheme 1). No one of the ligands exhibited time-dependent inhibitory activity (data not shown). From these data, one can conclude that in general, compounds containing electron withdrawing groups at the 4-position of phenyl moieties demonstrated an increased inhibition capacity. Indeed, the 4-fluor- (**4g**), and 4-cloro- (**4h**), and 4-nitro-substituted compounds (**4j**) showed IC₅₀ values of 2.4 ± 0.8 μM, 2.4 ± 0.4 μM, and 2.5 ± 0.2 μM, respectively. These results could thus be rationalized by polarization effects that modify the dipole vector of the compounds, facilitating van der Waals interactions. In accordance with previously reported data (24, 45), compounds with bulky substituents have shown better IC₅₀ values for inhibiting HisD activity. The 2-naphthyl substituted compound **4k** was able to inhibit the catalytic activity of *MtHisD* with an IC₅₀ of 1.1 ± 0.2 μM. This planar π-electron rich group can make hydrophobic interactions with side chains of the amino acid residues of the active site of *MtHisD*. The interaction mode of compound **4k** was studied by docking experiments, which will be described in the subsequent sections. Although hydrazone **4e** did not show an IC₅₀ value lower than 2.5 μM (9.8 ± 0.7 μM), this compound was selected for additional inhibition studies because of its high lipophilicity. This characteristic is interesting for further MIC determination.

The K_{is} values (Table 4) were determined with respect to L-Hol substrate for four selected compounds (IC₅₀ values lower than 2.5 μM, and molecule **4e**). All tested molecules showed a competitive inhibition profile determined from the straight-line patterns intersecting at the y-axis (30) (Fig. 5). The competitive inhibition of the synthesized molecules, for L-Hol, corroborated the maintenance of chemical characteristics of substrate/product. These results evidence direct competition of the two ligands (substrate and inhibitor) for a common binding pocket on the enzyme molecule (29), where the tested compounds bind to the free enzyme and exclude the substrate L-Hol binding. This mode of inhibition reduces the apparent affinity of the substrate by an amount that depends on the concentration and affinity of the inhibitor. Therefore, the substrate will bind to only the enzyme through the displacement of the inhibitor (46).

To verify the choice of binding mode of hydrazones **4a-k** at the active site of *MtHisD*,

molecular docking simulations were carried out for selected compounds showing K_{is} values lower than 5 μM . The selected molecules showed interactions with amino acid residues involved in both catalysis and substrate binding. These experiments considered the amino acid residues involved in binding of L-Hol, NAD^+ , and Zn^{+2} ion. These residues were determined in pH-rate profiles and molecular modeling experiments (23) based on the tridimensional structure of HisD of *E. coli* (*EcHisD*) (35). *MtHisD* is a homodimeric enzyme, and its monomer (subunits A and B) possesses four globular domains (23). The two active sites are located at the boundary of the homodimer interface. Domains 1, 2, and 4 are related to L-Hol and Zn^{+2} binding, and domain 1 to NAD^+ molecule binding (23). Ligand **4e** was obtained to perform hydrophobic contacts with His376, which is involved in L-Hol binding, (Fig. 6A), and Glu335. Participation of the latter in either catalysis or substrate binding had not been demonstrated in pH-rate profile experiments with *MtHisD* (23). However, in *EcHisD*-catalyzed reactions, Glu326 (corresponding to Glu335 in *MtHisD*) activates the water molecule at the second step of the reaction (35). Therefore, the inhibitory capacity of compound **4e** could be a consequence of its large structure occupying the binding site of the L-Hol pocket, rather than of its binding potential to enzyme residues involved in L-Hol binding. Compounds **4h** and **4k** implement hydrophobic contacts with His336 (Fig. 6B and 6C), also involved in L-Hol binding. This amino acid residue acts as a base to abstract the proton from a hydroxyl group, causing the α -carbon to adopt a sp^2 configuration (35). However, compound **4h** makes a hydrophobic interaction with Asp369, and Asp369 is involved in coordinating the Zn^{+2} ion (Fig. 6B). Considering that Zn^{+2} carries out an important function in the correct positioning of L-Hol (23, 35), it is expected that those compounds acting as competitive inhibitors of L-Hol interact with the Zn^{+2} -binding amino acid residues. The **4k** molecule makes a hydrogen bond (H-bond) with Asp369^{OD2} (Fig. 6C). The **4h** and **4k** candidates can have H-bond interactions with His376^{ND1}. The carbonyl backbones of this amino acid residue and of His336 are responsible for the formation of H-bonds with hydroxyl groups of the L-Hol substrate (23). The molecule **4h** interacts by H-bonding with Glu335^{OE2}, and this may interfere with activation of the water molecule and inhibit the nucleophilic attack on

the reactive carbon for L-Hal. Compound **4k** can make H-bonding interactions with Glu423^{OE1}, which is related to L-Hol binding similarly to His336 and His376 (23).

The hydrogen interactions of the N4 atom from **4k** imidazole portion with His336^{ND1} were determined to be very important because this amino acid residue acts as three of the four bases involved in the acid-base catalysis (35).

Finally, the number and relative force of the interactions performed by **4k** in molecular recognition can explain its higher inhibitory activity on *MtHisD*. Equilibrium fluorescence spectroscopy data were fitted to Equation 14. As *MtHisD* has four tryptophan amino acid residues and seven tyrosine residues, changes in protein Trp and Tyr fluorescence upon ligand binding were monitored. Titration of *MtHisD* with the best ligand in inhibition assays (**4k**) showed a hyperbolic curve (Fig. 7), yielding K_d values of $0.62 \pm 0.14 \mu\text{M}$, $0.7 \pm 0.1 \mu\text{M}$, and $0.79 \pm 0.15 \mu\text{M}$, at 20°C , 25°C , and 30°C , respectively. The K_d of **4k** binding to *MtHisD* at 25°C is in agreement with the K_{is} value of $0.47 \mu\text{M}$ for the same ligand. The K_d value of **4k** was lower than the K_d of $9 \mu\text{M}$ for L-Hol:*MtHisD* binary complex formation obtained by ITC (23).

The van't Hoff equation (Equation 15) allowed determination of the individual contributions of ΔH° and $T\Delta S^\circ$ of the inhibitor's Gibbs free energy of binding from measurements of K_d as a function of temperature (Fig. 8) (29). The values obtained for ΔH° and ΔS° were $-18 \pm 16 \text{ kJ mol}^{-1}$ ($-4.278 \pm 0.037 \text{ kcal mol}^{-1}$), and $5.77 \pm 0.052 \times 10^2 \text{ kJ mol}^{-1} \text{ K}^{-1}$ ($0.0138 \pm 0.0001 \text{ kcal mol}^{-1} \text{ K}^{-1}$), respectively. The negative value (favorable) of ΔH° achieved for ligation of compound **4k** with free *MtHisD* showed the release of heat, in contrast to *MtHisD*:L-Hol ligation, which is unfavorable. In other words, it needs to absorb heat (positive value) to occur ($\Delta H^\circ = 3.6 \pm 0.5 \text{ kcal mol}^{-1}$ (23)). However, the positive ΔS° value (favorable) obtained was lower than the ΔS° of binding for *MtHisD*:L-Hol binary complex formation ($0.035 \pm 0.013 \text{ kcal mol}^{-1} \text{ K}^{-1}$ (23)). Estimates for ΔG° values were calculated employing Equation 16, yielding a value for ΔG° of $-35.1 \pm 4.9 \text{ kJ mol}^{-1}$ ($-8.3956 \pm 1.17 \text{ Kcal mol}^{-1}$) in the temperature range of $20 - 30^\circ\text{C}$. The favorable (negative) Gibbs free energy of binding demonstrates the spontaneous formation of the *MtHisD*:**4k** complex. Compared to the *MtHisD*:L-Hol binary complex ΔG° value of $-7 \pm 3 \text{ kcal mol}^{-1}$ (23), binding of **4k** compound to free *MtHisD* is more favorable than

the L-Hol substrate binding. This result is in accordance with the competitive inhibition of the L-Hol profile by compound **4k**.

The minimum inhibitory concentration is defined as the lowest drug concentration that prevents a color change in the REMA plate method (34). Determination of MIC results for compound **4e** demonstrated that 100 µg mL⁻¹ of the inhibitor molecule is needed to stop Mtb growth. In addition, compounds **4h** and **4k** showed MICs > 100 µg mL⁻¹. These results show that improvements in the molecule to increase its

inhibitory potential and/or its ability to penetrate Mtb are necessary.

Finally, our results represent, in our opinion, an important advance in understanding the mechanism of the chemical reaction catalyzed by MtHisD. We also believe that the results here presented are useful for the rational design of inhibitory molecules targeting MtHisD activity, which hopefully could be further developed into novel alternative therapeutics against tuberculosis.

Acknowledgments: This work was supported by Quatro G P&D Ltda., and FAPERGS/SEBRAE (FAPERGS n. 013/2011). Financial support was also provided by National Institute of Science and Technology on Tuberculosis (Decit/SCTIE/MS-MCT-CNPq-FNDCT-CAPES), FAPERGS (ARD/2012), and CNPq (Process number 478959/2013-3). D.S.S. (CNPq, 304051/1975-06), L.A.B. (CNPq, 5201182/99-5), and O.N.S. (CNPq, 305984/2012-8), are research career awardees of the National Council for Scientific and Technological Development of Brazil (CNPq). The fellowships from CNPq, CAPES, and FAPERGS are also acknowledged.

Conflict of interest: The authors declare that they have no conflicts of interest with the contents of this article.

Author Contributions: JL carried out the kinetics and inhibition experiments, and wrote the paper. LKBM contributed to the kinetics and inhibitions assays, and review of manuscript. DCR and JESN helped in part of inhibition experiments. LFSMT and ONS performed molecular docking. ADV carried out the MIC determination. ASR, KP, and JL performed the synthesis and characterization of the compounds. DSS devised the experiments. LAB and PM assisted in most of the experiments and contributed to the manuscript writing and reviewing. All authors analyzed the results and approved the final version of the manuscript.

References

1. World Health Organization. (2014) Global tuberculosis control: WHO report 2014, Geneva, Switzerland, WHO/HTM/TB/2014.08
2. Andries, K., Verhasselt, P., Guillemont, J., Gohlmann, H. W. H., Neefs, J.-M., Winkler, H., Van Gestel, J., Timmerman, P., Zhu, M., Lee, E., Williams, P., de Chaffoy, D., Huitric, E., Hoffner, S., Cambau, E., Truffot-Pernot, C., Lounis, N., Jarlier, V. (2005) A diarylquinoline drug active on the ATP synthase of *Mycobacterium tuberculosis*. *Science*. **307**, 223-227
3. De Jonge, M. R., Koymans, L. H. M., Guillemont, J. E. G., Koul, A., and Andries, K. (2007) A computational model of the inhibition of *Mycobacterium tuberculosis* ATPase by a new drug candidate R207910. *Proteins*. **67**, 971-980
4. Diacon, A. H., Pym, A., Grobusch, M., Patientia, R., Rustomjee, R., Page-Shipp, L., Pistorius, C., Krause, R., Bogoshi, M., Churchyard, G., Venter, A., Allen, J., Palomino, J. C., De Marez, T., van Heeswijk, R. P. G., Lounis, N., Meyvisch, P., Verbeeck, J., Parys, W., de Beule, K., Andries, K., and Mc Neeley, D.F. (2009) The diarylquinoline TMC207 for multidrug-resistant tuberculosis. *N Engl J Med*. **360**, 2397-2405
5. Avorn, J. (2013). Approval of a tuberculosis drug based on a paradoxical surrogate measure. *JAMA*. **309**, 1349-1350
6. Lunardi, J., Nunes, J. E. S., Bizarro, C. V., Basso, L. A., Santos, D. S., and Machado, P. (2013) Targeting the histidine pathway in *Mycobacterium tuberculosis*. *Curr Top Med Chem*. **13**, 2866-2884

7. Ames, B. N., Garry, B., and Herzenberg, L. A. (1960) The genetic control of the enzymes of histidine biosynthesis in *Salmonella typhimurium*. *J. Gen. Microbiol.* **22**, 369-378
8. Alifano, P., Fani, R., Liò, P., Lazcano, A., Bazzicalupo, M., Carlamagno, M. S., and Bruni, C. B. (1996) Histidine biosynthetic pathway and genes: structure, regulation, and evolution. *Microbial Rev.* **60**, 44-69
9. Stepansky, A., and Leustek, T. (2006) Histidine biosynthesis in plants. *Amino Acids*. **30**, 127-142
10. Dancer, J. E., Ford, M. J., Hamilton, K., Kilkelly, M., Lindell, S. D., O'Mahony, M. J., and Saville-Stones, E. A. (1996) Synthesis of potent inhibitors of histidinol dehydrogenase. *Bioorg Med Chem Lett.* **6**, 2131-2136
11. Gohda, K., Ohta, D., Iwasaki, G., Ertl, P., and Jacob, O. (2001) Computational modeling of a binding conformation of the intermediate L-histidinal to histidinol dehydrogenase. *J Chem Inf Comput Sci.* **41**, 196-201
12. Due, A. V., Kuper, J., Geerlof, A., von Kries, J. P., and Wilmanns, M. (2011) Bisubstrate specificity in histidine/tryptophan biosynthesis isomerase from *Mycobacterium tuberculosis* by active site metamorphosis. *Proc Natl Acad Sci USA.* **108**, 3554-3559
13. Adams, E. (1954) The Enzymatic synthesis of histidine from histidinol. *J Biol Chem.* **209**, 829-846
14. Adams, E. (1955) L-histidinal, a biosynthetic precursor of histidine. *J Biol Chem.* **217**, 325-344
15. Loper, J. C., and Adams, E. (1965) Purification and properties of histidinol dehydrogenase from *Salmonella typhimurium*. *J Biol Chem.* **240**, 788-795
16. Kohler, S., Foulongne, V., Ouahrani-Bettache, S., Bourg, G., Teyssier, J., Ramuz, M., and Liautard, J. (2002) The analysis of the intramacrophagic virulome of *Brucella suis* deciphers the environment encountered by the pathogen inside the macrophage host cell. *Proc Natl Acad Sci USA.* **99**, 15711-15716
17. Fields, P. I., Swanson, R. V., Haidaris, C. G., and Heffron, F. (1986) Mutants of *Salmonella typhimurium* that cannot survive within the macrophage are avirulent. *Proc Natl Acad Sci USA.* **83**, 5189-5193
18. Pilatz, S., Breitbach, K., Hein, N., Fehlhaber, B., Schulze, J., Brenneke, B., Eberl, L., and Steinmetz, I. (2006) Identification of *Burkholderia pseudomallei* genes required for the intracellular life cycle and *in vivo* virulence. *Infect Immun.* **74**, 3576-3586
19. Parish, T. (2003) Starvation survival response of *Mycobacterium tuberculosis*. *J Bacteriol.* **185**, 6702-6706
20. Sassetti, C. M., Boyd, D. H., and Rubin, E. J. (2003) Genes required for mycobacterial growth defined by high density mutagenesis. *Mol Microbiol.* **48**, 77-84
21. Aguero, F., Al-Lazikani, B., Aslett, M., Berriman, M., Buckner, F. S., Campbell, R. K., Carmona, S., Carruthers, I. M., Chan, A. W. E., Chen, F., Crowther, G. J., Doyle, M. A., Hertz-Fowler, C., Hopkins, A. L., McAllister, G., Nwaka, S., Overington, J. P., Pain, A., Paolini, G. V., Pieper, U., Ralph, S. A., Riechers, A., Roos, D. S., Sali, A., Shanmugam, D., Suzuki, T., Van Voorhis, W. C., and Verlinde, C. L. M. J. (2008) Genomic-scale prioritization of drug targets: the TDR Targets database. *Nat Rev Drug Discov.* **7**, 900-907
22. DeJesus, M. A., Zhang, Y. J., Sassetti, C. M., Rubin, E. J., Sacchettini, J. C., and Ioerger, T. R. (2013) Bayesian analysis of gene essentiality based on sequencing of transposon insertion libraries. *Bioinformatics.* **29**, 695-703
23. Nunes, J. E. S., Ducati, R. G., Breda, A., Rosado, L. A., de Souza, B. M., Palma, M. S., Santos, D. S., Basso, L. A. (2011) Molecular, kinetic, thermodynamic, and structural analyses of *Mycobacterium tuberculosis hisD*-encoded metal-dependent dimeric histidinol dehydrogenase (EC 1.1.1.23). *Arch Biochem Biophys.* **512**, 143-153
24. Abdo, M.-R., Joseph, P., Mortier, J., Turtaut, F., Montero, J.-L., Masereel, B., Kohler, S., and Winum, J.-Y. (2011) Anti-virulence strategy against *Brucella suis*: synthesis, biological evaluation and molecular modeling of selective histidinol dehydrogenase inhibitors. *Org Biomol Chem.* **9**, 3681-3690

25. Segel, I. H. (1993) *Enzyme Kinetics – Behavior Analysis of Rapd Equilibrium and Steady-state Enzyme Systems*. Wiley, Classics Library Edition, Wiley- interscience, John Wiley & Sons, Inc. Hoboken, NJ
26. Lonhienne, T., Baise, E., Feller, G., Bouriotis, V., Gerday, C. (2001) Enzyme activity determination on macromolecular substrates by isothermal titration calorimetry: application to mesophilic and psychrophilic chitinases. *Biochim Biophys Acta.* **1545**, 349-356
27. Cook, P. F. (1991) *Enzyme Mechanism from Isotope Effects*, CRC Press, Boca Raton, Florida
28. Abdo, M.-R., Joseph, P., Boigegrain, R.-A, Montero, J.-L., Kohler, S., and Winum, J.-Y. (2008) *Brucella suis* histidinol dehydrogenase: synthesis and inhibition studies of substituted N-L-histidinylphenylsulfonyl hydrazide. *J Enzyme Inhib Med Chem.* **23**, 357-361
29. Copeland, R. A. (2005) *Evaluation of Enzymes Inhibitors in Drug Discovery: A Guide for Medicinal Chemists and Pharmacologists*, 1st Ed., Wiley-interscience, John Wiley & Sons, Inc. Hoboken, NJ
30. Lineweaver, H., and Burk, D. (1934) The determination of enzymes dissociation constant. *J Am Chem Soc.* **56**, 658-666
31. Copeland, R. A. (2000) *Enzymes: A Practical Introduction to Structure, Mechanism, and Data Analysis*, 2nd Ed, Wiley-interscience, John Wiley & Sons, Inc. Hoboken, NJ
32. Morris, G. M., Huey, R., Lindstrom, W., Sanner, M. F., Belew, R. K., Goodsell, D. S., and Olson, A. J. (2009) AutoDock4 and AutoDockTools4: Automated docking with selective receptor flexibility. *J Comput Chem.* **30**, 2785-2791
33. Goodsell, D. S., Olson, A. J. (1990) Automated docking of substrates to proteins by simulated annealing. *Proteins.* **8**, 195-202
34. Palomino, J.-C., Martin, A., Camacho, M., Guerra, H., Swings, J., and Portaels, F. (2002) Resazurin Microtiter Assay Plate: simple and inexpensive method for detection of drug resistance in *Mycobacterium tuberculosis*. *Antimicrob Agents Chemother.* **46**, 2720-2722
35. Barbosa, J. A. R. G., Sivaraman, J., Li, Y., Larocque, R., Matte, A., Schrang, J. D., and Cygler, M. (2002) Mechanism of action and NAD⁺-binding mode revealed by the crystal structure of L-histidinol dehydrogenase. *Proc Nati Acad Sci USA.* **99**, 1859-1864
36. Adams, E. (1955) Synthesis and properties of an α -amino aldehyde, histidinal. *J Biol Chem.* **217**, 317-324
37. Gorish, H., and Holke, W. (1985) Binding of histidinal to histidinol dehydrogenase. *Eur J Biochem.* **150**, 305-308
38. Grubmeyer, C., Teng, H. (1999) Mechanism of *Salmonella typhimurium* histidinol dehydrogenase: kinetic isotope effects and pH profiles. *Biochemistry.* **38**, 7355-7362
39. Gallicchio, E., Kubo, M. M., and Levy, R. M. (1998) Entropy-enthalpy compensation in solvation and ligand binding revisited. *J. Am. Chem. Soc.* **120**, 4526-4527
40. Lonhienne, T., Gerday, C., Feller, G. (2000) Psychrophilic enzymes: revisiting the thermodynamic parameters of activation may explain local flexibility. *Biochim Biophys Acta.* **1543**, 1-10
41. Olsson, T. S. G., Ladbury, J. E., Pitt, W. R., and Williams, M. A. (2011) Extent of enthalpy entropy compensation in protein–ligand interactions. *Protein Sci.* **20**, 1607-1618
42. Cook, P.F., and Cleland, W. W. (2007) *Enzyme Kinetics and Mechanism*, Garland Science Publishing, NY
43. Vopel, T., Makhatadze, G. (2012) Enzyme activity in the crowded milieu. *PLoS One.* **7**, e39418
44. Grubmeyer, C. T., Insinga, S., Bhatia, M., and Moazami, N. (1989) *Salmonella typhimurium* histidinol dehydrogenase: complete reaction stereochemistry and active site mapping. *Biochemistry.* **28**, 8174-8180
45. Abdo, M.-R., Joseph, P., Boigegrain, R.-A, Liautard, J.-P., Montero, J.-L., Kohler, S., and Winum, J.-Y. (2007) *Brucella suis* histidinol dehydrogenase: synthesis and inhibition studies of a series of substituted benzylidic ketones derived from histidine. *Bioorg Med Chem.* **15**, 4427-4433
46. Schon, A., Lam, S. Y., and Freire, E. (2011) Thermodynamics-based drug design: strategies for inhibiting protein–protein interactions. *Future Med Chem.* **3**, 1129-1137

Footnotes

¹ The abbreviations used are: *Bs*HisD, histidinol dehydrogenase of the *Brucella suis*; *Ec*HisD, histidinol dehydrogenase of the *Escherichia coli*; H-bond, hydrogen bond; HisD, histidinol dehydrogenase enzyme; ITC, isothermal titration calorimetry; L-Hal, L-histidinal; L-His, L-histidine; L-Hol, L-histidinol; LGA, Lamarckian Genetic Algorithm; MDR-TB, multi drug-resistant tuberculosis; MIC, minimum inhibitory concentration; *Mtb*, *Mycobacterium tuberculosis*; MtHisD, histidinol dehydrogenase of the *Mycobacterium tuberculosis*; PRPP, phosphoribosyl pyrophosphate; REMA, resazurin microtiter assay; SKIE, solvent kinetic isotope effects; *S*HisD, histidinol dehydrogenase of the *Salmonella typhimurium*; TB, tuberculosis; WHO, World Health Organization; XDRT-TB, extensively drug-resistant tuberculosis

Scheme 1. Structure of the synthetized compounds.

Figure 1. Monophasic curve obtained in stopped-flow experiments, with single exponential enhancement in the absorbance at 340 nm upon conversion of NAD⁺ to NADH catalyzed by 10 μM MtHisD. The baseline represents the experiment control performed with 50 mM NAD⁺ in 50 mM PIPES pH 7.2. The inset highlights the curve at the time of 3 s.

Figure 2. Arrhenius plot for the temperature dependence of k_{cat} . The linearity of the maximum velocity versus temperature function (ranging from 15 to 40 °C) suggests that there is no change in the rate-limiting step.

Figure 3. Solvent kinetic isotope effects in (A) varying concentration of L-Hol (4 – 200 μM) and fixed-saturating concentration of NAD⁺ (200 mM) at pH 7.2 (inset at pH 9.0), in (B) varying concentration of NAD⁺ (1 – 20 mM) and fixed-saturating concentration of L-Hol (200 μM) at pH 7.2 (inset at pH 9.0). The lines represent fits to Equation 9. The values were obtained in either 0 (●) or 90 (■) atom % D₂O.

Figure 4. Proton inventory using saturating concentrations of both substrates and variable atom % D₂O in 50 mM PIPES pH 7.2. The inset shows the proton inventory in 50 mM Tris-HCl pH 9.0.

Figure 5. Determination of inhibition mode for selected compounds. (A) Represents **4e**, (B) **4h**, (C) **4g**, and (D) **4k**. The Lineweaver – Burk plots display lines that intersect at the y-axis, which are diagnostic of competitive inhibition for all compounds tested. Thus, the V_{max} value is constant at all inhibitor concentrations, but the apparent value of K_{M} increases with increasing inhibitor concentration. Each line represents a different inhibitor concentration fitted to Equation 14 in a double reciprocal plot of MtHisD specific activity by L-Hol substrate.

Figure 6. Representation of MtHisD – ligand interactions. (A) Docking simulations for the enzyme with **4e**, (B) **4h**, and (C) **4k**.

Figure 7. Fluorescence spectroscopy of the equilibrium binding of compound **4k** to MtHisD, plotting the relative fluorescence change as a function of **4k** concentration at 25 °C.

Figure 8. Dissociation constant as a function of temperature. The curve was fitted using the van't Hoff equation (Equation 15), and the ΔH°, and ΔS° terms could be estimated.

Tables**Table 1.** Solvent kinetic isotope effects for MtHisD.

Parameters	Isotope effect pH 7.2	Isotope effect pH 9.0
$V/K_{L\text{-Hol}}$	1.52 ± 0.32	0.61 ± 0.10
$V_{L\text{-Hol}}$	1.24 ± 0.06	1.39 ± 0.01
V/K_{NAD^+}	0.98 ± 0.04	0.60 ± 0.08
V_{NAD^+}	1.30 ± 0.02	1.44 ± 0.06

Table 2. Comparison of steady-state kinetics constants of MtHisD in molecular crowding.

Substrate	Ficoll (g L^{-1})	$K_M (\text{M})$	$k_{\text{cat}} (\text{s}^{-1})$	$k_{\text{cat}}/K_M (\text{Ms}^{-1})^{\text{a}}$
L-Hol	--	$20 (\pm 5) \times 10^{-6}$	1.436 ± 0.001	$7 (\pm 2) \times 10^4$
	100	$17 (\pm 1) \times 10^{-6}$	1.209 ± 0.027	$7.3 (\pm 0.6) \times 10^4$
	200	$22 (\pm 5) \times 10^{-6}$	1.209 ± 0.083	$6 (\pm 1) \times 10^4$
NAD^+	--	$2.9 (\pm 0.1) \times 10^{-3}$	1.361 ± 0.038	$4.7 (\pm 0.2) \times 10^2$
	100	$2.7 (\pm 0.1) \times 10^{-3}$	1.134 ± 0.007	$4.2 (\pm 0.1) \times 10^2$
	200	$3.3 (\pm 0.4) \times 10^{-3}$	0.227 ± 0.015	$69 (\pm 10)$

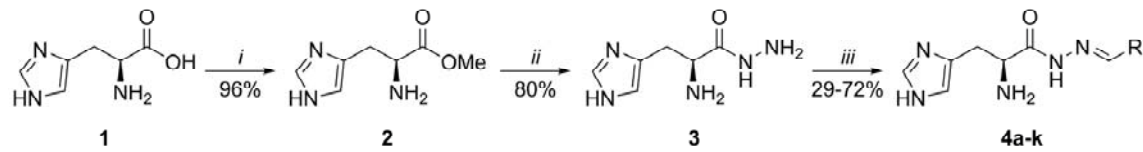
^a Specificity constant**Table 3.** The IC₅₀ values of the hydrazones derived from L-His.

Comp.	R	IC ₅₀ (μM)
4a	Ph	29 ± 3
4b	CH ₃ -4-C ₆ H ₄	5.5 ± 0.3
4c	Me ₂ N-4-C ₆ H ₄	9.1 ± 0.3
4d	MeO-4-C ₆ H ₄	5 ± 1
4e	Ph-4-O-Benzyl	9.8 ± 0.7
4f	HO-2-C ₆ H ₄	27 ± 2
4g	F-4-C ₆ H ₄	2.4 ± 0.8
4h	Cl-4-C ₆ H ₄	2.4 ± 0.4
4i	Br-4-C ₆ H ₄	7.7 ± 0.7
4j	O ₂ N-4-C ₆ H ₄	2.5 ± 0.2
4k	2-Naphthyl	1.1 ± 0.2

Table 4. Inhibition constants of select compounds.

Comp.	$K_{\text{is}} (\mu\text{M})$
4e	3.2 ± 0.6
4g	13 ± 2
4h	0.64 ± 0.07
4k	0.47 ± 0.06

Scheme 1



Comp.	R	Yield (%)
4a	Ph	40
4b	$\text{CH}_3\text{-}4\text{-C}_6\text{H}_4$	63
4c	$\text{Me}_2\text{N}\text{-}4\text{-C}_6\text{H}_4$	61
4d	$\text{MeO}\text{-}4\text{-C}_6\text{H}_4$	65
4e	Ph-4-O-Benzyl	72
4f	$\text{HO}\text{-}2\text{-C}_6\text{H}_4$	32
4g	F-4-C ₆ H ₄	50
4h	Cl-4-C ₆ H ₄	29
4i	Br-4-C ₆ H ₄	60
4j	$\text{O}_2\text{N}\text{-}4\text{-C}_6\text{H}_4$	69
4k	2-Naphthyl	34

Scheme 1. Reactants and conditions: *i*) = SOCl_2 , MeOH , 65°C , 16 h. *ii*) = (1) $\text{NH}_2\text{NH}_2\cdot\text{H}_2\text{O}$, MeOH , 65°C , 16 h; (2), 4-fluorobenzaldehyde, EtOH , 25°C , 1 h. *iii*) = Benzaldehyde, EtOH , 79°C , 4 h.

Figure 1

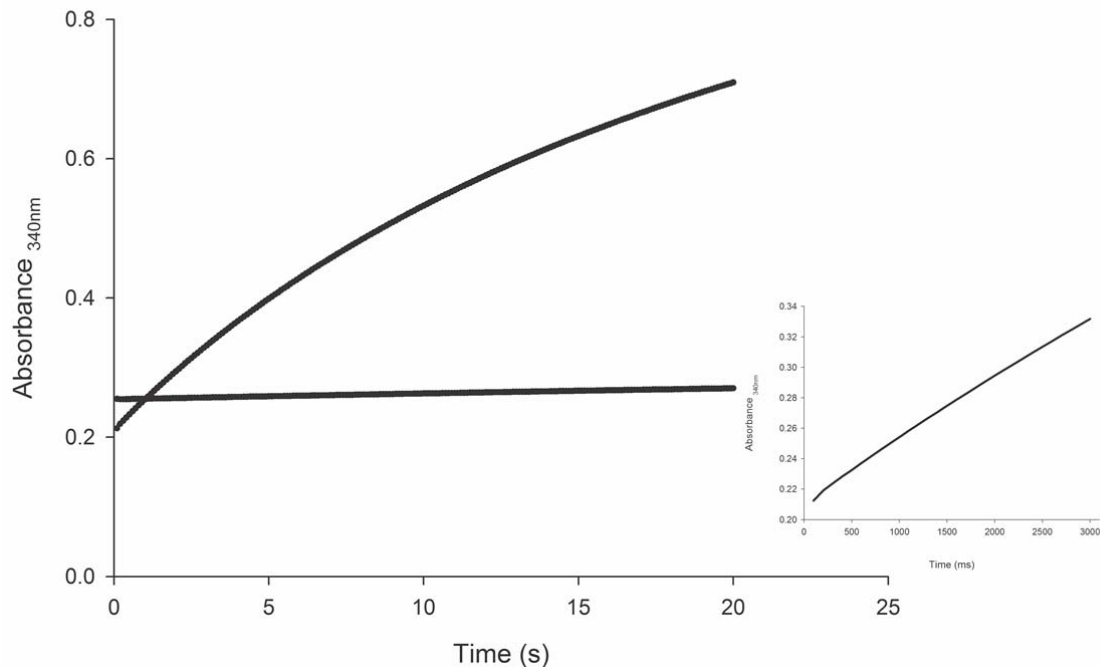


Figure 2

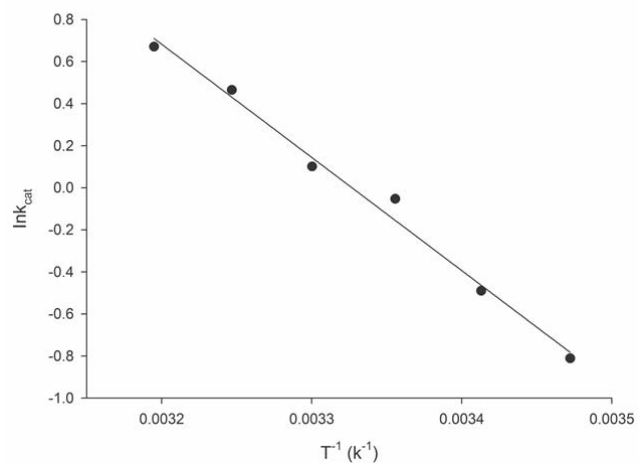


Figure 3

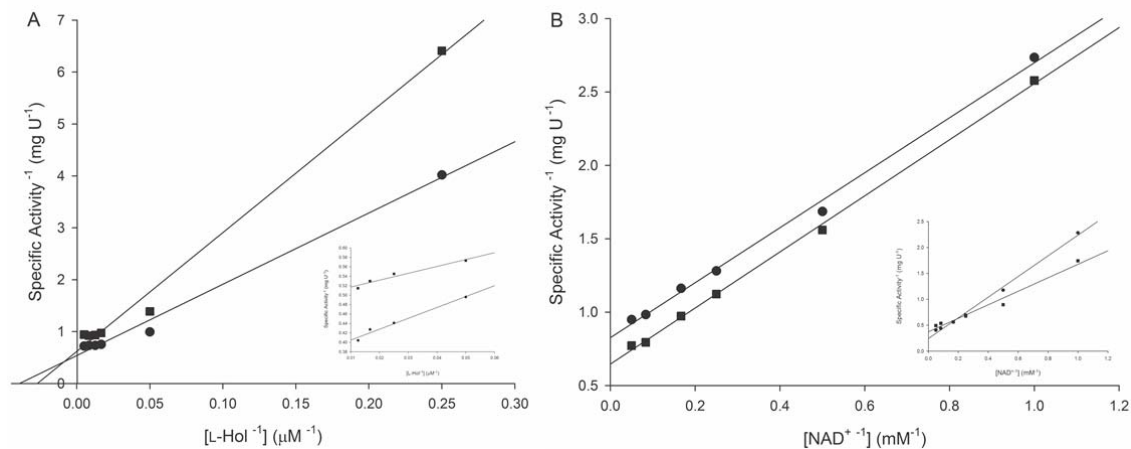


Figure 4

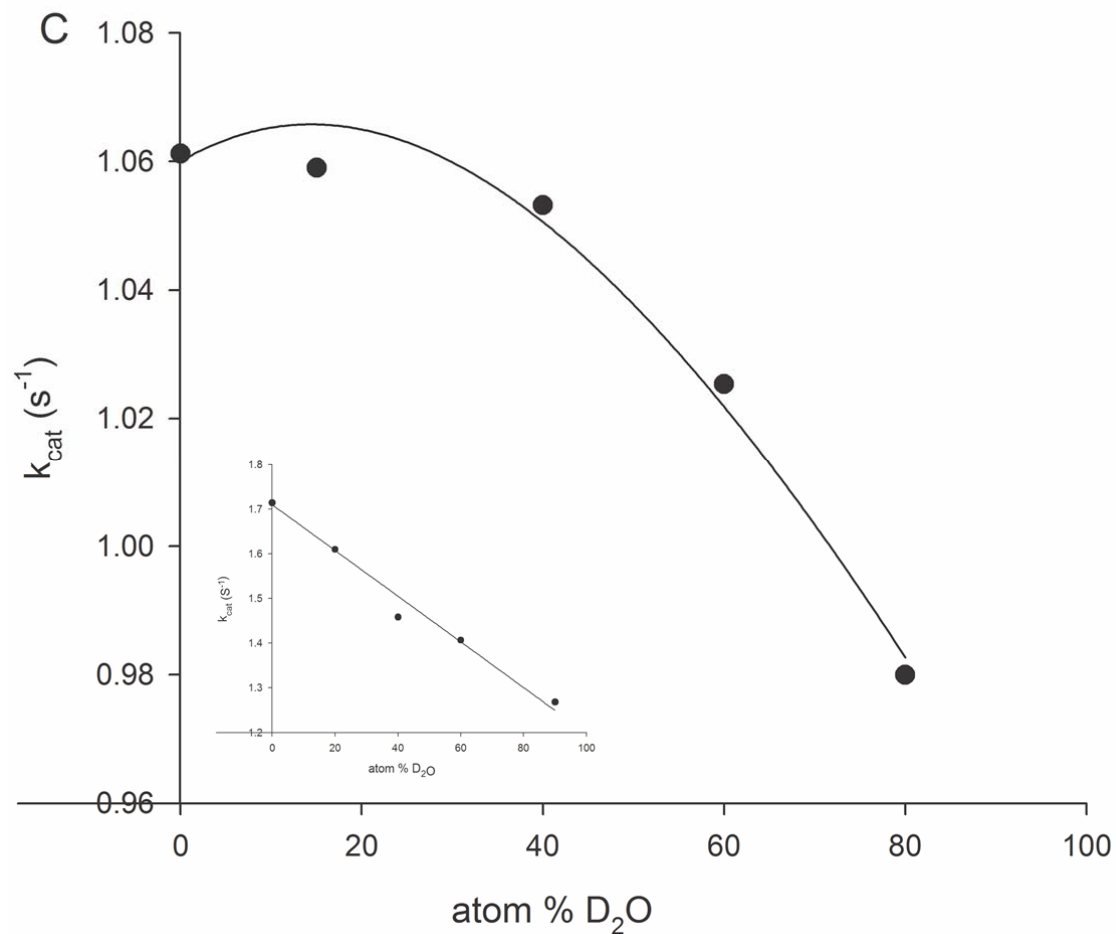


Figure 5

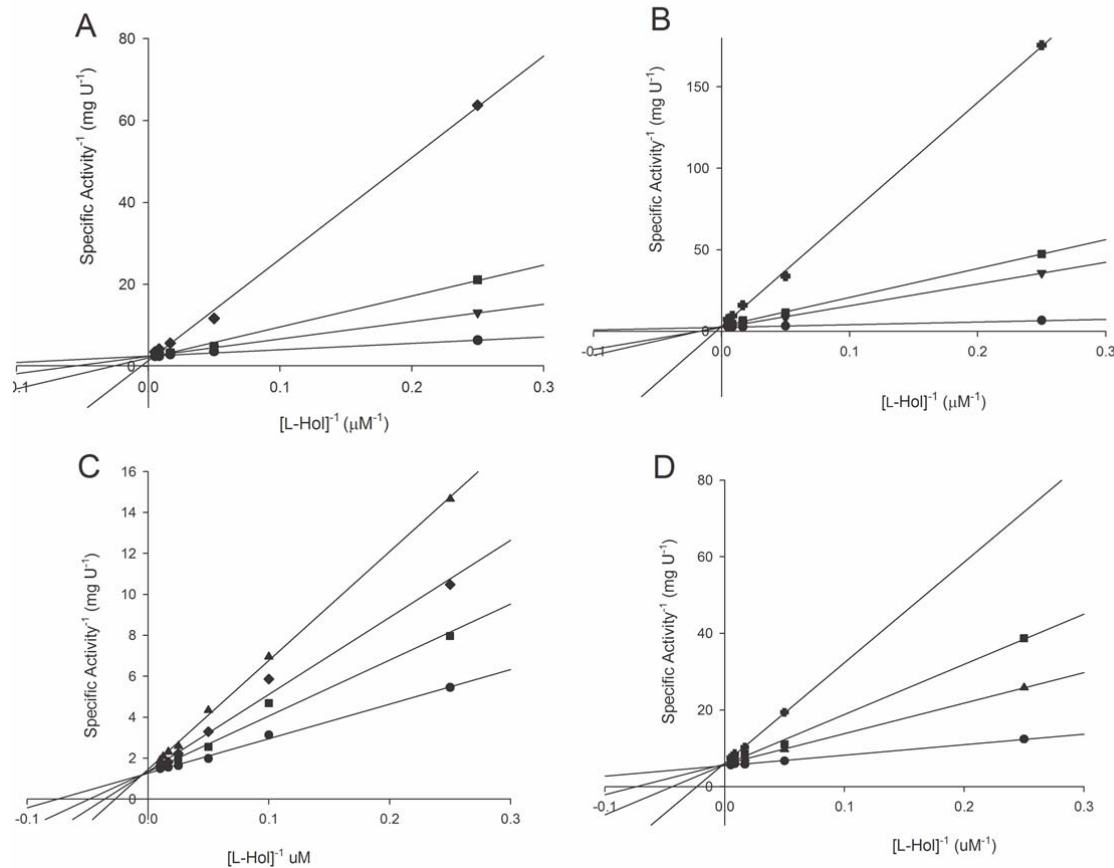


Figure 6

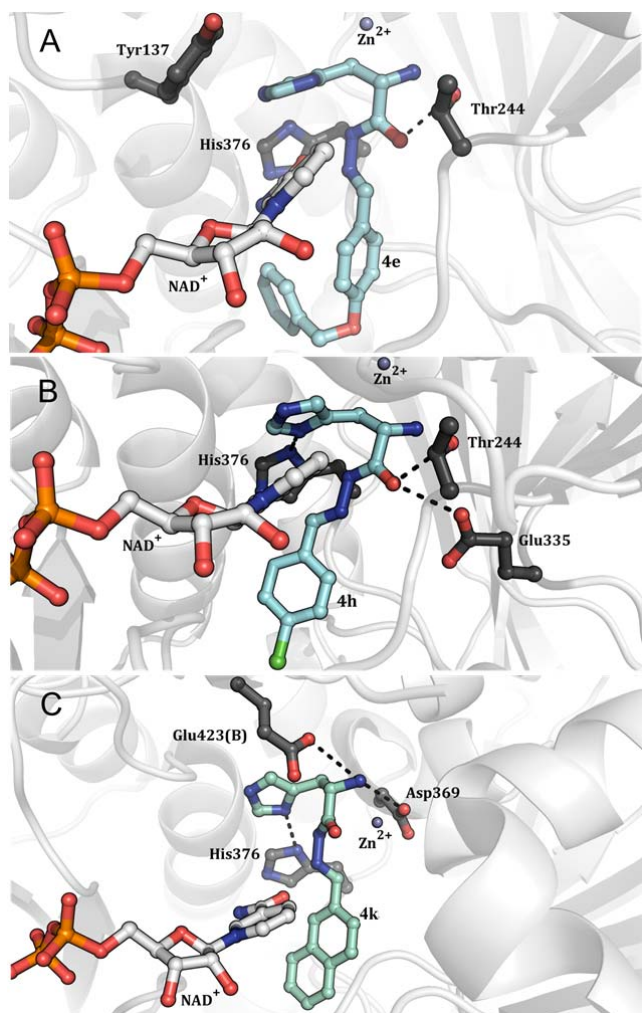


Figure 7

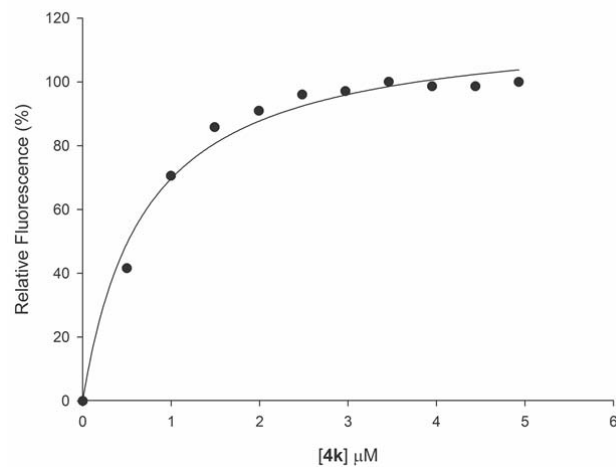
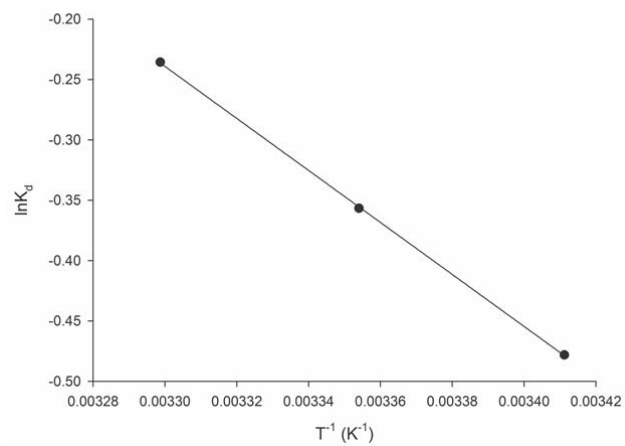


Figure 8



Supporting Information

***Mycobacterium tuberculosis* histidinol dehydrogenase: biochemical characterization and inhibition studies**

Juleane Lunardi , Leonardo Kras Borges Martinelli, Alessandra da Silva Raupp, José Eduardo Sacconi Nunes , Diana Carolina Rostirolla, Luís Fernando Saraiva Macedo Timmers, Anne Drumond Villela, Kenia Pissinate, Jones Limberger, Osmar Norberto de Souza, Diógenes Santiago Santos, Luiz Augusto Basso and Pablo Machado

Table of contents

- 1. Apparatus and analysis**
- 2. Procedure for the synthesis of L-histidine methyl ester dihydrochloride 2**
- 3. Procedure for the synthesis of (*S*)-2-amino-3-(1*H*-imidazol-4-yl)propanehydrazide 3**
- 4. General procedure for the synthesis of hydrazones 4**

1. Apparatus and analysis

All common reactants and solvents were used as obtained from commercial suppliers and used without further purification. Melting points were determined using a Microquímica MQAPF-302 apparatus. ^1H NMR spectra were acquired on an Anasazi EFT-60 spectrometer (^1H at 60.13 MHz) at 30 °C or on a Varian (Federal University of Rio Grande do Sul, UFRGS/Brazil) spectrometer (^1H at 400.13 MHz) at 25 °C. High-resolution mass spectra (HRMS) were obtained for all compounds on an LTQ Orbitrap Discovery mass spectrometer (Thermo Fisher Scientific, Bremen, Germany). This hybrid system combines the LTQ XL linear ion trap mass spectrometer with an Orbitrap mass analyzer. The experiments were performed using direct infusion of the sample in a solution of acetonitrile (50%), methanol (50%), and formic acid (0.1%), in positive-ion mode using electrospray ionization. Elemental composition calculations were performed using a specific tool included in the Qual Browser module of the Xcalibur (Thermo Fisher Scientific, release 2.0.7) software. Fourier transform infrared (FTIR) spectra were recorded using a universal attenuated total reflectance (UATR) attachment on a PerkinElmer Spectrum 100 spectrometer in the wavenumber range of 650-4000 cm^{-1} with a resolution of 4 cm^{-1} .

2. Procedure for the synthesis of L-histidine methyl ester dihydrochloride 2.

L-Histidine monohydrochloride monohydrate (2 mmol, 0.419 g) was reacted with a solution of thionyl chloride in CH_2Cl_2 (1 M, 10 mL) in refluxing methanol (15 mL) for 16 h. Subsequently, the solvent mixture was evaporated under reduced pressure. The solid obtained was washed with diethyl ether (3 x 15 mL). Finally, the solid was dried under reduced pressure. The product was used without further purification.

White powder; yield: 0.464 g (96%); m.p. 195-197 °C; ^1H NMR (60 MHz, DMSO-d₆): δ 3.36 (d, 2H, CH₂), 3.74 (s, 3H, OCH₃), 4.51 (t, 1H, CH), 7.57 (s, 1H, Im-H^{*}), 9.14 (s, 1H, Im-H^{*}), 10.83 (Br, 3H, NH, NH₂); IR (UATR) ν / cm^{-1} 1757 (C=O); HRMS (ESI) calcd for C₇H₁₁N₃O₂ + H: 170.0924, found: 170.0921 (M + H)⁺; Im-H^{*}: imidazole hydrogens.

*3. Procedure for the synthesis of (S)-2-amino-3-(1*H*-imidazol-4-yl)propanehydrazide 3.*

L-Histidine methyl ester dihydrochloride **2** (2.0 mmol, 0.338 g) was solubilized in dry methanol (10 mL). To this solution, hydrazine hydrate (4.1 mmol, 0.205 g) in dry methanol (5 mL) was added. After the addition, the reaction mixture was stirred for 16 h at 65 °C. Subsequently, the solvent was evaporated under reduced pressure and the oil obtained was dissolved with ethanol (15 mL). To this solution, 4-fluorobenzaldehyde (2.1 mmol, 0.260 g) was added and the reaction mixture was stirred for 1 h at 25 °C. The 4-(fluorobenzylidene)hydrazine was filtered off furnishing the analytically pure product **3**.

Yellow pale oil; yield: 0.271 g (80%); ^1H NMR (60 MHz, DMSO-d₆): δ 2.75-2.90 (m, 2H, CH₂), 3.67 (t, 1H, CH), 5.84 (Br, 6H, H-N), 6.86 (s, 1H, Im-H^{*}), 7.58 (s, 1H, Im-H^{*}); IR (UATR) ν / cm⁻¹ 1678 (C=O); HRMS (ESI) calcd for C₆H₁₁N₅O + H: 170.1036, found: 170.1028 (M + H)⁺; Im-H^{*}: imidazole hydrogens.

4. General procedure for the synthesis of hydrazones 4.

Benzaldehyde (1 mmol) was reacted with hydrazide **3** (1.0 mmol, 0.169 g) in refluxing ethanol (3 mL) for 4 h. After cooling to room temperature, the solvent was evaporated under reduced pressure. The obtained hydrazone was dissolved in dry CH₂Cl₂ (10 mL) and the mixture was washed with aqueous NaCl (5%, w/v, 2 x 8 mL) and saturated NaHCO₃ solution (2 x 8 mL). Finally, the organic layer was dried over anhydrous magnesium sulfate. The mixture was filtered, and the solvent was evaporated under reduced pressure. When necessary, the products were purified using silica gel chromatography or were recrystallized from hexane. All evaluated compounds were > 90% pure based on HPLC experiments. The stereochemistry of the double bond was assigned based on the observed imine proton chemical shifts [1]. It is noteworthy that some signals were duplicated in ^1H NMR spectra. This effect was attributed to tautomeric equilibria between protonated and deprotonated forms as basic or acid media restored the ^1H NMR spectra of the compounds to one set of signals.

3.1. (*S,E*)-2-amino-*N'*-benzylidene-3-(1*H*-imidazol-4-yl)propanehydrazide (**4a**)

White powder; yield: 0.103 g (40%); m.p. 207-209 °C; ¹H NMR (400 MHz, DMSO-d₆): δ 3.05-3.19 (m, 2H, CH₂), 4.16 (t, 0.5H, CH), 4.80 (t, 0.5H, CH), 6.97 (d, 1H, Im-H^{*}), 7.43-7.44 (m, 3H, Ar), 7.63 (s, 0.5H, Im-H^{*}), 7.67-7.68 (m, 2H, Ar), 8.09 (s, 0.5H, CH), 8.33 (s, 0.5H, CH); IR (UATR) v / cm⁻¹ 1686 (C=O); HRMS (ESI) calcd for C₁₃H₁₅N₅O + H: 258.1349, found: 258.1348 (M + H)⁺; Im-H^{*}: imidazole hydrogens.

3.2. (*S,E*)-2-amino-3-(1*H*-imidazol-4-yl)-*N'*-(4-methylbenzylidene)propanehydrazide (**4b**)

White powder; yield: 0.171 g (63%); m.p. 236-238 °C; ¹H NMR (400 MHz, DMSO-d₆): δ 2.37 (s, 1.5H, CH₃), 2.51 (s, 1.5H, CH₃), 3.03-3.20 (m, 2H, CH₂), 4.16 (t, 0.5H, CH), 4.80 (t, 0.5H, CH), 7.00 (d, 1H, Im-H^{*}), 7.26 (d, 2H, Ar), 7.59 (d, 2H, Ar), 7.74 (d, 1H, Im-H^{*}), 8.03 (s, 0.5H, CH), 8.26 (s, 0.5H, CH), 11.85 (br, 0.5H, NH); IR (UATR) v / cm⁻¹ 1679 (C=O); HRMS (ESI) calcd for C₁₄H₁₇N₅O + H: 272.1506, found: 272.1482 (M + H)⁺; Im-H^{*}: imidazole hydrogens.

3.3. (*S,E*)-2-amino-*N'*-(4-(dimethylamino)benzylidene)-3-(1*H*-imidazol-4-yl)propanehydrazide (**4c**)

Yellow powder; yield: 0.183 g (61%); m.p. 218-220 °C; ¹H NMR (400 MHz, DMSO-d₆): δ 2.97 (s, 6H, N(CH₃)₂), 3.05-3.20 (m, 2H, CH₂), 4.14 (t, 0.5H, CH), 4.76 (t, 0.5H, CH), 6.73 (d, 2H, Ar), 6.98 (d, 1H, Im-H^{*}), 7.50 (d, 2H, Ar), 7.68 (d, 1H, Im-H^{*}), 7.96 (s, 0.5H, CH), 8.16 (s, 0.5H, CH), 11.65 (br, 1H, NH); IR (UATR) v / cm⁻¹ 1683 (C=O); HRMS (ESI) calcd for C₁₅H₂₀N₆O + H: 301.1771, found: 301.1770 (M + H)⁺; Im-H^{*}: imidazole hydrogens.

3.4. (*S,E*)-2-amino-3-(1*H*-imidazol-4-yl)-*N'*-(4-methoxybenzylidene)propanehydrazide (**4d**)

White powder; yield: 0.187 g (65%); m.p. 214-216 °C; ¹H NMR (400 MHz, DMSO-d₆): δ 2.54-2.69 (m, 2H, CH₂), 3.30 (s, 3H, OCH₃), 3.65 (t, 0.5H, CH), 4.28 (t, 0.5H, CH), 6.46 (s, 0.5H, Im-H^{*}), 6.50 (d, 2H, Ar), 7.12-7.15 (m, 2H, Ar), 7.19 (s, 0.5H, Im-H^{*}), 7.53 (s, 0.5H, Im-H^{*}), 7.76 (s, 0.5H, Im-H); IR (UATR) v / cm⁻¹ 1685 (C=O); HRMS (ESI) calcd for C₁₄H₁₇N₅O₂ + H: 288.1455, found: 288.1433 (M + H)⁺; Im-H^{*}: imidazole hydrogens.

3.5. *(S,E)-2-amino-N'-(4-(benzyloxy)benzylidene)-3-(1H-imidazol-4-yl)propanehydrazide (4e)*

Yellow powder; yield: 0.261 g (72%); m.p. 215-217 °C; ^1H NMR (400 MHz, DMSO-d₆): δ 3.05-3.17 (m, 2H, CH₂), 4.14 (t, 0.5H, CH), 4.77 (t, 0.5H, CH), 5.15 (s, 2H, CH₂), 6.97 (d, 1H, Im-H^{*}), 7.07-7.09 (m, 2H, Ar), 7.32-7.46 (m, 5H, Ar), 7.63-7.64 (m, 2H, Ar), 7.68 (s, 0.5H, Im-H^{*}), 8.01 (s, 0.5H, CH), 8.24 (s, 0.5H, CH); IR (UATR) v / cm⁻¹ 1679 (C=O); HRMS (ESI) calcd for C₂₀H₂₁N₅O₂ + H: 364.1768, found: 364.1751 (M + H)⁺; Im-H^{*}: imidazole hydrogens.

3.6. *(S,E)-2-amino-N'-(2-hydroxybenzylidene)-3-(1H-imidazol-4-yl)propanehydrazide (4f)*

Yellow powder; yield: 0.087 g (32%); m.p. 202-204 °C; ^1H NMR (400 MHz, DMSO-d₆): δ 3.07-3.18 (m, 2H, CH₂), 4.17 (t, 0.5H, CH), 4.80 (t, 0.5H, CH), 6.99 (d, 1H, Im-H^{*}), 7.09-7.13 (m, 2H, Ar), 7.34-7.36 (m, 1H, Ar), 7.57-7.58 (m, 1H, Ar), 7.64 (d, 0.5H, Im-H^{*}), 8.15 (s, 0.5H, CH), 8.43 (s, 0.5H, CH); IR (UATR) v / cm⁻¹ 1693 (C=O); HRMS (ESI) calcd for C₁₃H₁₅N₅O₂ + H: 274.1299, found: 274.1277 (M + H)⁺; Im-H^{*}: imidazole hydrogens.

3.7. *(S,E)-2-amino-N'-(4-fluorobenzylidene)-3-(1H-imidazol-4-yl)propanehydrazide (4g)*

White powder; yield: 0.138 g (50%); m.p. 221-223 °C; ^1H NMR (400 MHz, DMSO-d₆): δ 3.05-3.18 (m, 2H, CH₂), 4.17 (t, 0.5H, CH), 4.80 (t, 0.5H, CH), 6.97 (d, 1H, Im-H^{*}), 7.27-7.29 (m, 2H, Ar), 7.66 (d, 1H, Im-H^{*}), 7.74-7.76 (m, 2H, Ar), 8.08 (s, 0.5H, CH), 8.33 (s, 0.5H, CH); IR (UATR) v / cm⁻¹ 1682 (C=O); HRMS (ESI) calcd for C₁₃H₁₄FN₅O + H: 276.1255, found: 276.1254 (M + H)⁺; Im-H^{*}: imidazole hydrogens.

3.8. *(S,E)-2-amino-N'-(4-chlorobenzylidene)-3-(1H-imidazol-4-yl)propanehydrazide (4h)*

White powder; yield: 0.085 g (29%); m.p. 228-230 °C; ^1H NMR (400 MHz, DMSO-d₆): δ 3.05-3.17 (m, 2H, CH₂), 4.17 (t, 0.5H, CH), 4.80 (t, 0.5H, CH), 6.97 (d, 1H, Im-H^{*}), 7.49-7.51 (m, 2H, Ar), 7.64 (s, 0.5H, Im-H^{*}), 7.69-7.73 (m, 2H, Ar), 8.07 (s, 0.5H, CH), 8.32 (s, 0.5H, CH); IR (UATR) v / cm⁻¹ 1680 (C=O); HRMS (ESI) calcd for C₁₃H₁₄ClN₅O + H: 292.0960, found: 292.0959 (M + H)⁺; Im-H^{*}: imidazole hydrogens.

3.9. (*S,E*)-2-amino-*N'*-(4-bromobenzylidene)-3-(1*H*-imidazol-4-yl)propanehydrazide (4i)

White powder; yield: 0.202 g (60%); m.p. 228-229 °C; ^1H NMR (400 MHz, DMSO-d₆): δ 3.08-3.17 (m, 2H, CH₂), 4.18 (t, 0.5H, CH), 4.81 (t, 0.5H, CH), 6.99 (d, 1H, Im-H^{*}), 7.65 (s, 4H, Ar), 7.71 (s, 0.5H, Im-H^{*}), 8.07 (s, 0.5H, CH), 8.32 (s, 0.5H, CH); IR (UATR) v / cm⁻¹ 1682 (C=O); HRMS (ESI) calcd for C₁₃H₁₄BrN₅O + H: 336.0454, found: 336.0437 (M + H)⁺; Im-H^{*}: imidazole hydrogens.

3.10. (*S,E*)-2-amino-3-(1*H*-imidazol-4-yl)-*N'*-(4-nitrobenzylidene)propanehydrazide (4j)

Yellow powder; yield: 0.209 g (69%); m.p. 219-221 °C (Dec.); ^1H NMR (400 MHz, DMSO-d₆): δ 3.05-3.13 (m, 2H, CH₂), 4.20 (t, 0.5H, CH), 4.85 (t, 0.5H, CH), 6.98 (d, 1H, Im-H^{*}), 7.66 (d, 1H, Im-H^{*}), 7.94 (d, 2H, Ar), 8.17 (s, 0.5H, CH), 8.27 (d, 2H, Ar), 8.45 (s, 0.5H, CH); IR (UATR) v / cm⁻¹ 1680 (C=O); HRMS (ESI) calcd for C₁₃H₁₄N₆O₃ + H: 303.1200, found: 303.1209 (M + H)⁺; Im-H^{*}: imidazole hydrogens.

3.11. (*S,E*)-2-amino-3-(1*H*-imidazol-4-yl)-*N'*-(naphthalen-2-ylmethylen)propanehydrazide (4k)

White powder; yield: 0.105 g (34%); m.p. 121-123 °C; ^1H NMR (400 MHz, DMSO-d₆): δ 3.15-3.26 (m, 2H, CH₂), 4.25 (t, 0.5H, CH), 4.90 (t, 0.5H, CH), 7.00 (d, 1H, Im-H^{*}), 7.56 (s, 2H, Ar), 7.67 (d, 1H, Im-H^{*}), 7.84 (s, 4H, Ar), 8.09-8.11 (m, 1H, Ar), 8.35 (s, 0.5H, CH), 8.61 (s, 0.5H, CH); IR (UATR) v / cm⁻¹ 1682 (C=O); HRMS (ESI) calcd for C₁₇H₁₇N₅O + H: 308.1506, found: 308.1492 (M + H)⁺; Im-H^{*}: imidazole hydrogens.

Reference:

- [1] Preisch, E., Bühlmann, P. and Affolter, C., *Structure determination of organic compounds: tables of spectral data*, Springer: 2000.

Capítulo 3

**“Targeting the Histidine Pathway in
Mycobacterium tuberculosis”**

Artigo de revisão publicado no
periódico *Current Topics in Medicinal
Chemistry*, 2013.

Targeting the Histidine Pathway in *Mycobacterium tuberculosis*

Juleane Lunardi^{1,2,3}, José Eduardo S. Nunes^{1,3}, Cristiano V. Bizarro^{1,2}, Luiz Augusto Basso^{1,2}, Diógenes Santiago Santos^{1,2,*} and Pablo Machado^{1,2,*}

¹Instituto Nacional de Ciéncia e Tecnologia em Tuberculose (INCT-TB), Centro de Pesquisas em Biologia Molecular e Funcional (CPBMF), Pontifícia Universidade Católica do Rio Grande do Sul (PUCRS), 90619-900, Porto Alegre, RS, Brazil; ²Programa de Pós-Graduação em Biologia Celular e Molecular (PPGBCM), Faculdade de Biociências, PUCRS, Porto Alegre, RS, Brazil. ³Quatro G Pesquisa & Desenvolvimento, 90619-900, Porto Alegre, RS, Brazil

Abstract: Worldwide, tuberculosis is the leading cause of morbidity and mortality due to a single bacterial pathogen, *Mycobacterium tuberculosis* (Mtb). The increasing prevalence of this disease, the emergence of multi-, extensively, and totally drug-resistant strains, complicated by co-infection with the human immunodeficiency virus, and the length of tuberculosis chemotherapy have led to an urgent and continued need for the development of new and more effective antitubercular drugs. Within this context, the L-histidine biosynthetic pathway, which converts 5-phosphoribosyl 1-pyrophosphate to L-histidine in ten enzymatic steps, has been reported as a promising target of antimicrobial agents. This pathway is found in bacteria, archaebacteria, lower eukaryotes, and plants but is absent in mammals, making these enzymes highly attractive targets for the drug design of new antimycobacterial compounds with selective toxicity. Moreover, the biosynthesis of L-histidine has been described as essential for Mtb growth *in vitro*. Accordingly, a comprehensive overview of *Mycobacterium tuberculosis* histidine pathway enzymes as attractive targets for the development of new antimycobacterial agents is provided, mainly summarizing the previously reported inhibition data for Mtb or orthologous proteins.

Keywords: Drug design, enzymatic inhibitors, antimycobacterial, L-histidine biosynthesis, molecular target, *Mycobacterium tuberculosis*.

INTRODUCTION

Human tuberculosis (TB) is a chronic infection that is primarily caused by *Mycobacterium tuberculosis* (Mtb). Despite more than half a century of chemotherapy, the disease is responsible for the deaths of more than 1.4 million people worldwide per year [1]. In 2011, the incident cases were estimated at 8.7 million, including 0.5 million women, making TB one of the top killers of women worldwide [1]. TB is considered the second leading cause of death from infectious disease, after human immunodeficiency virus (HIV). TB is also the leading cause of morbidity and mortality due to a single bacterial pathogen and has been treated by the World Health Organization (WHO) as a global public health emergency since 1993 [1-3]. Immunological tests have indicated that one-third of the global population is infected with a dormant or latent form of Mtb, with an associated risk of developing active TB as a consequence of infection reactivation. Indeed, in the latent TB infection the Mtb remain inactive for a lifetime without causing disease and can become active in people who have debilitated immune systems. Therefore, immunocompromised, HIV-positive individuals have an increased risk of developing so-called reactivation TB from latent infections [4], as do patients receiving an anti-tumor necrosis factor therapy [5], and also

individuals with diabetes [6]. Isoniazid has been used for the treatment of latent TB infection in persons at greatest risk of disease progression [7-9]. However, there are significant limitations to this intervention, and new drugs to improve the treatment have been deemed essential to the elimination of tuberculosis [10].

The management of TB has faced another challenge in recent years with the occurrence of multi-drug-resistant (MDR-TB), extensively drug-resistant (XDR-TB), and totally drug-resistant (TDR-TB) strains, increasing the difficulty, duration, and cost of treatment and the morbidity of the disease [11, 12]. Resistance can develop as a result of primary contact with a resistant strain (primary resistance) or during the course of treatment owing to selective pressure in favor of resistant mutants. At a minimum, MDR-TB strains are resistant to isoniazid and rifampicin, the most important drugs used in the treatment of TB [11]. XDR-TB is a form that is resistant to isoniazid and rifampicin, any fluoroquinolone, and any of the second-line injectable drugs (amikacin, kanamycin, or capreomycin) [11]; these strains do not respond to the standard six-month treatment with first-line anti-TB drugs. According to WHO, an intensive phase of 8 months of medication and a total duration of 20 months of treatment is recommended to treat the disease caused by resistant strains [13]. Therefore, the need for new drugs to treat TB is an urgent issue. Recently, studies with diarylquinolines (DARQs), a new class of potent inhibitors of Mtb ATP synthase [14-18], led the U.S. Food and Drug Administration (FDA) to approve SIRTURO™ (bedaquiline), a DARQ an-

*Address correspondence to these authors at the Instituto Nacional de Ciéncia e Tecnologia em Tuberculose (INCT-TB), Centro de Pesquisas em Biologia Molecular e Funcional (CPBMF), Pontifícia Universidade Católica do Rio Grande do Sul (PUCRS), 90619-900, Porto Alegre, RS, Brazil; Tel/Fax: +55-51-33203629; E-mail: diogenes@pucrs.br; pablo.machado@pucrs.br

timycobacterial drug, as a component of combination therapy to treat adults with multi-drug resistant pulmonary tuberculosis when other alternatives are not available [19]. This indication was based on the analysis of time to sputum culture conversion from two controlled Phase 2 trials in patients with pulmonary MDR-TB [18]. The discovery was a very important step in the search for new treatment options for tuberculosis, as bedaquiline was the first new anti-tuberculosis drug developed since the 1960s. Ideally, a new drug to treat TB should be effective against MDR and XDR strains, be able to eliminate latent forms of the bacillus, shorten the treatment course, thus simplifying the medication by reducing the pill burden, reduce the number of daily doses, and not produce important drug interactions with anti-HIV medications [20].

The complete genome sequencing of *MtbH37Rv* [21] has allowed the identification of potential molecular targets for drug development. The identification, selection, and evaluation of new drug targets, together with the druggability and assayability, are important aspects to consider in the drug discovery process [22], as such knowledge allows the design of chemical structures based on the structure of targets (structure-based drug design) and/or ligands (ligand-based drug design). Nevertheless, in the post-genomic era, the rate of target innovation has remained low and constant, with an average in the last 20 years of 5.3 first-against-target drugs per year [23]. New macromolecular targets may lead to the development of new drugs with innovative mechanisms of action, endowed with selective toxicity, and active against resistant strains of *Mtb*.

Within this context, the proteins that function in the L-histidine biosynthetic pathway emerge as novel attractive targets for the design of new compounds to treat TB. The L-histidine pathway comprises ten enzymatic steps that include complex and non-trivial reactions to convert phosphoribosyl pyrophosphate (PRPP) and ATP to L-histidine, (Scheme 1). The pathway is present in prokaryotic organisms, lower eukaryotic organisms, and plants but is absent in mammals [24–26]. Consequently, the enzymes that constitute this biosynthetic pathway are potential targets for new antimicrobial drugs and herbicides based on the principle of selective toxicity. The importance of the histidine biosynthetic pathway has also been shown by Aguero *et al.* [27], whose report a ranked list of 50 *Mtb* targets, taking into account such aspects as enzymes with a solved structure or structure model, essentiality in any species but not having a human ortholog, and expression during latency or dormancy. The enzymes phosphoribosyl-AMP pyrophosphatase (HisG), imidazole glycerol-phosphate dehydratase (HisB), and histidinol dehydrogenase (HisD) appear in this list.

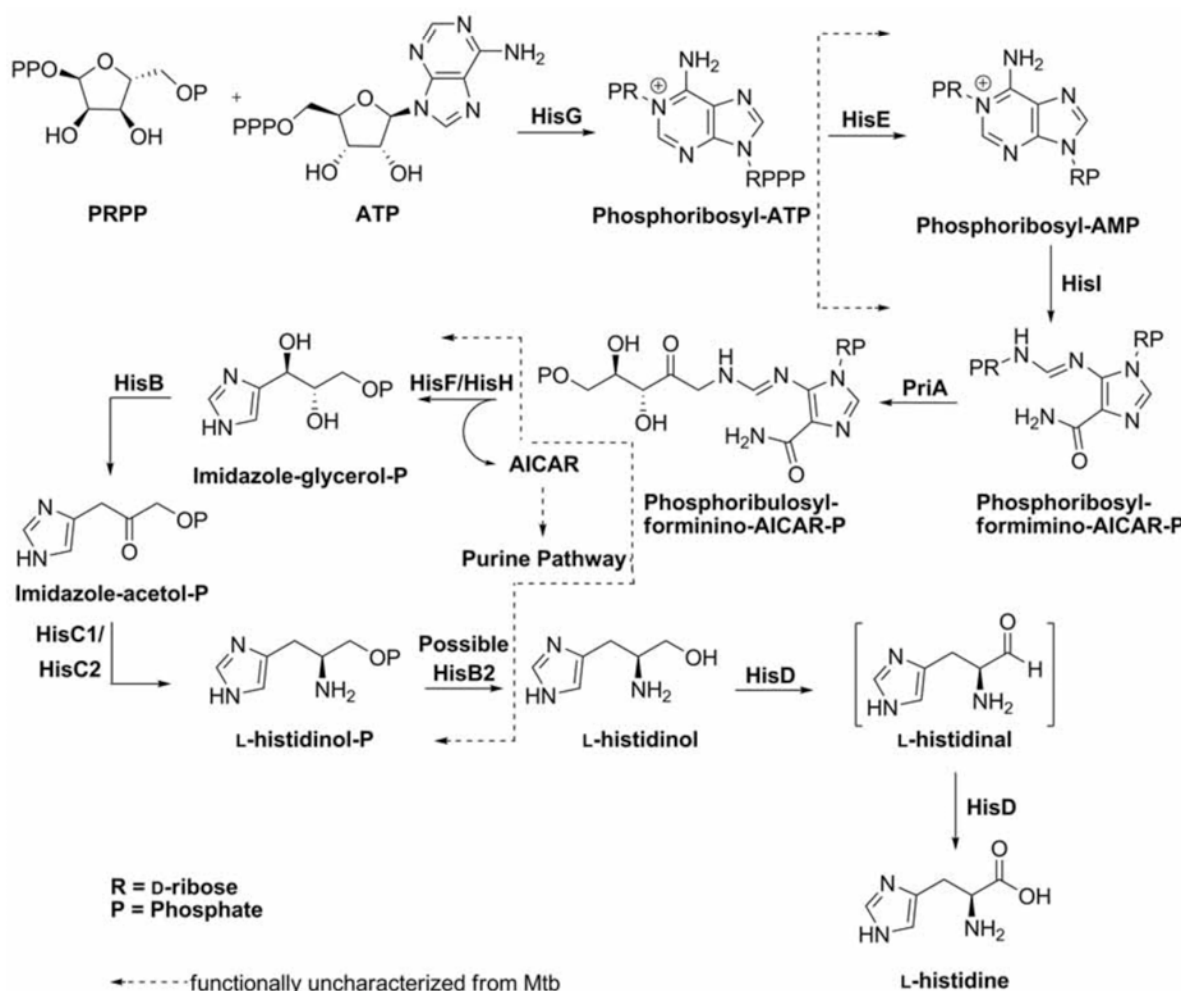
The essentiality of a gene product is a necessary attribute of a molecular target selection for drug development. For instance, molecular genetic screenings have been undertaken to systematically identify essential genes in the *Mtb* genome. Several genes coding for enzymes from the histidine biosynthesis pathway were found to be essential for *Mtb* survival in a *Himar1*-based transposon mutagenesis study [28]. The genes *priA* (*Rv1603*), *hisB* (*Rv1601*), *hisC1* (*Rv1600*), *hisD* (*Rv1599*), *hisF* (*Rv1605*), *hisG* (*Rv2121c*), *hisH* (*Rv1602*), *hisE* (*Rv2122c*), and *hisI* (*Rv1606*) were classified as “required for optimal growth”, whereas *hisC2* (*Rv3772*) was the

only gene coding for a histidine biosynthetic enzyme classified as “non-essential”. Based on a deep sequencing approach using next-generation sequencers, the genomic location of transposon insertions in individual *Mtb* mutants were recently mapped with high accuracy [29]. The essential nature of the genes in *Mtb* culture was then reassessed using these high-quality data with a novel statistical analysis method [30]. Interestingly, 185 of the 614 genes previously considered as essential [28] were predicted by this new approach to be non-essential (81), uncertain (75), or were classified in a “no-data” category (29). The indispensability of the *hisF* gene was re-examined, and this sequence is now considered “uncertain” in terms of essentiality, whereas *hisE* is considered too short to have a statistically relevant classification.

However, data from gene essentiality studies should be considered carefully when selecting molecular targets for further research. Indeed, it was found that a L-histidine auxotroph, an *Mtb* mutant strain with deletion of a central 0.7-kb fragment of *hisDC*, was unable to survive single-amino acid starvation for more than 8 weeks but behaved similar to wild-type strains when subjected to complete starvation, surviving for more than 14 weeks in a medium containing only sterile distilled water [31]. Presumably, under complete starvation conditions, the bacteria entered a state of persistence in which *de novo* L-histidine biosynthesis is not essential as it is under standard culture conditions depleted of L-histidine. These results emphasize that gene essentiality information should be always considered within the context of the particular conditions in which the experiments were performed. Further developments in animal models for latent tuberculosis and the analysis of gene knockout strains using these models will provide important clues regarding the essentiality of L-histidine biosynthesis enzymes in latency or dormancy.

In addition, it is also worth considering the repertoire of amino acid transporters presented by *Mtb* cells. If invading bacteria are able to acquire L-histidine from the host cell in enough quantities to supply its physiological requirements, then the L-histidine biosynthetic enzymes would presumably be dispensable in *Mtb* pathogenesis, and therefore irrelevant as targets for drug development. Although there is no specific L-histidine transporter described for *Mtb*, the genomic data available was considered, as well as classical permeability and culture experiments, in order to appreciate what is currently known about L-histidine acquisition from the host by *Mtb* cells.

The L-histidine biosynthetic pathway has been elucidated in detail in *Salmonella typhimurium* and *Escherichia coli* [32]. Although there is a tendency to assume that essential pathways are universally conserved, it remains unclear whether this information can be generalized between structurally and metabolically distinct organisms [28]. Indeed, *Mtb* shows differences in gene organization and functionality compared to organisms for which L-histidine biosynthesis has been better characterized. Therefore, investigation of this pathway can also shed light on concepts of enzyme evolution. Furthermore, the three-dimensional structures of only three *Mtb* L-histidine-pathway-enzymes phosphoribosyl isomerase A (*PriA*), pyrophosphoribosyl-ATP pyrophosphohydrolase (*HisE*) and phosphoribosyl-AMP pyrophosphatase



Scheme 1. The ten catalyzed steps of the L-histidine biosynthetic pathway.

(HisG) have been elucidated [33–35]. However, the availability of three-dimensional structures is a powerful tool for the drug discovery process. It is noteworthy that more than 90% of the targets for all approved drugs present a structure that is similar to a known protein in the Protein Data Bank (PDB), highlighting the importance of structure determination [23].

Therefore, the present review aims to demonstrate the potential of targeting the Mtb L-histidine biosynthetic pathway in the design of novel drug-like compounds endowed with effective antimycobacterial activity. To this end, the essentiality, assayability, druggability, and chemical mechanism of gene products, when available, is described. Within this context, reported enzyme inhibitors of the Mtb L-histidine pathway and also for related orthologous proteins are presented as important evidence of the druggability and assayability of these targets, in addition to serving as the structural template for future medicinal chemistry programs. Additionally, the analysis of the chemical mechanisms of the catalyzed reactions allows the inference of reaction intermediates that are energetically close to the active complex structures. Indeed, analog compounds for the transition state of enzymatically favorable reactions have been reported to be among the most potent inhibitors known [36].

HisG (Rv2121c)

(Other designations: ATP phosphoribosyltransferase, N-1-(5'-phosphoribosyl)-ATP).

Encoded by the *hisG* gene (MTB Rv2121c, 855 bp, 284 aa, 30480.8 Da, and isoelectric point (pI) = 4.71), HisG catalyzes the first step in the metabolic pathway of L-histidine biosynthesis. HisG promotes the nucleophilic substitution of 5-phosphoribosyl-1-pyrophosphate (PRPP) with ATP in the presence of Mg²⁺ ion, producing phosphoribosyl ATP and inorganic pyrophosphate (PPi), (Scheme 1). This enzyme plays a critical regulatory role in the biosynthesis of L-histidine, as it regulates the pathway through a negative feedback mechanism via allosteric inhibition by the product L-histidine [25].

As with other gene products of this biosynthetic pathway, HisG shows potential as a drug target for combating tuberculosis because it was found to be essential for the growth of strain MtbH37Rv *in vitro* in *Himar1*-based transposon experiments [24–26]. However, it is noteworthy that formal proof of the essentiality of the gene still needs to be provided, as knockout experiments for the *Mycobacterium tuberculosis* HisG (*MtHisG*) gene have not yet been reported. Recently, gene disruption and complementation experiments

showed that *Corynebacterium glutamicum* HisG (*CgHisG*) is essential for L-histidine metabolism in minimal medium [37]. This function was tested using a *hisG*-null *C. glutamicum* mutant that failed to grow on minimal medium and was restored when supplemented with L-histidine.

The structure of *MtHisG* in the apo form (PDB accession code 1NH7) has been reported based on the single-crystal X-ray diffraction [33]. Moreover, the protein structure containing AMP and L-histidine inhibitors (Fig. 1) was also described (PDB accession 1NH8) [33], and the structural bases of the interaction mode of the substrates and allosteric regulation mechanism as a function of available L-histidine have been inferred from these data. The molecular arrangement of *MtHisG* is distinct from other phosphoribosyltransferase family members, constituting a unique type IV PRTase fold. The protein contains 10 α -helices and 15 β -strands in three continuous domains. The *N*-terminal domains (I and II) contain the catalytic residues of *MtHisG*, with highly negative electrostatic potential residues that are presumably involved in binding the Mg²⁺ ion [33]. The conserved residues attributed to ATP binding are contained in domain I, and the PRPP binding site is in domain II (residues 149–161). AMP, an inhibitor of *MtHisG* catalytic activity, binds in a cleft between the two domains, with most of the non-covalent interactions occurring with residues from domain II [33]. The binding site of allosteric inhibitor L-histidine was observed far from the active site, at approximately 40 Å, in C-terminal domain III [33]. According to the solved structure, Asp218 and Thr238 form polar contacts with α -amino groups, whereas Ala273 interacts with the imidazole ring of L-histidine (Fig. 1). The residues Leu234 and Leu253 were observed to form the remainder of the non-covalent hydrogen bond network (Fig. 1) [33]. Upon the binding of L-histidine, the protein is obtained as a hexamer, with either altered topology or reduced access to the active site. Accordingly, it has been reported that L-histidine and its analog 1,2,4-triazole-3-alanine inhibit *Arabidopsis thaliana* HisG (*AtHisG*), with IC₅₀ values of 45 μ M and 650 μ M, respectively [38]. The inhibitory activity of L-histidine has been

also described for *Salmonella typhimurium* HisG (*StHisG*) and *Lactococcus lactis* HisG (*LlHisG*), with K_i values of 70 μ M and 81 μ M, respectively [39, 40]. Recently, site-direct mutagenesis experiments revealed that four residues (Asn215, Leu231, Thr235, and Ala270) from domain III of *CgHisG* are involved in L-histidine binding [37]. Binding to these residues the L-histidine showed a K_i value of 110 μ M [37]. These data underscore the allosteric L-histidine site of *MtHisG* as a promising structure-based drug target; inhibition by L-histidine, within the context of this biosynthetic pathway, should be studied further.

Other than by allosteric inhibition, few compounds have been described in the literature as inhibiting HisG from Mtb or from orthologous proteins. AMP and ADP have been reported as competitive inhibitors of *StHisG* and showed improved inhibitory activities in the presence of L-histidine [41, 42]. For *Escherichia coli* HisG (*EcHisG*), the phenolic compounds pentachlorophenol and dicoumarol have exhibited moderate activity, with K_i values of 50 μ M and 60 μ M, respectively [43]. In another study, the inhibitory activity of dinitrophenol on *EcHisG* was described, showing an IC₅₀ of 400 μ M [44]. Pentachlorophenol, dicoumarol, and dinitrophenol act as competitive inhibitors related to ATP in the *EcHisG* reaction. An interesting finding was the activity of naphthylamine derivative **1** that was able to inhibit the activity of *AtHisG*, with an IC₅₀ of 50 nM (Fig. 2) [45]. Another scaffold proposed is compound **2**, which inhibited 92% of the *AtHisG* activity at 100 μ M (Fig. 2); it was suggested that the amino-triazolopyrimidine ring present in **2** occupies the adenine binding site for ATP and that the 4-chlorophenyl group is positioned at the ribose binding site for PRPP in *AtHisG* [45].

Cho *et al.* [46] reported the discovery of *MtHisG* inhibitors using a virtual screening approach, obtaining 11 compounds with IC₅₀ values presumably in the μ M range. The most potent compounds **3–6** were showed between 46% and 76% *MtHisG* inhibitory activity at a final concentration of 10 μ M (Fig. 3).

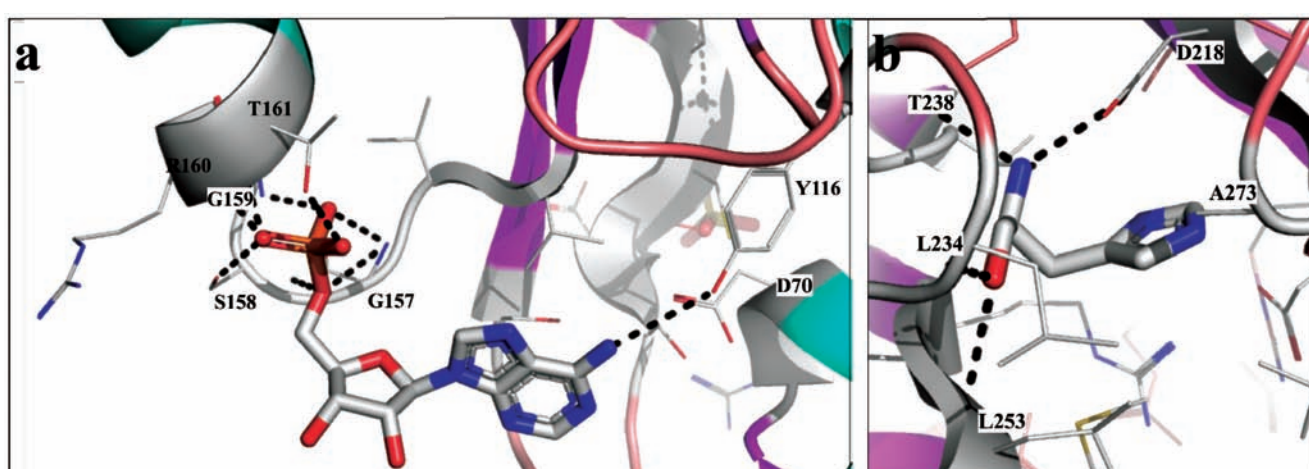


Fig. (1). *MtHisG* and its amino acid residues involved in the binding of ligands AMP and L-histidine. **a)** AMP in the active site and possible PRPP binding region. **b)** Binding of L-histidine in the allosteric site. Hydrogen bonds between each ligand and *MtHisG* residues are represented with dashed lines.

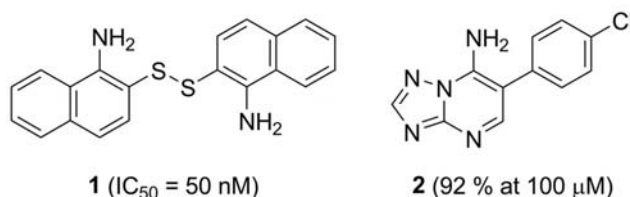


Fig. (2). Inhibitors of *AtHisG*.

The compounds **3** and **4** showed 76% and 71% of inhibition, respectively, at 10 μ M. Compounds **5** (71% at 10 μ M) and **6** (46% at 10 μ M) were also tested for their capacity of inhibition on the growth of *Mycobacterium smegmatis*; compound **5** showed weak inhibitory activity, whereas compound **6** resulted in 100% inhibition at 25 μ g/mL. Unfortunately, the MIC values were not reported. It is important to mention the difference in the predicted partition coefficient between compounds **5** and **6**: compound **6** exhibited LogP of 4.88, and compound **5** presented LogP of 3.85 [46]. The increased hydrophobicity could explain better *in vitro* activity of **6** against mycobacterial growth. However, further studies are necessary to clarify this point.

HisE and HisI (Rv2122c and Rv1606, Respectively)

(Other designations: pyrophosphoribosyl-ATP pyrophosphohydrolase, PR-ATP PH, pyrophosphoribosyl AMP cyclohydrolase, PR-AMP CH, hisIE, HIS4)

The products of the genes *hisE* (MTB Rv2122c, 282 bp, 93 aa, 10242.5 Da, pI = 4.38) and *hisI* (MTB Rv1606, 348 bp, 115 aa, 12464.9 Da, pI = 5.10), HisE and HisI, are responsible for the second and third steps, respectively, in L-histidine biosynthesis. HisE catalyzes the Mg²⁺ ion-dependent hydrolysis of the α-β-phosphodiester bond of pyrophosphoribosyl-ATP (PR-ATP) to produce pyrophospho-

ribosyl-AMP (PR-AMP); HisI catalyzes the unusual hydrolysis of the purine ring of PR-AMP between N1 and C6, generating phosphoribosyl-formimino-AICAR-phosphate (ProFAR). The purine ring opening is mediated by the nucleophilic attack of a metal (Zn^{2+})-activated H_2O molecule at C6, after electron reorganization, forming the amide group and imidazole ring of ProFAR via the formation of a tetrahedral intermediate, as shown in (Scheme 2). The stereochemistry of this intermediate has not been verified. In addition, has been reported that the intermediate is stabilized by the presence of a histidine residue that acts in a classical acid-basic proton transfer [47].

The organization of the *hisE* and *hisI* genes among organisms varies greatly, as the enzymes are monofunctional (Archaea and actinomycetes) [34, 47-49], bifunctional, fused to the *hisI* gene (plants and Eubacteria) [50-52], and multi-functional (yeast) [53-55].

In *Mtb*, two separate genes have been described as encoding HisE and HisI, though the complete functional characterization has not been reported. Together with *hisG*, the *hisE* gene is encoded in a different operon (Rv2121c–Rv2122c) in relation to the other genes of the L-histidine biosynthesis pathway. The crystal structure of *Mycobacterium tuberculosis* HisE (*MtHisE*) in two apo forms have been solved from diffractometry experiments [34] (PDB accession codes 1Y6X and 3C90), establishing that the enzyme belongs to the α -helical NTP pyrophosphatase superfamily and is composed entirely of α -helices and connecting loops (Fig. 4). The protein has a dimeric quaternary structure, with one probable active site in each monomer. An Mg^{2+} EXXE binding motif was suggested by homology with other enzymes from the family, though no electron density compatible with a magnesium ion could be clearly identified. Furthermore, no substrate cavity was proposed because the direct soaking of crystals and cocrystallization with ATP

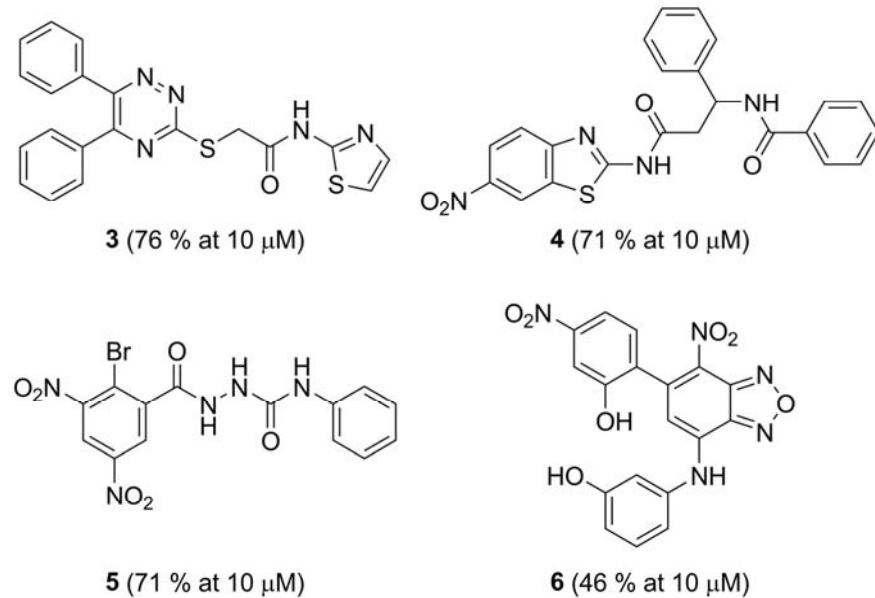
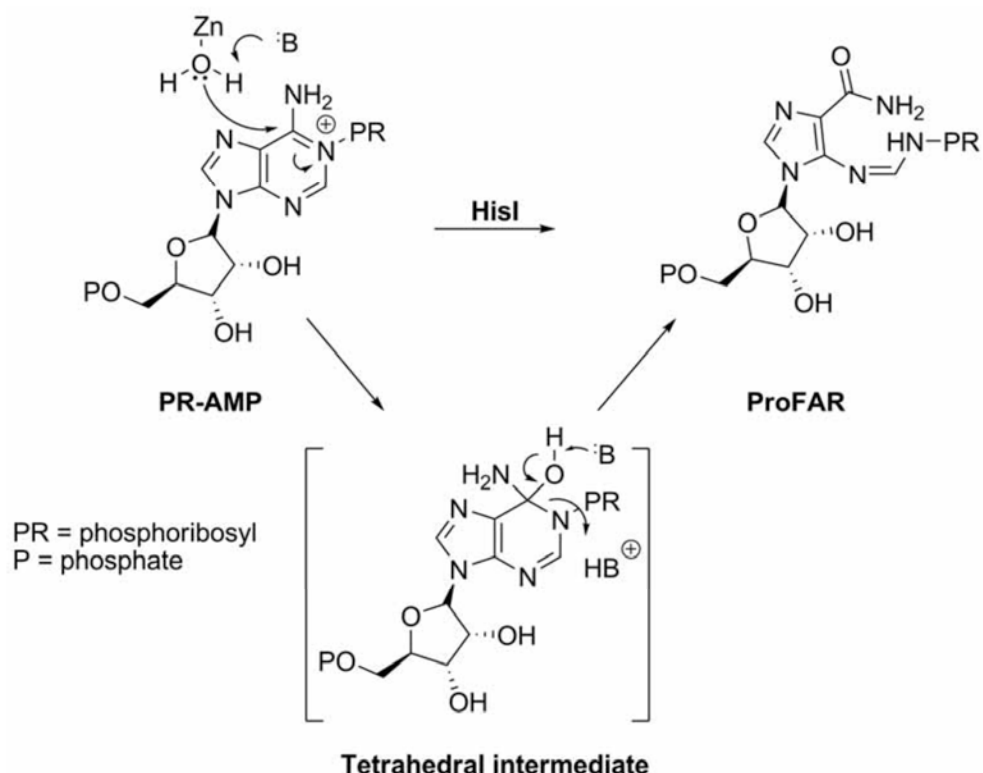


Fig. (3). Chemical structures of the most promising compounds for the *MtHisG* inhibition selected from the ChemBridge and NCI databases through virtual screening.



Scheme 2. Proposed mechanism for the conversion of PR-AMP to ProFAR, as catalyzed by the *hisI* gene product.

analogs failed to generate enzyme-substrate complexes, leaving the phosphoribosyl-ATP binding mode unclear. Thus, the possibility of a complex between HisE and HisI to fully form the active site in accordance with bifunctional enzymes from orthologous organism was not discarded. Unfortunately, HisI from Mtb has not yet been characterized and was only identified in a membrane fraction by proteomic analysis [56].

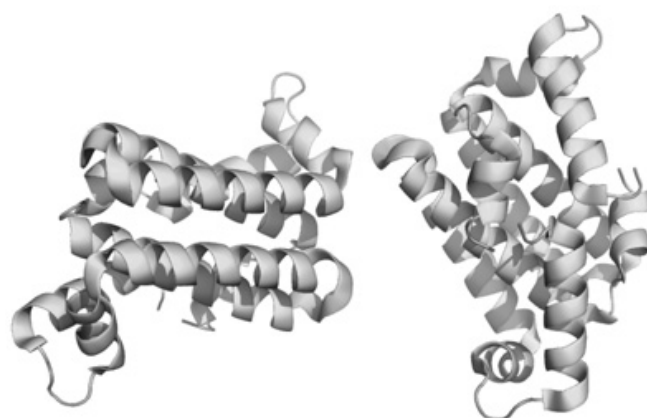


Fig. (4). Tridimensional structure of *Mycobacterium tuberculosis* HisE (MtHisE) in apo form obtained by X-ray diffractometry. The enzyme is entirely formed by α -helices and connecting loops. Two pairs of long central α -helices pack to form a four-helix bundle.

(The color version of the figure is available in the electronic copy of the article).

HisI from *Methanococcus vannielii* (*MvHisI*) has been purified and characterized as a Zn^{2+} -dependent metalloenzyme [57]. A direct spectrophotometric assay at 300 nm was used to determine the kinetic constants and pH-rate profiles, with a K_M value of 9.9 mM and k_{cat} of 4.1 s^{-1} . The enzyme also requires free Mg^{2+} for activity [57]. EDTA inhibition was shown to be related to magnesium ion chelation, whereas 1,10-phenanthroline was able to remove the tightly bound zinc ions from the enzyme. Recently, site-directed mutations of residues C93, C109, and C116 and the double mutant C109/C116 provided evidence that the Zn^{2+} ion is coordinated to these three cysteine residues in *MvHisI* [47]. Moreover, it was proposed that D92, D94, and D96, which flanks the C93 residue, coordinate Mg^{2+} , thus playing an important role in enzyme catalysis, cysteine activation, and zinc-binding capacity [47]. These data are corroborated by X-ray experiments of Cd^{2+} -substituted HisI from the archaeon *Methanobacterium thermoautotrophicum*, which revealed that the three cysteine and three aspartate residues appear to be coordinated to Cd^{2+} [48].

PR-AMP ($pK_a = 8.8 \pm 0.1$) can exist in tautomeric equilibrium with the protonated form [57]. The maximum turnover for PR-AMP was reported to occur at pH 7.5 and k_{cat}/K_M profile showed a single pK_a of 7.3 ± 0.1 , suggesting that the protonation of the substrate is not limiting for this conversion [57], an observation that is in accordance with the classical Curtin-Hammett principle [58]. It is noteworthy that the above three cysteines, three aspartates, and histidine are conserved in Mtb HisI (*MtHisI*). Certain inhibitors have been proposed for orthologous proteins and were identified through virtual screening studies and then tested on whole cells [59], with

some of these compounds being able to inhibit the *in vitro* growth of *S. aureus* and *E. coli*. It is noteworthy that confirmation of the activity of these compounds on the catalytic activity of HisI was not presented, though these compounds can be good starting points for further optimization using functional assays. To date, no inhibition studies with the *MtHisE* or *MtHisI* enzymes have been published.

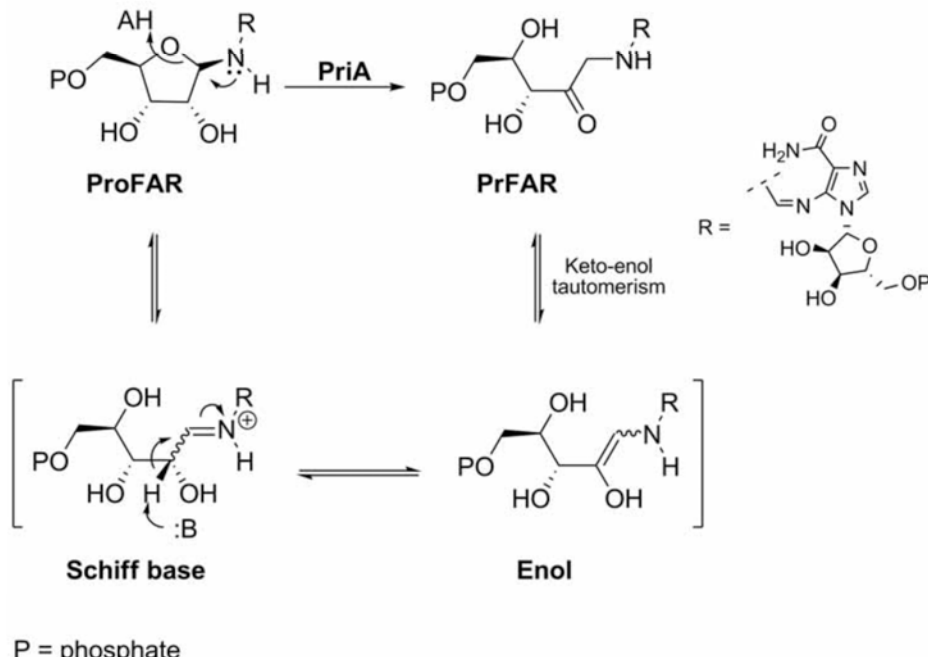
PriA (Rv1603)

(Other designations: hisA, *N'*-(5'-phosphoribosyl) formimino]-5-aminoimidazole-4-carboxamide ribonucleotide (ProFAR) isomerase, BBM II isomerase).

The fourth enzyme in the pathway, encoded by *priA* (MTB Rv1603, 738 bp, 245 aa, 25730.9 Da, pI = 4.42), the *N'*-(5'-phosphoribosyl)formimino]-5-aminoimidazole-4-carboxamide ribonucleotide (ProFAR) isomerase, has been described as a bifunctional enzyme that acts in both L-histidine and tryptophan biosynthesis [35]. In most organisms, two different genes, *hisA* and *trpF*, encode two distinct products that catalyze the isomerization of single-substrates, ProFAR and phosphoribosyl anthranilate (PRA), respectively. Both PriA and HisA have been studied in several organisms, such as bacteria, archaea, yeast, and higher plants, with regard to L-histidine biosynthesis [35, 52, 60-62]. These proteins catalyze an acid/base-assisted Amadori rearrangement, converting the aminoaldose ProFAR into its corresponding aminoketose, phosphoribulosyl-formimino-AICAR-phosphate (PrFAR) [35, 60-62], (Scheme 3). A plausible mechanism for this catalyzed reaction involves a Schiff base and an enol derivative as the intermediates [63], (Scheme 3). *Himar1*-based transposon mutagenesis in strain MtbH37Rv [28, 29] predicted the gene to be essential for mycobacterial survival, placing this enzyme among those that are potential targets for drug development.

HisA-like proteins are frequently compared to TrpF (phosphoribosylanthranilate (PRA) isomerase) because both enzymes assume a $(\beta\alpha)_8$ -barrel fold, the most frequent fold adopted by approximately 10% of the proteins with known structures [64, 65] and also common among enzymes involved in central metabolic pathways [66, 67]. Furthermore, these enzymes perform similar isomerization reactions, leading to the hypothesis that they should use similar strategies in their catalytic mechanisms. Indeed, the enzymes from *Thermotoga maritima* (*TmHisA* and *TmTrpF*) were investigated, showing that Asp8 from *TmHisA* and Cys7 from *TmTrpF*, both located in the C-terminal end of β -strand 1, are key residues that act as a general base during catalysis; Asp127 from *TmHisA* (C-terminal end of β -strand 5) and Asp126 from *TmTrpF* (C-terminal end of β -strand 6) were designated as general acids [60]. The similarities between these enzymes (amino acid sequence, structure, and reaction mechanism, in addition to protein engineering) support the idea that they might have evolved from a common ancestral enzyme with broader substrate specificity.

The search for *trpF* gene in the genomes of *Streptomyces coelicolor*, *Mycobacterium tuberculosis*, and *Mycobacterium leprae* failed [61], even though these actinomycetes are able to synthesize tryptophan. Further investigations showed that the *hisA* homolog identified in the genome of *S. coelicolor* (SCO2050) encoded a bifunctional isomerase that participates in both histidine and tryptophan biosynthesis, suggesting that the gene should be renamed *priA* (phosphoribosyl isomerase A) [61]. Indeed, an *S. coelicolor* mutant strain lacking *priA* activity proved to be auxotrophic for both histidine and tryptophan. In addition, complementation of an *E. coli* mutant lacking *hisA* and *trpF* activity with the *hisA* gene from Mtb (Rv1603) reestablished growth in minimal media, indicating that this enzyme displays the same bifunctionality [61]. These data were confirmed by Due *et al.* [35] using



Scheme 3. Proposed mechanism of the Amadori rearrangement catalyzed by PriA.

diffractometry (PDB accession codes 2Y85, 2Y88 and 2Y89) and kinetic studies with *Mtb* PriA (*Mt*PriA).

As ProFAR and PRA differ in molecular weight by a factor of almost two, the question that emerges is how *Mt*PriA is able to catalyze the reactions, considering that the size of the active site of the single-substrate HisA and TrpF enzymes are substantially different [35]. Three separate structures – the apo form (PDB 2Y89) and in the presence of two ligands (PrFAR, PDB 2Y88, and rCdRP, PDB 2Y85) demonstrated that *Mt*PriA undergoes a conformational change to generate two different active sites to catalyze each reaction. The Asp11 and Asp175 residues act as acids/bases during both isomerizations, though Asp175 (which is located on flexible loop 6) is recruited by a substrate-specific mechanism. For ProFAR isomerization, Asp175 is recruited by Arg19 (present on loop 1) to interact with the 4'-hydroxyl group of the ribulosyl moiety; in PRA isomerization, Arg143 (loop 5) is responsible for positioning Asp175 to perform the same interaction (Fig. 5). These findings indicate that the high loop flexibility allows substrate-induced recruitment to result in the bi-substrate specificity of *Mt*PriA [35]. Asp11, which is located on β -strand 1, has a restricted movement, interacting with the 2'-keto group (ProFAR) or 2'-hydroxyl group (PRA) of the ribulosyl moiety.

An active-site architecture analysis of the bi-substrate enzyme superimposed with its single-substrate versions showed that PriA displays higher similarities with HisA, whereas the superposition of the PriA structure onto TrpF does not present important structural similarity. Supporting this observation, inhibitory compounds screened from a library of 20,000 small molecules that inhibited *Mt*PriA, (Fig. 6), were also able to inhibit *Tm*HisA, though with diminished effectiveness [35]. However, when tested on *Tm*TrpF activity, the same compounds did not exhibit any inhibition on PRA conversion, indicating important structural differences between TrpF and PriA.

Inhibitors were screened using a coupled assay with the next enzyme in the pathway from *T. maritima* (*Tm*HisF) by measuring the decrease in absorbance at 300 nm due to difference in the extinction coefficients between ProFAR and 5-

phosphoribosyl-4-carboxamide-5-aminoimidazole (AICAR) ($\Delta\epsilon_{300\text{nm}}$ (ProFAR – AICAR) = 5.637 mM⁻¹.cm⁻¹). It is noteworthy that ProFAR is not commercially available and is thermolabile, which could be a drawback for investigations involving drug targeting of this enzyme. Despite this disadvantage, the fact that *Mt*PriA participates in two biosynthetic pathways, L-histidine and tryptophan, makes it an interesting target for the development of new antitubercular drugs.

HisH and HisF (Rv1602 and Rv1605, Respectively)

(Other designations: imidazole glycerol phosphate (IGP) synthase, HIS7 (in Eukarya)).

Encoded by the *hisH* (MTB Rv1602, 621 bp, 206 aa, 21386.4 Da, pI = 5.21) and *hisF* (MTB Rv1605, 804 bp, 267 aa, 27220.9 Da, pI = 4.47) genes, the HisH and HisF enzymes are responsible for the conversion of PrFAR into imidazole glycerol-phosphate (IGP), with the concomitant liberation of AICAR, in L-histidine biosynthesis [25]. This reaction links L-histidine with nitrogen metabolism and *de novo* purine biosynthesis. The link with purine pathway is devoted to AICAR liberation because this product is a key entry point in the purine pathway. In bacteria, the products of *hisH* and *hisF* have been described to form a stable dimeric complex endowed with glutamine amidotransferase and cyclase activity, respectively [25, 68, 69]. The ammonia produced with the catalytic activity of HisH is used at the active site of HisF, yielding imidazole glycerol-phosphate and AICAR as products. However, in Eukarya [55, 70, 71] and some δ -Proteobacteria [72], both the activities are accomplished by a single product of *HIS7*. The fusion, absent in prokaryotes, has been considered as an important hallmark of eukaryote evolution and has remained in nucleated cells over time [71]. Whether *Mtb* presents a bi-enzyme complex remains to be proven, as the *hisH* and *hisF* product have not yet been characterized. However, compared with other prokaryotes, the organization of genes in operons suggests that *Mtb* should also show this organization, with the probable formation of a bi-enzyme complex. The mechanism of conversion of PrFAR into IGP, as accomplished by HisF, involves steps of addition-elimination that are acid-base cata-

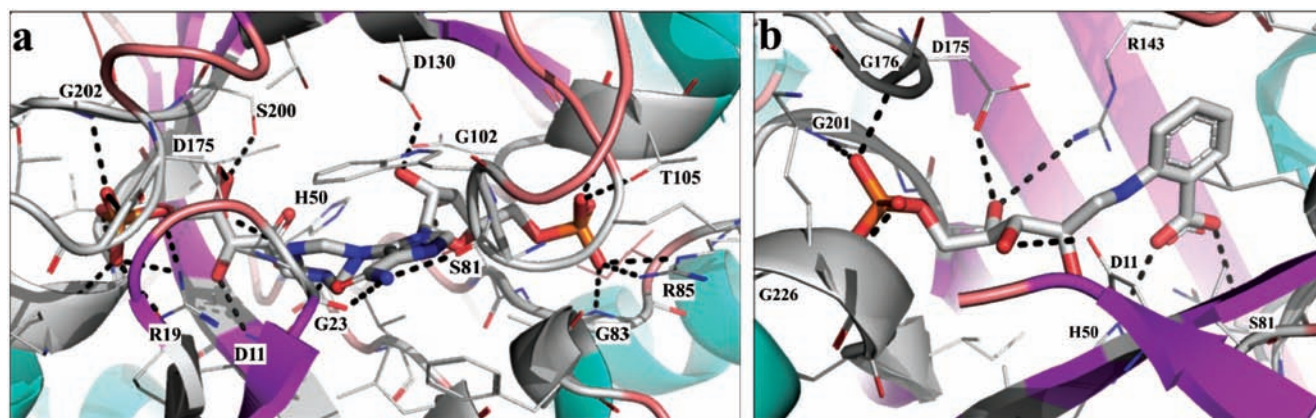


Fig. (5). Active site structures of the *Mt*PriA-PrFAR (a) and *Mt*PriA-rCdRP (b) complexes. The structures of both PriA-ligand complexes reveal the same pair of residues (Asp11 and Asp175) as candidates to catalyze the isomerization of the respective L-histidine and tryptophan biosynthesis substrates. Hydrogen bonds between each ligands and enzyme residues are represented with dashed lines. (The color version of the figure is available in the electronic copy of the article).

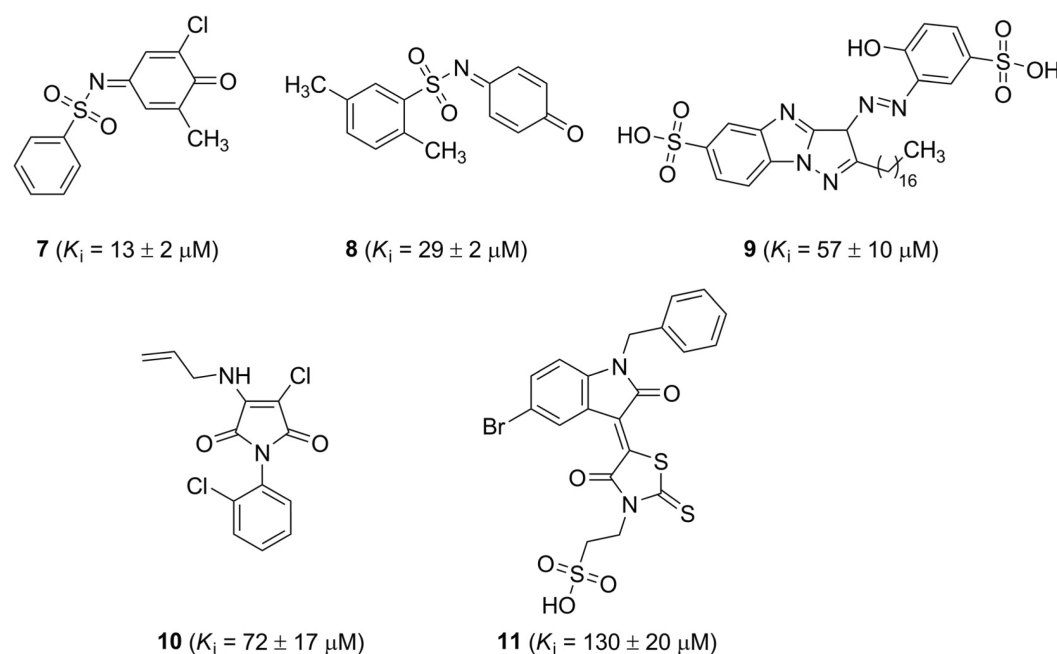


Fig. (6). Selected inhibitors of *MtPriA* (K_i related to ProFAR).

lyzed, hydrolysis of an imine group, and an intramolecular cyclocondensation (Scheme 4). The first step is the addition of ammonia to the carbonyl group of PrFAR. The elimination of a water molecule leads to imine derivative I. The subsequent hydrolysis of another imine group, already present in PrFAR, generates aldehyde derivative II, with the concomitant generation of AICAR. Lastly, an intramolecular cyclocondensation reaction with water elimination leads to the imidazole ring and IGP product. This mechanism has been inferred from results in *Thermotoga maritime* HisF (*TmHisF*) in which two aspartate residues (Asp11 and Asp 130) were observed as catalytically essential for *TmHisF* activity, as based on site-directed mutagenesis experiments [68]. These residues acted as an acid-base pair in the formation of IGP.

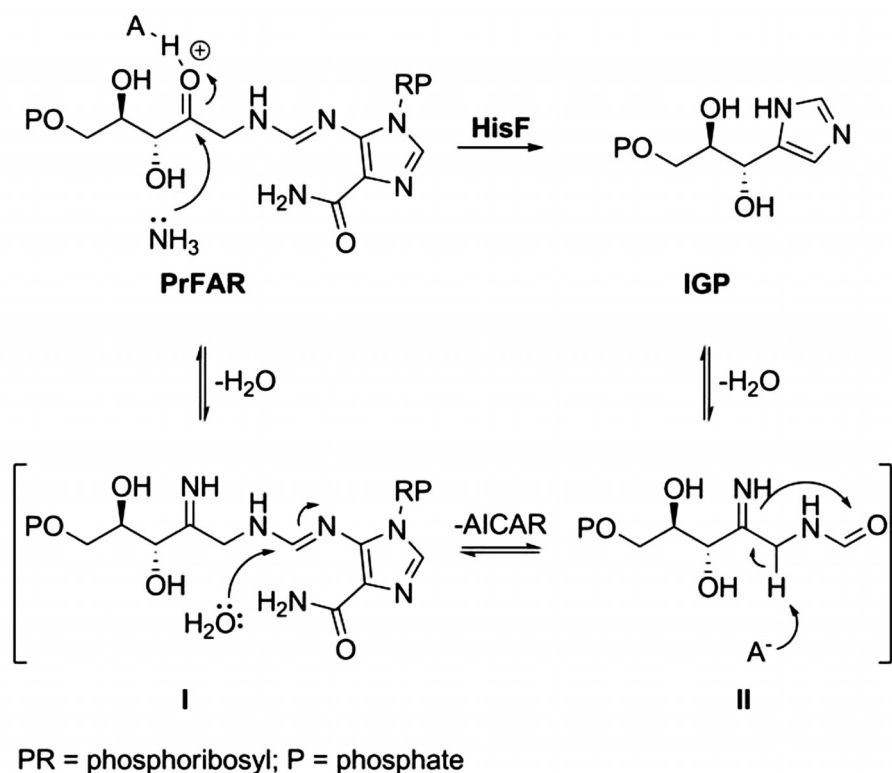
Neither *Mycobacterium tuberculosis* enzymes (*MtHisH* nor *MtHisF*) have been studied in Mtb. As these proteins integrate important metabolic pathways, the design of specific inhibitors or activators could lead to advances in the design of novel drugs. In addition, the overproduction of the *hisH* and *hisF* products induces growth inhibition on *Salmonella typhimurium* [73] and filamentation in *E. coli* [74]. Therefore, a systematic study of these genes and their products in Mtb could yield important findings for understanding their roles.

HisB (Rv1601)

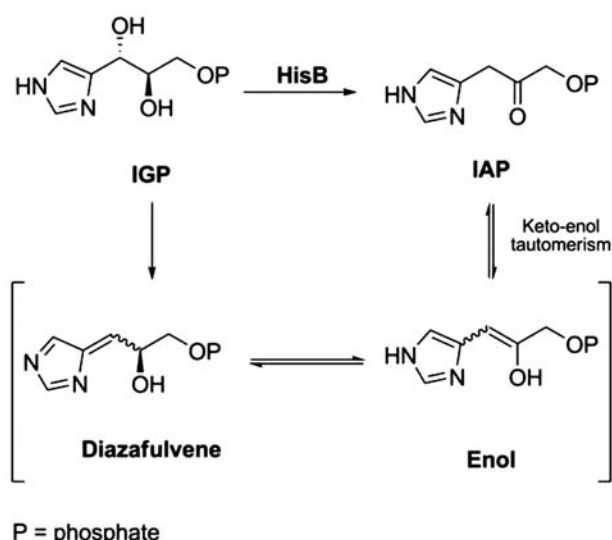
(Other designations: imidazole glycerol phosphate dehydratase, IGPD, HisB).

Imidazole glycerol phosphate dehydratase (IGPD, EC.4.2.1.19) is associated with a polypeptide encoded by the *hisB* gene (MTB Rv1601, 633 bp, 210 aa, 22769.6 Da, and pI = 6.85). IGPD is observed in fungi [75, 76], plants [77], Archaea, and some Eubacteria as a monofunctional unit, whereas other Eubacteria encode bifunctional enzymes dis-

playing a histidinol phosphate phosphatase (HPase) activity for the same polypeptide chain. With regard to the bifunctional enzymes, biochemical and genetic studies suggest that the enzymatic activities, IGPD (or HisB) and HPase (or HisN), are independent of one another and reside in separate domains. The HPase (EC.3.1.3.15) activity is found within the *N*-terminal domain (residues 1-167), whereas the *C*-terminal domain (residues 168-356) exhibits the IGPD activity [71]. HPase catalyzes the eighth step of histidine biosynthesis: the dephosphorylation of histidinol-phosphate to L-histidinol, the direct precursor of histidine. IGPD is responsible for the sixth step of histidine biosynthesis, catalyzing the dehydration of imidazole glycerol phosphate (IGP) to imidazole acetol phosphate (IAP) [78, 79]. The mechanism of this dehydration follows an unusual elimination reaction because the lack of adjacent electron-withdrawing groups α to the leaving proton makes this a nonacidic proton. In most dehydration reactions, the carbonyl and imine moieties are typically observed α and β to the departing proton and hydroxyl group, respectively [66]. The lack of this functional arrangement in IGP led to the proposition of a mechanism via the formation of an enol, preceded by a diazafulvene intermediate (Scheme 5) [80]. The elucidation of the tertiary structure of HisB from *Arabidopsis thaliana* (AtHisB) by X-ray diffractometry corroborated the proposed mechanism and stereochemistry of the reaction [81]. In the molecular modeling proposed, the formation of a diazafulvene intermediate was supported by the presence of two manganese ions stabilizing the imidazolate precursor [81]. The sequence alignment of Mtb HisB (*MtHisB*) and its counterpart from *A. thaliana* HisB (AtHisB) (47% sequence identity) revealed that all eight metal binding residues are completely conserved [82], indicating the possibility of the maintenance of the proposed mechanism across species. The glutamic acids (Glu21 and Glu173) involved in the proton transfer are also conserved [81, 82].



Scheme 4. Proposed mechanism for the conversion of PrFAR into IGP, as catalyzed by HisF.



Scheme 5. Substrate (IGP), intermediates, and the product (IAP) in the reaction catalyzed by HisB.

There is no evidence to date for a bifunctional *hisB* gene in Mtb, with IGPD being the unique activity for this gene [71, 82]. Using evolutionary models and studies of alignment, Brilli and Fani [71] observed a monofunctional *hisB* in Mtb CDC1551 (MT1637). Their findings indicate that gene fusion events and horizontal transfer in other organisms could have resulted in the *hisNB* gene (the nomenclature given to *hisB* bifunctional genes), with the HPase activity encoded by the *hisN* gene (paralogous to *gmhB*) and the IGPD activity by the *hisB* gene. The evolutionary model

implies that the *hisNB* gene formation occurred via duplication events and subsequent evolutionary divergence of the ancestor gene encoding a DDDD-phosphatase, such as D-glycero-D-manno-Heptose-1,7-bisphosphate phosphatase (GmhB), and posterior fusion with *hisB* [71, 72].

There is a debate regarding which enzyme is responsible for the eighth step of histidine biosynthesis in Mtb. The literature indicates that GmhB (Rv0114), also called HisB2, might be responsible. This enzyme is a member of the histidinol phosphate phosphatase subfamily of the haloalkanoic acid dehalogenase (HAD) enzyme superfamily [83, 84]. However, in a quick search, no candidates for enzymes conducting the eighth step appear in the vicinity of the gene clusters that comprise the genes involved in this pathway [71, 72, 85]. We performed an alignment of the protein sequence of MtbH37Rv GmhB with *Escherichia coli* bifunctional HisB (Gene ID: 12931411), revealing that GmhB aligns with the N-terminal region of bifunctional HisB (32% of identity) (data not shown), a region that was demonstrated to be responsible for HPase activity [71]. HisN has a limited biological distribution, whereas GmhB is found in a wide variety of Archaea and bacteria. More interesting is that GmhB catalyzes the dephosphorylation of D- α -D-heptose-1,7-PP in surface lipopolysaccharide (LPS) production in *E. coli* and *Aneurinibacillus thermoautotrophicus* [86, 87].

Although the preliminary crystal structure of *MtHisB* has been solved [82], to our knowledge, there is no kinetic study or inhibitor reported in the literature. In contrast, IGPD has been described as an important target for the rational development of novel herbicides [88-90] and antimicrobials [59].

The herbicide compounds have been designed to mimic both substrate and the putative reaction intermediate diazafulvene [91]. In these synthesized compounds, both triazole ring and a phosphonate group connected by a three-carbon chain are essential for strong IGPD inhibition. Among the compounds hitherto described, the racemic triazolylphosphonate **12**, (Fig. 7), has been described to show very potent inhibition of ($K_i = 0.6$ nM) and a slow dissociation ($K_{off} = 0.04$ min⁻¹) from *Saccharomyces cerevisiae* IGPD [75]. This compound was obtained to mimic the diazafulvene intermediate. In addition, triazolylphosphonate **13** and **14**, (Fig. 7) have been reported as potent inhibitors of IGPD purified from wheat germ, with K_i values of 8.5 ± 1.4 nM and 10 ± 1.6 nM, respectively [92]. These compounds could become starting points for obtaining new antimycobacterial compounds based on *MtHisB* inhibition. Utilizing the same strategy as for HisI, virtual screening of a library of 10^6 compounds using a homology model of HisB from *Staphylococcus aureus* (*S. aureus*) was conducted in an attempt to discover novel antimicrobial drugs. The better ranked compounds were tested in whole cells and only two of these showed strong inhibition on *S. aureus* strains. IGPD1 and IGPD13 compounds showed promising and even superior activity to the control in the tested conditions. It should be noted that the effectiveness of compounds in inhibit the catalytic activity of HisB was not demonstrated.

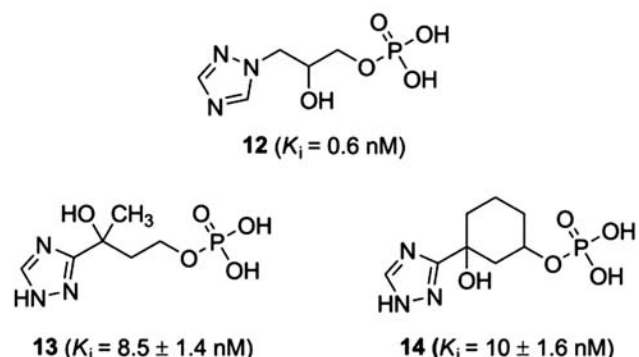


Fig. (7). Structure of some triazolylphosphonate compounds obtained as IGPD inhibitors.

HisC1 (Rv1600) and HisC2 (Rv3772)

(Other designations: HisC, HisC1, HisC2, histidinol-phosphate aminotransferase, imidazole acetol-phosphate transaminase, imidazole acetol-phosphate aminotransferase)

The genes *hisC1* (MTB Rv1600, 1143 bp, 380 aa, 40581.1 Da, and pI = 5.07) and *hisC2* (MTB Rv3772, 1062 bp, 353 aa, 38007.5 Da, and pI = 6.51) encode two possible histidinol-phosphate aminotransferases. These proteins may, in principle, catalyze the seventh step in the histidine biosynthesis pathway, a reversible transamination reaction in which the α -amino group of L-glutamate is transferred to imidazole acetol phosphate, leading to the production of α -ketoglutarate and L-histidinol-phosphate. However, the activity and functionality of both gene products from Mtb remains to be demonstrated. The amino acid sequence alignment of Mtb HisC1 (*MtHisC1*) and Mtb HisC2 (*MtHisC2*) show 29% sequence identity [93].

Histidinol-phosphate aminotransferases share certain mechanistic features with other pyridoxal-phosphate-dependent aminotransferases, requiring a pyridoxal-5'-phosphate (PLP) as a cofactor that covalently binds to an active-site lysine residue, leading to the formation of an aldehyde between pyridoxal-phosphate and the amino acid substrate as the first intermediate, following a ping-pong-Bi-Bi mechanism of catalysis [94].

The sequence analysis of members of family I of the aminotransferase superfamily, including aspartate, histidinol, and tyrosine aminotransferases, indicates that these proteins are evolutionarily related, with several residues associated with dimerization or catalysis and substrate-binding being conserved [94, 95]. The PLP-binding site of HisC is structurally similar to that found in other PLP-dependent enzymes, including *Thermus thermophilus* aspartate aminotransferase [96], *E. coli* MalY protein [97] apple 1-amino-cyclopropane-1carboxylate synthase [98], and *Trypanosoma cruzi* tyrosine aminotransferase [99]. The polar contacts of HisC from *E. coli* (*EcHisC*) and PLP are performed by Tyr55, Asn157, Asp184, Tyr187, Lys214, and Arg222 residues, which are conserved in family I aminotransferases [100].

Kinetic studies using *Bacillus subtilis* showed that the transamination reaction in the synthesis of tyrosine and phenylalanine could be primarily catalyzed by histidinol-phosphate aminotransferase. The K_M values for PLP, α -ketoglutarate, and phenylalanine were 11-, 5-, and 4-fold lower with HisC than with aromatic aminotransferase [101-103].

The *EcHisC* structure with piridoxamine-5'-phosphate (PMP), its PLP internal aldimine, was reported in 2001 by Sivaraman *et al.* [100] as was a tetrahedral complex with both PLP and L-histidinol phosphate covalently linked through the active-site residue Lys214, the residue forming the Schiff-base with PLP; the equivalent residue in HisC from *S. typhimurium* is Lys217 [94]. The three-dimensional structure of HisC from *Thermotoga maritima* was also elucidated in complex with the histidinol-phosphate adduct (in apo form), with pyridoxal-5'-phosphate complex, and in complex with PMP. Recently, preliminary X-ray diffractometry studies of *MtHisC1* [93] and *MtHisC2* [85] crystals have been reported. *MtHisC1* and *MtHisC2* were overexpressed in *Mycobacterium smegmatis* and purified to homogeneity using nickel-nitrilotriacetic acid metal affinity and gel-filtration chromatography, and the crystals were obtained using the hanging-drop vapor-diffusion technique [85, 93].

The inhibition of HisC from *S. aureus* has been targeted [59]: using virtual screening, a series of 10^6 compounds were assayed with a homology model of *SaHisC*. The selected compounds were directly tested in *S. aureus* and *E. coli*, showing only weak or partial inhibition. However, the interaction of these compounds with HisC lacks verification.

HisD (Rv1599)

(Other designations: histidinol dehydrogenase, HDH, NAD:L-histidinol oxidoreductase).

The protein histidinol dehydrogenase performs the last two steps in the biosynthesis of L-histidine. Encoded by the

hisD gene (MTB Rv1599, 1317 bp, 438 aa, 45346.2 Da, pI = 4.63) this zinc-metalloenzyme consists of two identical subunits and produces L-histidine from the α -amino alcohol, L-histidinol through two successive oxidation reactions via an aldehyde intermediate, histidinaldehyde or L-histidinal (Scheme 6) [104].

The importance of L-histidinol dehydrogenase for virulence has been demonstrated in some pathogenic bacteria, such as *Brucella suis* [105], *Salmonella typhimurium* [106], and *Burkholderia pseudomallei* [107]. In Mtb, the *hisD* gene has been described as possibly essential for survival and mycobacterial virulence [24–27, 103]. These findings, together with an apparent inability of histidine auxotrophs to survive single-amino acid starvation [31] and the identification of genes required for mycobacterial growth [28], make histidinol dehydrogenase a promising target for antitubercular agent development. In addition, these and other characteristics have ranked HisD among the top 50 targets in the TDR Targets database [27].

Studying HisD from *Salmonella typhimurium* (*StHisD*), Grubmeyer *et al.* [109] showed that the two reactions are successively catalyzed at one active site of each subunit of the enzyme, containing one Zn^{2+} atom and one NAD^+ -binding site each; the authors verified the metal dependency of the enzyme but without demonstrating the catalytic role. Lee and Grubmeyer [110] had previously demonstrated that removing metal ions caused the dissociation of subunits and that dimer formation required metal ions.

HisD has been isolated from *Arthrobacter histidinolorans* [111], *Neurospora crassa* [112], yeast [113], *Bacillus* spp. [114], *Salmonella typhimurium* [115], *B. suis* [116], and cabbage [117] and investigated both genetically and biochemically [115, 118–121].

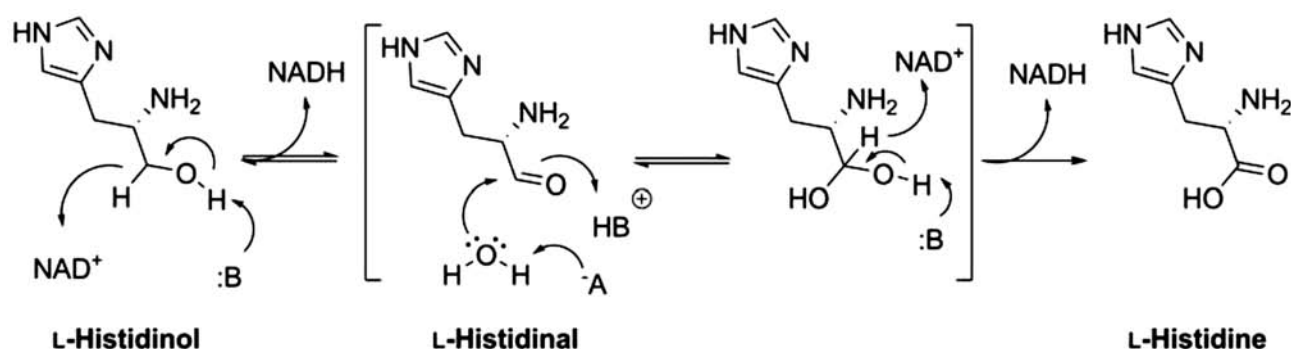
The kinetic characterization of Mtb histidinol dehydrogenase (*MtHisD*) encoded by the *hisD* gene was described as part of our ongoing project [122]. This enzyme is a homodimeric metalloprotein and follows a Bi-Uni-Uni-Bi ping-pong mechanism, with histidinol binding first to the enzyme and NAD^+ unable to bind to the free enzyme [122]. A molecular homology modeling of the *MtHisD* structure was constructed based on the *E. coli* HisD (*EcHisD*) structure; as determined by X-ray diffraction in the apo state and in complex with L-histidinol, Zn^{2+} , and NAD^+ at 1.7 Å resolution, the HisD monomer consists of four domains [123]. Through the molecular modeling of *MtHisD*, it was inferred that residues His336 and His376 from domain 2 and Glu423 in domain 4

are involved in L-histidinol binding; the Zn^{2+} ion was observed octahedrally coordinated to Gln267, His270, Asp369, and His428 [122]. The importance of histidine residue for metal binding was revealed by site-directed mutagenesis studies utilizing HisD from cabbage (*cbHisD*), whereby a His261-Asn mutation caused the loss of Zn^{2+} and inactivated the enzyme [124]. The NAD^+ -binding site includes Try129, Gly132, and Asn221 [122]. The mechanism of oxidation performed by HisD involves the abstraction of a proton and a hydride from L-histidinol (Scheme 6) [123]. According to the proposed molecular modeling of *MtHisD* [122], His336 acts as a base to abstract the proton from a hydroxyl group, causing the α -carbon to adopt an sp^2 configuration. Activated by Glu335, a water molecule performs the nucleophilic attack of the carbonyl group from L-histidinaldehyde, with the concomitant formation of a tetrahedral intermediate and restoration of neutrality of the base. A second proton and hydride abstraction leads to L-histidine formation. The hydride reduces the NAD^+ in the mechanism proposed in (Scheme 6).

The inhibition studies of orthologous proteins have demonstrated the possible druggability of *MtHisD*. Dancer *et al.* [125] studied HisD inhibitors targeting the isoforms from cabbage and *E. coli*, and compounds have been designed to interact with the lipophilic binding pocket adjacent to the active site of the enzyme. The best compounds showed IC_{50} values of approximately 40 μM and 20 μM for cabbage and *E. coli* HisD, respectively. Although it is difficult to compare IC_{50} values from two different experiments, the above results appear to be better than the previously reported methyl ketones evaluated as *StHisD* inhibitors [126].

Recently, a series of *B. suis* HisD (*BsHisD*) inhibitors have been reviewed [127]. Histidinol analogs containing an aromatic chain compatible with the presence of an adjacent lipophilic pocket represented the first series of inhibitors of *BsHisD* [126]. Abdo *et al.* [116] investigated the inhibitory effects of a series of substituted benzylic ketones derived from histidine on the activity of *BsHisD*, and three compounds showed effective inhibitory activity, with $IC_{50} \leq 10$ nM. Derivative **15** was found to be the most potent inhibitor, with an IC_{50} value of 3 nM (Fig. 8). The benzylic ketones **16** and **17** (Fig. 8) showed IC_{50} values of 6 nM and 10 nM, respectively [128]. A new series of compounds was proposed in an attempt to improve the potency of benzylic ketone derivatives.

The inhibitors of the second series were developed through the intercalation of a sulfonyl hydrazide moiety but



Scheme 6. Proposed mechanism for the formation of L-histidine catalyzed by the *hisD* product.

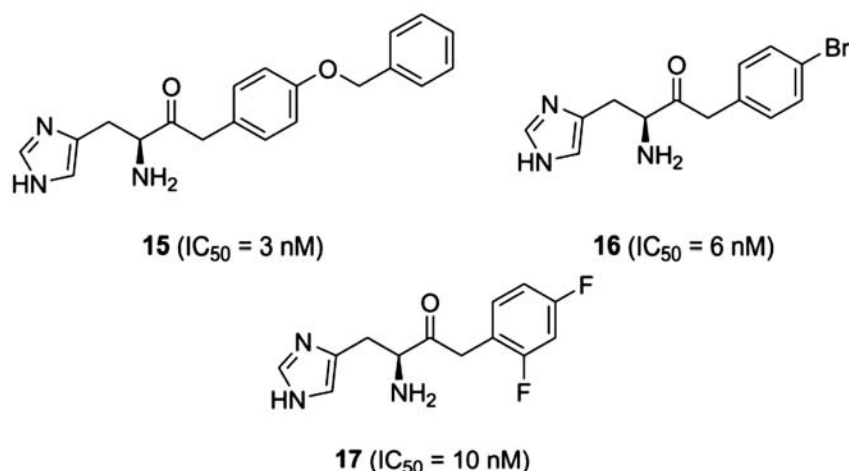


Fig. (8). Inhibitors of *BsHisD*.

did not provide more potent inhibitors. Indeed, the majority compounds of this series exhibited very poor inhibition capacity, with $IC_{50} \geq 100 \mu\text{M}$ [127].

The third series of potential inhibitors was designed with an extension of the aromatic chain by a second aromatic ring, which was separated by a variety of linkers; this series exhibited good inhibition capacities, with $IC_{50} \leq 70 \text{ nM}$ [128]. Compounds **18** and **19** (Fig. 9) were able to inhibit *BsHisD*, with IC_{50} values of 3 nM and 8.5 nM, respectively. The inhibitors of the third series (Fig. 9) had a rigid structure comprising a carbon-carbon triple bond between both aromatic moieties. Compound **18** exhibited 100% inhibition of *B. suis* growth in a minimal medium at a concentration of 50 μM , in contrast to an untreated control culture; the compound also showed an inhibition profile that included a reduction in intramacrophagic replication that was slightly higher than 10^3 -fold at 24 h post-infection at a concentration of 10 μM compared to untreated macrophage-like THP1 cells [128]. The results obtained by Abdo [128] and reviewed by Lopez [127] demonstrated the impact of the second aromatic moiety added to the inhibitor.

As already mentioned with regard to other proteins present in the histidine biosynthetic pathway, these compounds may be starting points for the development of alternative antimycobacterial agents based on the inhibition of *MtHisD*.

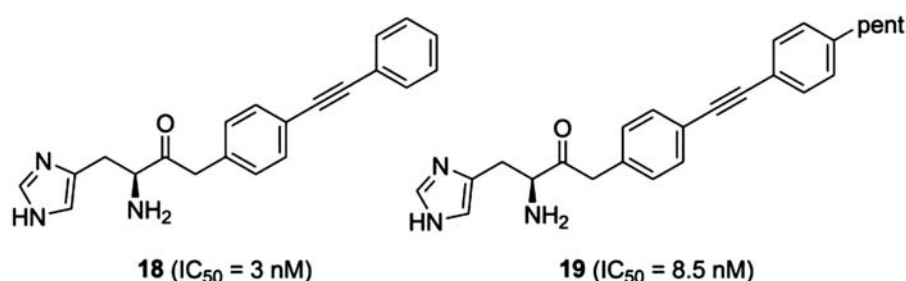
L-Histidine Acquisition from the Host Cell

The nutritional requirements of different mycobacterial species have been studied and characterized, although little is known about the identity and properties of specific transporters [129, 130]. In *Mycobacterium phlei*, it was shown that, unlike proline, the uptake of histidine, leucine, lysine, tryptophan, glutamic acid, and glutamine was blocked by respiratory inhibitors [131]. L-histidine can support the growth of the saprophytic *Mycobacterium smegmatis* as the only carbon or nitrogen source [132], but the same is not observed for the parasitic *Mycobacterium bovis* BCG [133]. This is in agreement with a general trend found, in which saprophytic mycobacteria, in contrast to intracellular parasitic species, are able to grow in a broader spectrum of compounds when used as the only substrate available [129].

The arginine transporter is the only inner-membrane amino acid transporter from mycobacteria characterized genetically and by transport experiments [133]. It was found that the Rv0522 gene product from *Mycobacterium bovis* BCG is an L-arginine and also a γ -aminobutyric acid permease [133].

The amino acid L-histidine could also be obtained from the medium or from the host cell indirectly, by uptaking histidine-containing oligopeptides. *M. smegmatis*, for example, can use the dipeptide β -alanyl-L-histidine (carnosine) as the sole carbon and nitrogen sources [132]. Later, the oligopeptide permease operon (oppBCDA) of *M. bovis* BCG was cloned and a mutant opp strain constructed by homologous recombination [134]. In this study, 25 di- and tripeptides, four of them containing histidine, were used as the sole carbon and/or nitrogen sources by wild-type and opp mutant BCG strain. Interestingly, neither the wild-type nor the opp mutant *M. bovis* BCG strain was able to grow using any of these peptides as the sole carbon source, stressing again the marked differences in transport mechanisms between saprophytic and parasitic mycobacteria.

In a comparative analysis of transporter proteins encoded by the clinical strain Mt CDC1551 and *Mycobacterium leprae*, 285 potential transporters from different categories were identified in the Mt genome, including inner-membrane channel-forming proteins, outer-membrane porin-type proteins, secondary carriers, primary active transporters and poorly defined systems [135]. Most of these sequences are not currently annotated as transport proteins in the Mt genome, so this work will pave the way for a better understanding of transport mechanisms in mycobacteria. Within the transport proteins found, four of them could be directly involved with L-histidine uptake. An Amino Acid-Polyamine-Organocation (APC) superfamily member, similar to the cationic amino acid transporter (CAT-1) of *Achaeoglobus fulgidus* was identified. Interestingly, the murine CAT-1 transporter is an efficient carrier for L-histidine at pH 5.5, when this amino acid is largely protonated, but not at pH 7.4, when L-histidine is neutral [136]. Three ATP-Binding Cassette (ABC) superfamily members similar to amino acid and oligopeptide transporters from other

**Fig. (9).** Third series of *BsHisD* inhibitors.

organisms were also identified [135]. However, the relevance of these proteins, if any, to L-histidine uptake by Mtb remains to be studied. Finally, an important point is based on economic energy perspective, if the Mtb could import this amino acid from host cell the L-histidine pathway could have been silenced over the thousands of years of evolution.

CONCLUSION

Mtb has been considered to be the most successful pathogen in the world because of the ability of the bacillus to persist in the host. Although the bactericidal activity of some

antitubercular drugs can be observed *in vitro*, these compounds need prolonged administration to obtain comparable effects [137, 138]. The emergence of MDR-TB and XDR-TB strains and the urgency to combat “latent” TB strains emphasize the need to develop new anti-TB agents that are more effective and less toxic, with the aim of reducing the duration of treatment, advancing the treatment of drug-resistant TB, and providing efficient treatment for latent TB infection. New drugs, such as SIRTURO™ (bedaquiline), demonstrate the importance of research on the drug design of new antimycobacterial compounds target-based. Bedaquiline is the first TB therapy in 40 years with a new mechanism of

Table 1. Summary of Information From L-Histidine Pathway.

Enzyme	Isolated in Mtb (Ref.) ^a	Essentiality (Ref.)	Cristalographic Structure from Mtb (PDB code)	Druggability Index (0-1) [27]	Inhibitors from Mtb or Orthologous Proteins (Ref.)
HisG	Isolated and functionally characterized [33]	Essential [24-26, 30]	1NH7 and 1NH8 [33]	0.2	[41-46]
HisE	Isolated [34]	Without statistical classification [30]	1Y6X and 3C90 [34]	-	-
HisI	Identified ^b [49, 56]	Essential [28-30]	-	0.2	-
PriA	Isolated and functionally characterized [35]	Essential [28-30]	2Y85, 2Y88 and 2Y89 [35]	0.2	[35]
HisH	Identified ^c [56]	Essential [28-30]	-	0.2	-
HisF	Identified ^c [56]	Uncertain [30]	-	0.2	-
HisB	Isolated [82]	Essential [28-30]	Crystallization and preliminary X-ray diffraction Studies. [82]	0.3	[91, 92]
HisC1	Isolated [93]	Essential [28-30]	Crystallization and preliminary X-ray diffraction studies [93]	-	[59]
HisC2	Isolated [85]	Non-Essential [28-30]	Crystallization and preliminary X-ray diffraction studies [85]	-	-
HisD	Isolated and functionally characterized [122]	Essential [28-30]	-	0.3	[116, 125, 126, 128]

^aIsolated from microorganism was referred as an amplified, cloned, expressed, and purified gene product.^bIdentified by mass spectrometry in Triton X-114 extracts of MtbH37Rv, membrane protein fraction and whole cell lysates.^cIdentified by mass spectrometry in whole cell lysates of MtbH37Rv.

action and the first one to be approved by the FDA to specifically treat multi-drug resistant TB [19]. However, the possibility of mutation with the rapid appearance of new resistant strains cannot reduce the effort for obtaining novel anti-tuberculosis drugs. Moreover, the safety of this compound needs be completely established because the molecule has been correlated to cardiac arrest [139].

The present review highlights the importance of the histidine biosynthesis pathway and its connection to other biosynthetic pathways, such as purine (connected through the AICAR cycle) and tryptophan biosynthesis [25, 35], and the essentiality of the genes in this pathway [28-31] (Table 1). However, one can conclude that histidine biosynthesis pathway is still poorly studied in Mtb: of the ten enzymatic steps of this pathway, only three gene products have been functionally characterized (HisG, PriA, and HisD); action indispensable for drug design. Furthermore, some components still have not been described in Mtb, such as the gene for the seventh reaction and the enzyme involved in the eighth reaction. Some enzymes characterized as bifunctional in such organisms as *E. coli* and *S. typhimurium* have not been shown to be bifunctional in Mtb: for example, for HisB, only IGPD activity has been described. The genes encoding HisE and HisI vary greatly among organisms, as the enzymes are as monofunctional (Archaea and actinomycetes), bifunctional (plants and Eubacteria), and multifunctional (yeast) [34, 48, 49, 51, 53-55, 57, 140]. In Mtb, two separate genes are described as encoding HisE and HisI [34]. These aspects are very interesting for studies of enzyme evolution. The fifth reaction in histidine biosynthesis, performed by HisH and HisF, is also not well established in Mtb. Because this step links the L-histidine pathway with nitrogen metabolism and *de novo* purine biosynthesis [25], it is a very important reaction and requires further study. Furthermore, the three-dimensional structure has been solved for only three enzymes of Mtb (PriA, HisE, and HisG) [33-35], though this characteristic is of utmost importance in the design of novel inhibitors targeting this pathway (Table 1).

In this work, we also reviewed the targets of Mtb L-histidine biosynthesis that are already well characterized in the literature. PriA is a linkage point of this pathway with tryptophan biosynthesis [35], making this enzyme very important, as is HisG, the first enzyme in the pathway, which is feedback regulated by the product histidine [25]. Another critical enzyme for histidine biosynthesis is HisD, which is responsible for the two last reactions and is considered a promising target for inhibitor design.

It is noteworthy that the genes *hisE*, *hisB*, and *hisD* have been ranked among the top 50 targets by the TDR Targets database. In addition, seven genes from L-histidine pathway (*priA*, *hisB*, *hisC1*, *hisD*, *hisG*, *hisH*, and *hisI*) have been described as essential for Mtb growth (Table 1).

Some substrates in the L-histidine pathway are extremely unstable [25], which, in turn, makes the study of some of the steps challenging. Furthermore, several compounds are not commercially available making kinetic and inhibition studies laborious and indicating a need to develop methods to synthesize these substrates.

This review clearly demonstrates the applicability of the L-histidine pathway as a target for the development of new

anti-tuberculosis drugs. We remain optimistic for the future expansion of synthetic procedures to yield small molecules designed to target the gene products of this pathway, with the possibility of obtaining innovative drugs.

CONFLICT OF INTEREST

The author(s) confirm that this article content has no conflicts of interest.

ACKNOWLEDGEMENTS

Financial support for this work was provided by QuatroG P&D Ltda. and SEBRAE/FAPERGS (FAPERGS n. 013/2011). Financial support was also provided by National Institute of Science and Technology on Tuberculosis (Decit/SCTIE/MS-MCT-CNPq- FNDCTCAPES), Millennium Initiative Program (CNPq - Brazil), to D.S.S. and L.A.B., and Support Newly Doctor from FAPERGS (ARD/2012) to P.M. D.S.S. (CNPq, 304051/1975-06) and L.A.B. (CNPq, 5201182/99-5), are research career awardees of the National Council for Scientific and Technological Development of Brazil (CNPq).

ABBREVIATIONS

PRPP	=	5-phosphoribosyl-1-pyrophosphate
AICAR	=	5-phosphoribosyl-4-carboxamide-5-aminoimidazole
HisG	=	ATP Phosphoribosyltransferase
ATPase	=	ATP synthase
GmhB	=	D-glycero-D-mano-Heptose-1,7-bisphosphate phosphatase
DARQs	=	Diarylquinolines
XDR-TB	=	Extensively drug-resistant
HAD	=	Haloalkanoic acid dehalogenase
HisD	=	Histidinol dehydrogenase
HPase	=	Histidinol Phosphate Phosphatase
HisC	=	Histidinol-phosphate aminotransferase
IAP	=	Human immunodeficiency virus (HIV) imidazole acetol phosphate
HisB	=	Imidazole glycerol phosphate Dehydratase (IGPD)
HisF	=	Imidazole glycerol phosphate synthase (HisH)
IGP	=	Imidazole glycerol-phosphate
PPi	=	Inorganic pyrophosphate
LPS	=	Lipopolysaccharide
MIC	=	Minimum inhibitory concentration
MDR-TB	=	Multi drug-resistant
Mtb	=	<i>Mycobacterium tuberculosis</i>
PRA	=	Phosphoribosyl anthranilate
PriA	=	Phosphoribosyl isomerase A

ProFAR	=	Phosphoribosyl-formimino-AICAR-phosphate
TrpF	=	Phosphoribosylanthranilate isomerase
PRTase	=	Phosphoribosyltransferase
PrFAR	=	Phosphoribulosyl-formimino-AICAR-phosphate
PMP	=	Piridoxamine-5'-phosphate
PDB	=	Protein Data Bank
PLP	=	Pyridoxal-5'phosphate
HisI	=	Pyrophosphoribosyl AMP Cyclohydrolase
PR-AMP	=	Pyrophosphoribosyl-AMP
PR-ATP	=	Pyrophosphoribosyl-ATP
HisE	=	Pyrophosphoribosyl-ATP Pyrophosphohydrolase
TDR-TB	=	Totally drug-resistant
TB	=	Tuberculosis
FDA	=	U.S. Food and Drug Administration
WHO	=	World Health Organization

REFERENCES

- [1] World Health Organization *Global tuberculosis report 2012*; World Health Organization: Geneva, 2012.
- [2] World Health Organization *Global tuberculosis control WHO report 2010*; World Health Organization: Geneva, 2010.
- [3] World Health Organization *Global tuberculosis control: WHO report 2011*; World Health Organization: Geneva, 2011.
- [4] Barry, C. E., 3rd; Bosshoff, H. I.; Dartois, V.; Dick, T.; Ehrt, S.; Flynn, J.; Schnappinger, D.; Wilkinson, R. J.; Young, D. The spectrum of latent tuberculosis: rethinking the biology and intervention strategies. *Nat. Rev. Microbiol.*, **2009**, 7, 845-855.
- [5] Keane, J.; Gershon, S.; Wise, R. P.; Mirabile-Levens, E.; Kasznica, J.; Schwieterman, W. D.; Siegel, J. N.; Braun, M. M. Tuberculosis associated with infliximab, a tumor necrosis factor alpha-neutralizing agent. *N. Engl. J. Med.*, **2001**, 345, 1098-1104.
- [6] Dooley, K. E.; Chaisson, R. E. Tuberculosis and diabetes mellitus: convergence of two epidemics. *Lancet Infect. Dis.*, **2009**, 9, 737-746.
- [7] Cruz-Knight, W.; Blake-Gumbs, L. Tuberculosis: an overview. *Prim. Care.*, **2013**, 40, 743-756.
- [8] Preventive therapy against tuberculosis in people living with HIV. *Wkly. Epidemiol. Rec.*, **1999**, 74, 385-398.
- [9] Jasmer, R. M.; Nahid, P.; Hopewell, P. C. Latent Tuberculosis Infection. *N. Engl. J. Med.*, **2002**, 347, 1860-1866.
- [10] Tuberculosis elimination revisited: obstacles, opportunities, and a renewed commitment. Advisory Council for the Elimination of Tuberculosis (ACET). *MMWR Recomm. Rep.*, **1999**, 48, 1-13.
- [11] World Health Organization Multidrug and extensively drug-resistant TB (M/XDR-TB) **2010** global report on surveillance and response. http://whqlibdoc.who.int/publications/2010/9789241599191_eng.pdf (accessed October 1, 2012).
- [12] Velayati, A. A.; Farnia, P.; Masjedi, M. R.; Ibrahim, T. A.; Tabarsi, P.; Haroun, R. Z.; Kuan, H. O.; Ghanavi, J.; Farnia, P.; Varahram, M. Totally drug-resistant tuberculosis strains: evidence of adaptation at the cellular level. *Eur. Respir. J.*, **2009**, 34, 1202-1203.
- [13] World Health Organization *Guidelines for the programmatic management of drug-resistant tuberculosis*; World Health Organization: Geneva, 2011.
- [14] Van Gestel, J.; Guillemont, J.; Venet, M.; Poignet, H.; Decrane, L.; Vernier, D.; Odds, F. Quinoline Derivatives and Their Use as Mycobacterial Inhibitors, WO2004011436A1. **2005**.
- [15] Andries, K.; Verhasselt, P.; Guillemont, J.; Göhlmann, H. W. H.; Neefs, J.-M.; Winkler, H.; Van Gestel, J.; Timmerman, P.; Zhu, M.; Lee, E.; Williams, P.; de Chaffoy, D.; Huitric, E.; Hoffner, S.; Cambau, E.; Truffot-Pernot, C.; Lounis, N.; Jarlier, V. A diarylquinoline drug active on the ATP synthase of *Mycobacterium tuberculosis*. *Science*, **2005**, 307, 223-227.
- [16] De Jonge, M. R.; Koymans, L. H. M.; Guillemont, J. E. G.; Koul, A.; Andries, K. A computational model of the inhibition of *Mycobacterium tuberculosis* ATPase by a new drug candidate R207910. *Proteins*, **2007**, 67, 971-980.
- [17] Koul, A.; Dendouga, N.; Vergauwen, K.; Molenberghs, B.; Vranckx, L.; Willebroeds, R.; Ristic, Z.; Lill, H.; Dorange, I.; Guillemont, J.; Bald, D.; Andries, K. Diarylquinolines target subunit c of mycobacterial ATP synthase. *Nat. Chem. Biol.*, **2007**, 3, 323-324.
- [18] Diacon, A. H.; Pym, A.; Grobusch, M.; Patientia, R.; Rustomjee, R.; Page-Shipp, L.; Pistorius, C.; Krause, R.; Bogoshi, M.; Churchyard, G.; Venter, A.; Allen, J.; Palomino, J. C.; De Marez, T.; van Heeswijk, R. P. G.; Lounis, N.; Meyvisch, P.; Verbeeck, J.; Parys, W.; de Beule, K.; Andries, K.; Mc Neeley, D. F. The diarylquinoline TMC207 for multidrug-resistant tuberculosis. *N. Engl. J. Med.*, **2009**, 360, 2397-2405.
- [19] Press Announcements > FDA approves first drug to treat multi-drug resistant tuberculosis. <http://www.fda.gov/NewsEvents/Newsroom/PressAnnouncements/ucm333695.htm> (accessed March 17, 2013).
- [20] Koul, A.; Arnoult, E.; Lounis, N.; Guillemont, J.; Andries, K. The challenge of new drug discovery for tuberculosis. *Nature*, **2011**, 469, 483-490.
- [21] Cole, S. T.; Brosch, R.; Parkhill, J.; Garnier, T.; Churcher, C.; Harris, D.; Gordon, S. V.; Eiglmeier, K.; Gas, S.; Barry, C. E., 3rd; Tekia, F.; Badcock, K.; Basham, D.; Brown, D.; Chillingworth, T.; Connor, R.; Davies, R.; Devlin, K.; Feltwell, T.; Gentles, S.; Hamlin, N.; Holroyd, S.; Hornsby, T.; Jagels, K.; Krogh, A.; McLean, J.; Moule, S.; Murphy, L.; Oliver, K.; Osborne, J.; Quail, M. A.; Rajandream, M. A.; Rogers, J.; Rutter, S.; Seeger, K.; Skelton, J.; Squares, R.; Squares, S.; Sulston, J. E.; Taylor, K.; Whitehead, S.; Barrell, B. G. Deciphering the biology of *Mycobacterium tuberculosis* from the complete genome sequence. *Nature*, **1998**, 393, 537-544.
- [22] Gashaw, I.; Ellinghaus, P.; Sommer, A.; Asadullah, K. What makes a good drug target? *Drug Discov. Today.*, **2011**, 16, 1037-1043.
- [23] Overington, J. P.; Al-Lazikani, B.; Hopkins, A. L. How many drug targets are there? *Nat. Rev. Drug Discov.*, **2006**, 5, 993-996.
- [24] Ames, B. N.; GARRY, B.; HERZENBERG, L. A. The genetic control of the enzymes of histidine biosynthesis in *Salmonella typhimurium*. *J. Gen. Microbiol.*, **1960**, 22, 369-378.
- [25] Alifano, P.; Fani, R.; Liò, P.; Lazzano, A.; Bazzicalupo, M.; Carluomagno, M. S.; Bruni, C. B. Histidine biosynthetic pathway and genes: structure, regulation, and evolution. *Microbiol. Rev.*, **1996**, 60, 44-69.
- [26] Stepansky, A.; Leustek, T. Histidine biosynthesis in plants. *Amino Acids*, **2006**, 30, 127-142.
- [27] Agüero, F.; Al-Lazikani, B.; Aslett, M.; Berriman, M.; Buckner, F. S.; Campbell, R. K.; Carmona, S.; Carruthers, I. M.; Chan, A. W. E.; Chen, F.; Crowther, G. J.; Doyle, M. A.; Hertz-Fowler, C.; Hopkins, A. L.; McAllister, G.; Nwaka, S.; Overington, J. P.; Pain, A.; Paolini, G. V.; Pieper, U.; Ralph, S. A.; Riechers, A.; Roos, D. S.; Sali, A.; Shanmugam, D.; Suzuki, T.; Van Voorhis, W. C.; Verlinde, C. L. M. J. Genomic-scale prioritization of drug targets: the TDR Targets database. *Nat. Rev. Drug Discov.*, **2008**, 7, 900-907.
- [28] Sassetti, C. M.; Boyd, D. H.; Rubin, E. J. Genes required for mycobacterial growth defined by high density mutagenesis. *Mol. Microbiol.*, **2003**, 48, 77-84.
- [29] Griffin, J. E.; Gawronski, J. D.; Dejesus, M. A.; Ioerger, T. R.; Akerley, B. J.; Sassetti, C. M. High-resolution phenotypic profiling defines genes essential for mycobacterial growth and cholesterol catabolism. *PLoS Pathog.*, **2011**, 7, e1002251.
- [30] DeJesus, M. A.; Zhang, Y. J.; Sassetti, C. M.; Rubin, E. J.; Sacchettini, J. C.; Ioerger, T. R. Bayesian analysis of gene essentiality based on sequencing of transposon insertion libraries. *Bioinformatics*, **2013**, 29, 695-703.
- [31] Parish, T. Starvation survival response of *Mycobacterium tuberculosis*. *J. Bacteriol.*, **2003**, 185, 6702-6706.

- [32] Brenner, M., A., B. N. The histidine operon and its regulation. In *Metabolic pathways; Metabolic regulation*; H. J. Vogel: Academic Press Inc., New York, **1971**; Vol. vol. 5, pp. 349-387.
- [33] Cho, Y.; Sharma, V.; Sacchettini, J. C. Crystal structure of ATP phosphoribosyltransferase from *Mycobacterium tuberculosis*. *J. Biol. Chem.*, **2003**, *278*, 8333-8339.
- [34] Javid-Majd, F.; Yang, D.; Ioerger, T. R.; Sacchettini, J. C. The 1.25 Å resolution structure of phosphoribosyl-ATP pyrophosphohydrolase from *Mycobacterium tuberculosis*. *Acta Crystallogr. D Biol. Crystallogr.*, **2008**, *64*, 627-635.
- [35] Due, A. V.; Kuper, J.; Geerlof, A.; von Kries, J. P.; Wilmanns, M. Bisubstrate specificity in histidine/tryptophan biosynthesis isomerase from *Mycobacterium tuberculosis* by active site metamorphosis. *Proc. Natl. Acad. Sci. U.S.A.*, **2011**, *108*, 3554-3559.
- [36] Schramm, V. L. Enzymatic Transition States, Transition-State Analogs, Dynamics, Thermodynamics, and Lifetimes. *Annu. Rev. Biochem.*, **2011**, *80*, 703-732.
- [37] Zhang, Y.; Shang, X.; Deng, A.; Chai, X.; Lai, S.; Zhang, G.; Wen, T. Genetic and biochemical characterization of *Corynebacterium glutamicum* ATP phosphoribosyltransferase and its three mutants resistant to feedback inhibition by histidine. *Biochimie*, **2012**, *94*, 829-838.
- [38] Ohta, D.; Fujimori, K.; Mizutani, M.; Nakayama, Y.; Kunpaisal-Hashimoto, R.; Münzer, S.; Kozaki, A. Molecular cloning and characterization of ATP-phosphoribosyl transferase from *Arabidopsis*, a key enzyme in the histidine biosynthetic pathway. *Plant Physiol.*, **2000**, *122*, 907-914.
- [39] Kleeman, J. E.; Parsons, S. M. Reverse direction substrate kinetics and inhibition studies on the first enzyme of histidine biosynthesis, adenosine triphosphate phosphoribosyltransferase. *Arch. Biochem. Biophys.*, **1976**, *175*, 687-693.
- [40] Champagne, K. S.; Piscitelli, E.; Francklyn, C. S. Substrate recognition by the hetero-octameric ATP phosphoribosyltransferase from *Lactococcus lactis*. *Biochemistry*, **2006**, *45*, 14933-14943.
- [41] Morton, D. P.; Parsons, S. M. Biosynthetic direction substrate kinetics and product inhibition studies on the first enzyme of histidine biosynthesis, adenosine triphosphate phosphoribosyltransferase. *Arch. Biochem. Biophys.*, **1976**, *175*, 677-686.
- [42] Morton, D. P.; Parsons, S. M. Inhibition of ATP phosphoribosyltransferase by AMP and ADP in the absence and presence of histidine. *Arch. Biochem. Biophys.*, **1977**, *181*, 643-648.
- [43] Dall-Larsen, T.; Kryvi, H.; Klungsoyr, L. Dinitrophenol, dicoumarol and pentachlorophenol as inhibitors and parasite substrates in the ATP phosphoribosyltransferase reaction. *Eur. J. Biochem.*, **1976**, *66*, 443-446.
- [44] Dall-Larsen, T.; Fasold, H.; Klungsoyr, L.; Kryvi, H.; Meyer, C.; Ortanderl, F. Affinity labelling to - SH groups in adenosine - triphosphate - phosphoribosyl transferase with the dinitrophenyl group from S-dinitrophenyl-6-mercaptopurine-riboside 5'-phosphate. *Eur. J. Biochem.*, **1975**, *60*, 103-107.
- [45] Gohda, K.; Ohta, D.; Kozaki, A.; Fujimori, K.; Mori, I.; Kikuchi, T. Identification of Novel Potent Inhibitors for ATP-Phosphoribosyl Transferase Using Three-Dimensional Structural Database Search Technique. *Quant. Struct.-Act. Rel.*, **2001**, *20*, 143-147.
- [46] Cho, Y.; Ioerger, T. R.; Sacchettini, J. C. Discovery of novel nitrobenzothiazole inhibitors for *Mycobacterium tuberculosis* ATP phosphoribosyl transferase (HisG) through virtual screening. *J. Med. Chem.*, **2008**, *51*, 5984-5992.
- [47] D'Ordine, R. L.; Linger, R. S.; Thai, C. J.; Davisson, V. J. Catalytic zinc site and mechanism of the metalloenzyme PR-AMP cyclohydrolase. *Biochemistry*, **2012**, *51*, 5791-5803.
- [48] Sivarajan, J.; Myers, R. S.; Boju, L.; Sulea, T.; Cygler, M.; Jo Davisson, V.; Schrag, J. D. Crystal structure of *Methanobacterium thermoautotrophicum* phosphoribosyl-AMP cyclohydrolase HisI. *Biochemistry*, **2005**, *44*, 10071-10080.
- [49] Målen, H.; Pathak, S.; Søfteland, T.; de Souza, G. A.; Wiker, H. G. Definition of novel cell envelope associated proteins in Triton X-114 extracts of *Mycobacterium tuberculosis* H37Rv. *BMC Microbiol.*, **2010**, *10*, 132.
- [50] Smith, D. W.; Ames, B. N. Phosphoribosyladenosine monophosphate, an intermediate in histidine biosynthesis. *J. Biol. Chem.*, **1965**, *240*, 3056-3063.
- [51] Carlomagno, M. S.; Chiariotti, L.; Alifano, P.; Nappo, A. G.; Bruni, C. B. Structure and function of the *Salmonella typhimurium* and *Escherichia coli* K-12 histidine operons. *J. Mol. Biol.*, **1988**, *203*, 585-606.
- [52] Fujimori, K.; Tada, S.; Kanai, S.; Ohta, D. Molecular cloning and characterization of the gene encoding N'-(5'-phosphoribosyl)-formimino]-5-aminoimidazole-4-carboxamide ribonucleotide (BBM II) isomerase from *Arabidopsis thaliana*. *Mol. Gen. Genet.*, **1998**, *259*, 216-223.
- [53] Crane, D. I.; Gould, S. J. The *Pichia pastoris* HIS4 gene: nucleotide sequence, creation of a non-reverting his4 deletion mutant, and development of HIS4-based replicating and integrating plasmids. *Curr. Genet.*, **1994**, *26*, 443-450.
- [54] Donahue, T. F.; Farabaugh, P. J.; Fink, G. R. The nucleotide sequence of the HIS4 region of yeast. *Gene*, **1982**, *18*, 47-59.
- [55] Legerton, T. L.; Yanofsky, C. Cloning and characterization of the multifunctional his-3 gene of *Neurospora crassa*. *Gene*, **1985**, *39*, 129-140.
- [56] De Souza, G. A.; Leversen, N. A.; Målen, H.; Wiker, H. G. Bacterial proteins with cleaved or uncleaved signal peptides of the general secretory pathway. *J. Proteomics.*, **2011**, *75*, 502-510.
- [57] D'Ordine, R. L.; Klem, T. J.; Davisson, V. J. N. 1-(5'-phosphoribosyl)adenosine-5'-monophosphate cyclohydrolase: purification and characterization of a unique metalloenzyme. *Biochemistry*, **1999**, *38*, 1537-1546.
- [58] Carey, F. A.; Sundberg, R. J. *Advanced organic chemistry*; Plenum Press: New York, 1983.
- [59] Henriksen, S. T.; Liu, J.; Estiu, G.; Oltvai, Z. N.; Wiest, O. Identification of novel bacterial histidine biosynthesis inhibitors using docking, ensemble rescoring, and whole-cell assays. *Bioorg. Med. Chem.*, **2010**, *18*, 5148-5156.
- [60] Henn-Sax, M.; Thoma, R.; Schmidt, S.; Hennig, M.; Kirschner, K.; Sterner, R. Two (betaalpha)(8)-barrel enzymes of histidine and tryptophan biosynthesis have similar reaction mechanisms and common strategies for protecting their labile substrates. *Biochemistry*, **2002**, *41*, 12032-12042.
- [61] Barona-Gómez, F.; Hodgson, D. A. Occurrence of a putative ancient-like isomerase involved in histidine and tryptophan biosynthesis. *EMBO Rep.*, **2003**, *4*, 296-300.
- [62] Quevillon-Cheruel, S.; Leulliot, N.; Graille, M.; Blondeau, K.; Janin, J.; van Tilburgh, H. Crystal structure of the yeast His6 enzyme suggests a reaction mechanism. *Protein Sci.*, **2006**, *15*, 1516-1521.
- [63] Leopoldseder, S.; Claren, J.; Jürgens, C.; Sterner, R. Interconverting the catalytic activities of (betaalpha)(8)-barrel enzymes from different metabolic pathways: sequence requirements and molecular analysis. *J. Mol. Biol.*, **2004**, *337*, 871-879.
- [64] Wierenga, R. K. The TIM-barrel fold: a versatile framework for efficient enzymes. *FEBS Lett.*, **2001**, *492*, 193-198.
- [65] Höcker, B.; Jürgens, C.; Wilmanns, M.; Sterner, R. Stability, catalytic versatility and evolution of the (beta alpha)(8)-barrel fold. *Curr. Opin. Biotechnol.*, **2001**, *12*, 376-381.
- [66] Gerlt, J. A.; Babbitt, P. C. Divergent evolution of enzymatic function: mechanistically diverse superfamilies and functionally distinct suprafamilies. *Annu. Rev. Biochem.*, **2001**, *70*, 209-246.
- [67] Todd, A. E.; Orengo, C. A.; Thornton, J. M. Evolution of function in protein superfamilies, from a structural perspective. *J. Mol. Biol.*, **2001**, *307*, 1113-1143.
- [68] Beismann-Driemeyer, S.; Sterner, R. Imidazole glycerol phosphate synthase from *Thermotoga maritima*. Quaternary structure, steady-state kinetics, and reaction mechanism of the bienzyme complex. *J. Biol. Chem.*, **2001**, *276*, 20387-20396.
- [69] Klem, T. J.; Chen, Y.; Davisson, V. J. Subunit interactions and glutamine utilization by *Escherichia coli* imidazole glycerol phosphate synthase. *J. Bacteriol.*, **2001**, *183*, 989-996.
- [70] Chittur, S. V.; Chen, Y.; Davisson, V. J. Expression and purification of imidazole glycerol phosphate synthase from *Saccharomyces cerevisiae*. *Protein Expr. Purif.*, **2000**, *18*, 366-377.
- [71] Brilli, M.; Fani, R. Molecular evolution of hisB genes. *J. Mol. Evol.*, **2004**, *58*, 225-237.
- [72] Fani, R.; Brilli, M.; Fondi, M.; Lió, P. The role of gene fusions in the evolution of metabolic pathways: the histidine biosynthesis case. *BMC Evol. Biol.*, **2007**, *7 Suppl 2*, S4.

- [73] Murray, M. L.; Hartman, P. E. Overproduction of hisH and hisF gene products leads to inhibition of cell division in *Salmonella*. *Can. J. Microbiol.*, **1972**, *18*, 671-681.
- [74] Frandsen, N.; D'Ari, R. Excess histidine enzymes cause AICAR-independent filamentation in *Escherichia coli*. *Mol. Gen. Genet.*, **1993**, *240*, 348-354.
- [75] Hawkes, T. R.; Thomas, P. G.; Edwards, L. S.; Rayner, S. J.; Wilkinson, K. W.; Rice, D. W. Purification and characterization of the imidazoleglycerol-phosphate dehydratase of *Saccharomyces cerevisiae* from recombinant *Escherichia coli*. *Biochem. J.*, **1995**, *306*(Pt 2), 385-397.
- [76] Parker, A. R.; Moore, T. D.; Edman, J. C.; Schwab, J. M.; Davisson, V. J. Cloning, sequence analysis and expression of the gene encoding imidazole glycerol phosphate dehydratase in *Cryptococcus neoformans*. *Gene.*, **1994**, *145*, 135-138.
- [77] Mano, J.; Hatano, M.; Koizumi, S.; Tada, S.; Hashimoto, M.; Scheidegger, A. Purification and Properties of a Monofunctional Imidazoleglycerol-Phosphate Dehydratase from Wheat. *Plant Physiol.*, **1993**, *103*, 733-739.
- [78] Ames, B. N.; Mitchell, H. K. The biosynthesis of histidine; imidazoleglycerol phosphate, imidazoleacetol phosphate, and histidinol phosphate. *J. Biol. Chem.*, **1955**, *212*, 687-696.
- [79] Ames, B. N. The biosynthesis of histidine; D-erythro-imidazoleglycerol phosphate dehydratase. *J. Biol. Chem.*, **1957**, *228*, 131-143.
- [80] Parker, A. R.; Moore, J. A.; Schwab, J. M.; Davisson, V. J. *Escherichia coli* imidazoleglycerol phosphate dehydratase: spectroscopic characterization of the enzymic product and the steric course of the reaction. *J. Am. Chem. Soc.*, **1995**, *117*, 10605-10613.
- [81] Glynn, S. E.; Baker, P. J.; Sedelnikova, S. E.; Davies, C. L.; Eadsforth, T. C.; Levy, C. W.; Rodgers, H. F.; Blackburn, G. M.; Hawkes, T. R.; Viner, R.; Rice, D. W. Structure and mechanism of imidazoleglycerol-phosphate dehydratase. *Structure*, **2005**, *13*, 1809-1817.
- [82] Ahangar, M. S.; Khandokar, Y.; Nasir, N.; Vyas, R.; Biswal, B. K. HisB from *Mycobacterium tuberculosis*: cloning, overexpression in *Mycobacterium smegmatis*, purification, crystallization and preliminary X-ray crystallographic analysis. *Acta Crystallogr. Sect. F Struct. Biol. Cryst. Commun.*, **2011**, *67*, 1451-1456.
- [83] Nguyen, H. H.; Wang, L.; Huang, H.; Peisach, E.; Dunaway-Mariano, D.; Allen, K. N. Structural determinants of substrate recognition in the HAD superfamily member D-glycero-D-manno-heptose-1,7-bisphosphate phosphatase (GmhB). *Biochemistry*, **2010**, *49*, 1082-1092.
- [84] Wang, L.; Huang, H.; Nguyen, H. H.; Allen, K. N.; Mariano, P. S.; Dunaway-Mariano, D. Divergence of biochemical function in the HAD superfamily: D-glycero-D-manno-heptose-1,7-bisphosphate phosphatase (GmhB). *Biochemistry*, **2010**, *49*, 1072-1081.
- [85] Nasir, N.; Vyas, R.; Chugh, C.; Ahangar, M. S.; Biswal, B. K. Molecular cloning, overexpression, purification, crystallization and preliminary X-ray diffraction studies of histidinol phosphate aminotransferase (HisC2) from *Mycobacterium tuberculosis*. *Acta Crystallogr. Sect. F Struct. Biol. Cryst. Commun.*, **2012**, *68*, 32-36.
- [86] Kneidinger, B.; Graninger, M.; Puchberger, M.; Kosma, P.; Messner, P. Biosynthesis of nucleotide-activated D-glycero-D-manno-heptose. *J. Biol. Chem.*, **2001**, *276*, 20935-20944.
- [87] Kneidinger, B.; Marolda, C.; Graninger, M.; Zamyatina, A.; McArthur, F.; Kosma, P.; Valvano, M. A.; Messner, P. Biosynthesis pathway of ADP-L-glycero-beta-D-manno-heptose in *Escherichia coli*. *J. Bacteriol.*, **2002**, *184*, 363-369.
- [88] Cox, J. M.; Hawkes, T. R.; Bellini, P.; Ellis, R. M.; Barrett, R.; Swarborough, J. J.; Russell, S. E.; Walker, P. A.; Barnes, N. J.; Knee, A. J.; Lewis, T.; Davies, P. R. The Design and Synthesis of Inhibitors of Imidazoleglycerol Phosphate Dehydratase as Potential Herbicides. *Pestic. Sci.*, **1997**, *50*, 297-311.
- [89] Lindell, S. D.; Earnshaw, C. G.; Wright (deceased), B. J.; Carver, D. S.; O'Mahony, M. J.; Saville-Stones, E. A. Synthesis of inhibitors of imidazole glycerol phosphate dehydratase. *Bioorg. Med. Chem. Lett.*, **1996**, *6*, 547-552.
- [90] Schweitzer, B. A.; Loida, P. J.; CaJacob, C. A.; Chott, R. C.; Colantes, E. M.; Hegde, S. G.; Mosier, P. D.; Profeta, S. Discovery of imidazole glycerol phosphate dehydratase inhibitors through 3-D database searching. *Bioorg. Med. Chem. Lett.*, **2002**, *12*, 1743-1746.
- [91] Gohda, K.; Kimura, Y.; Mori, I.; Ohta, D.; Kikuchi, T. Theoretical evidence of the existence of a diazafulvene intermediate in the reaction pathway of imidazoleglycerol phosphate dehydratase: design of a novel and potent heterocycle structure for the inhibitor on the basis of the electronic structure-activity relationship study. *Biochim. Biophys. Acta*, **1998**, *1385*, 107-114.
- [92] Mori, I.; Fonne-Pfister, R.; Matsunaga, S.; Tada, S.; Kimura, Y.; Iwasaki, G.; Mano, J.; Hatano, M.; Nakano, T.; Koizumi, S.; Scheidegger, A.; Hayakawa, K.; Ohta, D. A Novel Class of Herbicides (Specific Inhibitors of Imidazoleglycerol Phosphate Dehydratase). *Plant Physiol.*, **1995**, *107*, 719-723.
- [93] Nasir, N.; Vyas, R.; Biswal, B. K. Sample preparation, crystallization and structure solution of HisC from *Mycobacterium tuberculosis*. *Acta Crystallogr. Sect. F Struct. Biol. Cryst. Commun.*, **2013**, *69*, 445-448.
- [94] Hsu, L. C.; Okamoto, M.; Snell, E. E. L-Histidinol phosphate aminotransferase from *Salmonella typhimurium*. Kinetic behavior and sequence at the pyridoxal-P binding site. *Biochimie*, **1989**, *71*, 477-489.
- [95] Jensen, R. A.; Gu, W. Evolutionary recruitment of biochemically specialized subdivisions of Family I within the protein superfamily of aminotransferases. *J. Bacteriol.*, **1996**, *178*, 2161-2171.
- [96] Nakai, T.; Okada, K.; Akutsu, S.; Miyahara, I.; Kawaguchi, S.; Kato, R.; Kuramitsu, S.; Hirotsu, K. Structure of *Thermus thermophilus* HB8 aspartate aminotransferase and its complex with maleate. *Biochemistry*, **1999**, *38*, 2413-2424.
- [97] Clausen, T.; Schlegel, A.; Peist, R.; Schneider, E.; Steegborn, C.; Chang, Y. S.; Haase, A.; Bourenkov, G. P.; Bartunik, H. D.; Boos, W. X-ray structure of MalY from *Escherichia coli*: a pyridoxal 5'-phosphate-dependent enzyme acting as a modulator in mal gene expression. *EMBO J.*, **2000**, *19*, 831-842.
- [98] Capitani, G.; Hohenester, E.; Feng, L.; Storici, P.; Kirsch, J. F.; Jansonius, J. N. Structure of 1-aminocyclopropane-1-carboxylate synthase, a key enzyme in the biosynthesis of the plant hormone ethylene. *J. Mol. Biol.*, **1999**, *294*, 745-756.
- [99] Blankenfeldt, W.; Nowicki, C.; Montemartini-Kalisz, M.; Kalisz, H. M.; Hecht, H. J. Crystal structure of *Trypanosoma cruzi* tyrosine aminotransferase: substrate specificity is influenced by cofactor binding mode. *Protein Sci.*, **1999**, *8*, 2406-2417.
- [100] Sivaraman, J.; Li, Y.; Larocque, R.; Schrag, J. D.; Cygler, M.; Matte, A. Crystal structure of histidinol phosphate aminotransferase (HisC) from *Escherichia coli*, and its covalent complex with pyridoxal-5'-phosphate and l-histidinol phosphate. *J. Mol. Biol.*, **2001**, *311*, 761-776.
- [101] Weigert, D. A.; Nester, E. W. Purification and properties of two aromatic aminotransferases in *Bacillus subtilis*. *J. Biol. Chem.*, **1976**, *251*, 6974-6980.
- [102] Weigert, D. A.; Nester, E. W. Regulation of histidinol phosphate aminotransferase synthesis by tryptophan in *Bacillus subtilis*. *J. Bacteriol.*, **1976**, *128*, 202-211.
- [103] Nester, E. W.; Montoya, A. L. An enzyme common to histidine and aromatic amino acid biosynthesis in *Bacillus subtilis*. *J. Bacteriol.*, **1976**, *126*, 699-705.
- [104] Loper, J. C.; ADAMS, E. Purification and properties of histidinol dehydrogenase from *Salmonella typhimurium*. *J. Biol. Chem.*, **1965**, *240*, 788-795.
- [105] Köhler, S.; Foulongne, V.; Ouahrani-Bettache, S.; Bourg, G.; Teysier, J.; Ramuz, M.; Liautard, J.-P. The analysis of the intramacrophagic virulome of *Brucella suis* deciphers the environment encountered by the pathogen inside the macrophage host cell. *Proc. Natl. Acad. Sci. U.S.A.*, **2002**, *99*, 15711-15716.
- [106] Fields, P. I.; Swanson, R. V.; Haidaris, C. G.; Heffron, F. Mutants of *Salmonella typhimurium* that cannot survive within the macrophage are avirulent. *Proc. Natl. Acad. Sci. U.S.A.*, **1986**, *83*, 5189-5193.
- [107] Pilatz, S.; Breitbach, K.; Hein, N.; Fehlhaber, B.; Schulze, J.; Brenneke, B.; Eberl, L.; Steinmetz, I. Identification of *Burkholderia pseudomallei* genes required for the intracellular life cycle and in vivo virulence. *Infect. Immun.*, **2006**, *74*, 3576-3586.
- [108] Parish, T.; Stoker, N. G. Mycobacteria: bugs and bugbears (two steps forward and one step back). *Mol. Biotechnol.*, **1999**, *13*, 191-200.

- [109] Grubmeyer, C.; Skiadopoulos, M.; Senior, A. E. L-histidinol dehydrogenase, a Zn²⁺-metalloenzyme. *Arch. Biochem. Biophys.*, **1989**, 272, 311-317.
- [110] Grubmeyer, C. T.; Chu, K. W.; Insinga, S. Kinetic mechanism of histidinol dehydrogenase: histidinol binding and exchange reactions. *Biochemistry*, **1987**, 26, 3369-3373.
- [111] Dhawale, M. R.; Creaser, E. H.; Loper, J. C. Evolutionary mechanism of adaptation of *Arhrobacter histodinolovorans* and *Pseudomonas aeruginosa* to use L-histidinol as a sole source of nitrogen and carbon. *J. Gen. Microbiol.*, **1972**, 73, 353-358.
- [112] Minson, A. C.; Creaser, E. H. Purification of a trifunctional enzyme, catalysing three steps of the histidine pathway, from *Neurospora crassa*. *Biochem. J.*, **1969**, 114, 49-56.
- [113] Keesey, J. K., Jr; Bigelis, R.; Fink, G. R. The product of the his4 gene cluster in *Saccharomyces cerevisiae*. A trifunctional polypeptide. *J. Biol. Chem.*, **1979**, 254, 7427-7433.
- [114] Lindsay, J. A.; Creaser, E. H. Purification and properties of histidinol dehydrogenases from psychrophilic, mesophilic and thermophilic bacilli. *Biochem. J.*, **1977**, 165, 247-253.
- [115] Yourno, J. Composition and subunit structure of histidinol dehydrogenase from *Salmonella typhimurium*. *J. Biol. Chem.*, **1968**, 243, 3277-3288.
- [116] Abdo, M.-R.; Joseph, P.; Boigegrain, R.-A.; Liautard, J.-P.; Montero, J.-L.; Köhler, S.; Winum, J.-Y. *Brucella suis* histidinol dehydrogenase: synthesis and inhibition studies of a series of substituted benzylidene ketones derived from histidine. *Bioorg. Med. Chem.*, **2007**, 15, 4427-4433.
- [117] Nagai, A.; Scheidegger, A. Purification and characterization of histidinol dehydrogenase from cabbage. *Arch. Biochem. Biophys.*, **1991**, 284, 127-132.
- [118] Roth, J. R.; Antón, D. N.; Hartman, P. E. Histidine regulatory mutants in *Salmonella typhimurium*. I. Isolation and general properties. *J. Mol. Biol.*, **1966**, 22, 305-323.
- [119] Loper, J. C. Histidinol dehydrogenase from *Salmonella typhimurium*. Crystallization and composition studies. *J. Biol. Chem.*, **1968**, 243, 3264-3272.
- [120] Greeb, J.; Atkins, J. F.; Loper, J. C. Histidinol dehydrogenase (hisD) mutants of *Salmonella typhimurium*. *J. Bacteriol.*, **1971**, 106, 421-431.
- [121] Bitar, K. G.; Firca, J. R.; Loper, J. C. Histidinol dehydrogenase from *salmonella typhimurium* and *Escherichia coli*. Purification, some characteristics and the amino acid sequence around a reactive thiol group. *Biochim. Biophys. Acta.*, **1977**, 493, 429-440.
- [122] Nunes, J. E. S.; Ducati, R. G.; Breda, A.; Rosado, L. A.; de Souza, B. M.; Palma, M. S.; Santos, D. S.; Bassó, L. A. Molecular, kinetic, thermodynamic, and structural analyses of *Mycobacterium tuberculosis* hisD-encoded metal-dependent dimeric histidinol dehydrogenase (EC 1.1.1.23). *Arch. Biochem. Biophys.*, **2011**, 512, 143-153.
- [123] Barbosa, J. A. R. G.; Sivaraman, J.; Li, Y.; Larocque, R.; Matte, A.; Schrag, J. D.; Cygler, M. Mechanism of action and NAD⁺-binding mode revealed by the crystal structure of L-histidinol dehydrogenase. *Proc. Natl. Acad. Sci. U.S.A.*, **2002**, 99, 1859-1864.
- [124] Nagai, A.; Ohta, D. Histidinol dehydrogenase loses its catalytic function through the mutation of His261-->Asn due to its inability to ligate the essential Zn. *J. Biochem.*, **1994**, 115, 22-25.
- [125] Dancer, J. E.; Ford, M. J.; Hamilton, K.; Kilkelly, M.; Lindell, S. D.; O'Mahony, M. J.; Saville-Stones, E. A. Synthesis of potent inhibitors of histidinol dehydrogenase. *Bioorg. Med. Chem. Lett.*, **1996**, 6, 2131-2136.
- [126] Grubmeyer, C. T.; Insinga, S.; Bhatia, M.; Moazami, N. *Salmonella typhimurium* histidinol dehydrogenase: complete reaction stereochemistry and active site mapping. *Biochemistry*, **1989**, 28, 8174-8180.
- [127] Lopez, M.; Köhler, S.; Winum, J.-Y. Zinc metalloenzymes as new targets against the bacterial pathogen Brucella. *J. Inorg. Biochem.*, **2012**, 111, 138-145.
- [128] Abdo, M.-R.; Joseph, P.; Mortier, J.; Turtaut, F.; Montero, J.-L.; Maserel, B.; Köhler, S.; Winum, J.-Y. Anti-virulence Strategy against *Brucella suis*: Synthesis, Biological Evaluation and Molecular Modeling of Selective Histidinol Dehydrogenase Inhibitors. *Org. Biomol. Chem. OBC*, **2011**, 9, 3681.
- [129] Niederweis, M. Nutrient acquisition by mycobacteria. *Microbiology*, **2008**, 154, 679-692.
- [130] Cook, G. M.; Berney, M.; Gebhard, S.; Heinemann, M.; Cox, R. A.; Danilchanka, O.; Niederweis, M. Physiology of Mycobacteria. *Adv. Microb. Physiol.*, **2009**, 55, 81-319.
- [131] Prasad, R.; Kalra, V. K.; Brodie, A. F. Different mechanisms of energy coupling for transport of various amino acids in cells of *Mycobacterium phlei*. *J. Biol. Chem.*, **1976**, 251, 2493-2498.
- [132] Bhatt, A.; Green, R.; Coles, R.; Condon, M.; Connell, N. D. A Mutant of *Mycobacterium smegmatis* Defective in Di peptide Transport. *J. Bacteriol.*, **1998**, 180, 6773-6775.
- [133] Seth, A.; Connell, N. D. Amino Acid Transport and Metabolism in Mycobacteria: Cloning, Interruption, and Characterization of an l-Arginine/-Aminobutyric Acid Permease in *Mycobacterium bovis* BCG. *J. Bacteriol.*, **2000**, 182, 919-927.
- [134] Green, R. M.; Seth, A.; Connell, N. D. A Peptide Permease Mutant of *Mycobacterium bovis* BCG Resistant to the Toxic Peptides Glutathione and S-Nitrosoglutathione. *Infect. Immun.*, **2000**, 68, 429-436.
- [135] Youm, J.; Saier, M. H. Comparative analyses of transport proteins encoded within the genomes of *Mycobacterium tuberculosis* and *Mycobacterium leprae*. *Biochim. Biophys. Acta.*, **2012**, 1818, 776-797.
- [136] Kim, J. W.; Closs, E. I.; Albritton, L. M.; Cunningham, J. M. Transport of cationic amino acids by the mouse ecotropic retrovirus receptor. *Nature*, **1991**, 352, 725-728.
- [137] Hingley-Wilson, S. M.; Lougheed, K. E. A.; Ferguson, K.; Leiva, S.; Williams, H. D. Individual *Mycobacterium tuberculosis* universal stress protein homologues are dispensable in vitro. *Tuberculosis (Edinb)*, **2010**, 90, 236-244.
- [138] Gomez, J. E.; McKinney, J. D. M. tuberculosis persistence, latency, and drug tolerance. *Tuberculosis (Edinb)*, **2004**, 84, 29-44.
- [139] Avorn, J. Approval of a tuberculosis drug based on a paradoxical surrogate measure. *JAMA*, **2013**, 309, 1349-1350.
- [140] Fujimori, K.; Ohta, D. Isolation and characterization of a histidine biosynthetic gene in *Arabidopsis* encoding a polypeptide with two separate domains for phosphoribosyl-ATP pyrophosphohydrolase and phosphoribosyl-AMP cyclohydrolase. *Plant Physiol.*, **1998**, 118, 275-283.

Capítulo 4

Considerações Finais

Referências

Considerações Finais

O *Mycobacterium tuberculosis* é considerado o patógeno de maior sucesso no mundo, devido à sua capacidade de permanecer latente no hospedeiro. O surgimento de cepas resistentes como MDR-TB, XDR-TB tem aumentado a necessidade de novos medicamentos para o tratamento desta doença que, somente no ano de 2013, chegou a 1,5 milhão de mortes no mundo (1).

Neste contexto, o desenho de novos fármacos que levem em consideração o princípio da toxicidade seletiva é uma estratégia muito interessante, para o possível desenvolvimento de novos medicamentos. Assim, a via de biossíntese da histidina e as enzimas envolvidas nesta via são de extrema importância, pois esta rota biossintética não está presente em mamíferos (51).

Com este trabalho foi possível compreendermos um pouco melhor esta via de biossíntese e, principalmente, aprofundarmos os estudos sobre o mecanismo da *MtHisD*, enzima que é responsável pelas duas últimas reações da via de biossíntese de L-His.

A histidinol desidrogenase catalisa duas reações de oxirredução sucessivas, neste processo ocorre a formação de dois intermediários (L-histidinal e L-histidindiol). Além do intermediário não se desligar do sítio da enzima, apenas um único sítio é responsável pela oxidação de ambos, L-Hol e L-Hal. O L-histidinal, quando não complexado com a enzima, é muito instável, o que dificulta o estudo da chamada meia reação (110). Essas características tornam a reação enzimática da HisD extremamente complexa e dificultam o entendimento do seu mecanismo enzimático (81-83, 110).

Os dados já existentes na literatura quanto à caracterização cinética da enzima *MtHisD* (95) foram de extrema importância para o desenvolvimento desse trabalho, visto que a análise do mecanismo deve ser uma prioridade para o desenvolvimento de fármacos (111). Assim, para o melhor conhecimento do mecanismo desta enzima nós realizamos experimentos que

buscaram aprofundar o conhecimento das etapas enzimáticas da reação e as interações da enzima com seus substratos.

Com os resultados obtidos no experimento de cinética em estado pré-estacionário, realizado no equipamento *Stopped-flow*, foi possível determinarmos que a liberação dos produtos não contribui para a etapa limitante da reação catalisada pela *MtHisD*. Grubmeyer e Teng (112) em seu trabalho com a HisD de *S. typhimurium*, concluíram por experimentos de cinética em estado pré-estacionário e efeitos isotópicos, que tanto a primeira quanto a segunda meia-reação da *StHisD* contribuem para a etapa limitante da catálise, os autores também mostraram que a liberação dos produtos não influencia a etapa limitante da reação.

Pela determinação da energia de ativação foi possível calcularmos os valores dos parâmetros termodinâmicos do estado de transição ($\Delta H^\#$, $\Delta S^\#$ e $\Delta G^\#$) da reação. Os resultados de $\Delta H^\#$ positivo (desfavorável), $\Delta S^\#$ negativo (desfavorável) demonstram a ausência de um sistema compensatório entre entalpia e entropia. O valor de $\Delta G^\#$ positivo (não espontâneo) nos mostra que há uma barreira energética a ser superada para a transição do complexo enzima-substrato (ES) para o seu estado ativado ES[#].

O estudo de efeitos isotópicos do solvente (SKIE), em pH 7,2, demonstra que há uma modesta participação de prótons do solvente na catálise e na ligação do L-Hol à *MtHisD*, enquanto que na ligação do NAD⁺ parece não haver participação de prótons do solvente. Além disso, pelo inventário de prótons, em pH 7,2, chegamos à conclusão de que mais de um próton é transferido do solvente para a reação e que, ambas, normal e inversa contribuição do solvente influenciam o SKIE (*Dome-shaped*), o que já foi reportado para a enzima de *S. typhimurium* (112). O mecanismo de catálise da HisD de *E. coli* (85) descreve que moléculas de água vizinhas fazem interações com os estados de transição da reação, o que corrobora para a possibilidade de dois ou mais estados de transição estarem influenciando o SKIE. Devido à dificuldade de estudo da meia reação, não é possível determinarmos os valores dos fatores de fracionamento para esta reação, assim maiores estudos são necessários para podermos afirmar, exatamente, quais e quantos estados de reagentes e ou de transição estão contribuindo para o SKIE.

Os efeitos isotópicos cinéticos do solvente determinados em pH 9,0 mostraram um SKIE normal na catálise e um SKIE inverso para a ligação dos dois substratos (L-Hol e NAD⁺). O inventário de prótons sugere que um único próton do estado de transição contribui para o SKIE neste pH. A diferença dos SKIE nos dois pH utilizados no nosso trabalho pode estar relacionada com os valores de pK_a dos resíduos envolvidos na catálise e na ligação do L-Hol pela *MtHisD* (95). De qualquer forma, os resultados obtidos nos experimentos em pH 7,2 (próximo ao pH fisiológico) reproduzem com maior confiabilidade o ambiente encontrado pelo MTB ao infectar células humanas.

Dando continuidade à questão de simular o ambiente da célula hospedeira, realizamos experimentos de volume excluído (*molecular crowding*) para analisar a influência do meio nos parâmetros cinéticos em estado estacionário da reação (K_M , k_{cat} e constante de especificidade). Esse ensaio tenta reproduzir, da maneira mais verossímil, o ambiente celular, com uma alta concentração de macromoléculas, através do uso de um polímero inerte (113). A ausência de diferenças nestes parâmetros obtidos em meio aquoso e no meio contendo o polímero inerte validam os resultados obtidos neste trabalho.

Tendo em vista a importância do desenvolvimento de novos inibidores da *MtHisD*, compostos químicos com ação inibitória da atividade enzimática podem ser obtidos a partir de análogos estruturais aos substratos, aos produtos ou ao estado de transição da reação enzimática (50). Desta forma, o planejamento e síntese de possíveis inibidores, os quais foram utilizados nos estudos de inibição deste trabalho, tem por base a síntese de compostos com características estruturais derivadas do substrato (L-Hol), intermediário (L-Hal) e produto (L-His) da reação da *MtHisD*, propondo, assim, a manutenção da possível interação polar não-covalente mediada pelo grupamento imidazol do L-Hol com o resíduo de aminoácido His336, que pode estar envolvido na ligação do substrato e na catálise (85, 97). A síntese e planejamento dos compostos foi realizada em colaboração com o Laboratório de Química do Centro de pesquisas em Biologia Molecular em Funcional (CPBMF) da PUCRS.

As 11 hidrazonas derivadas da histidina que foram sintetizadas apresentaram valores de IC₅₀ que variaram de 1,1 até 29 μM. Quatro

compostos tiveram sua constante de inibição (K_i) determinada e todos apresentaram um perfil de inibição competitivo ao substrato L-Hol, ou seja, competem pelo sítio de ligação deste substrato, o que era esperado devido à conservação da porção histidinil presente nas moléculas sintetizadas, porção que, por sua vez, interage com os resíduos His376 e His336 que ligam o substrato L-Hol (85, 95).

A docagem molecular (realizada em colaboração com o Laboratório de Bioinformática, Modelagem e Simulação de Biossistemas (LABIO) da PUCRS, sob co-ordenação do Prof. Dr. Osmar Norberto de Souza) nos mostrou as interações entre os ligantes e a enzima, utilizando uma modelagem da *MtHisD*, realizada por Nunes e colaboradores (95), baseada na estrutura tridimensional da *EcHisD* (85). Os compostos com K_i mais baixos (**4h** e **4k**) apresentaram interações hidrofóbicas e de hidrogênio com as duas histidinas (His376 e His336) que estão relacionadas à formação de ligações de hidrogênio com o grupo hidroxil do L-Hol. O Glu423 também está relacionado à ligação do L-Hol, o que torna relevante a ligação de hidrogênio que o composto **4k** realiza com este resíduo. Outros resíduos como Asp369, que atua na ligação do Zn^{+2} , e Glu335, que na enzima *EcHisD* (Glu326) ativa a molécula de água durante o segundo passo da reação, também possuem interações com os compostos **4h** e **4k**. O metal Zn^{+2} está relacionado a orientação do substrato L-Hol no seu sítio de ligação na enzima (85), por este motivo a interação da porção histidinil com o Zn^{+2} e a adição de substituintes com características hidrofóbicas na posição R dos compostos parece ser de extrema importância para a orientação da ligação destes no sítio de ligação do substrato L-Hol.

Através de estudos de fluorescência determinamos a constante de dissociação (K_d) da ligação do composto **4k** com a *MtHisD*, obtendo um K_d menor do que o K_d para o substrato L-Hol (95). Com a determinação do K_d em diferentes temperaturas foi possível calcularmos os valores dos parâmetros termodinâmicos de ligação (ΔH° , ΔS° e ΔG°) da enzima com o composto. A comparação destes parâmetros com os da ligação da enzima com o L-Hol, obtidos por calorimetria de titulação isotérmica (95), nos mostra que a ligação ao composto possui um ΔH° negativo (favorável), ou seja, a ligação do composto à enzima livre libera calor. Este resultado é o oposto do

que foi evidenciado para a formação do complexo binário *MtHisD:L-Hol*, que possui um ΔH° positivo (desfavorável), em outras palavras, necessita da absorção de calor para ocorrer. Todavia, o valor positivo de ΔS° obtido para a ligação do composto foi menor que o valor de ΔS° para a ligação do substrato à enzima. Além disso, o valor de ΔG° (negativo) obtido foi tão ou mais favorável quanto o da ligação ao substrato, o que corrobora com o perfil de inibição competitivo do composto **4k** pelo sítio do substrato. Estes resultados demonstram que a formação do complexo binário *MtHisD:4k* é espontânea.

A concentração inibitória mínima (MIC) (ensaios realizados pela Dr. Anne D. Vilella no Laboratório NB3 do CPBMP) dos compostos **4e**, **4h** e **4k** para inibir o crescimento do MTB, foi determinada pelo método de placas REMA (114). O composto **4e** demonstrou capacidade de inibir o crescimento do MTB na concentração de $100 \mu\text{g mL}^{-1}$, já os compostos **4h** e **4k** mostraram inibição em concentrações $>100 \mu\text{g mL}^{-1}$. Esse experimento indica que modificações nos compostos, que potencializem a habilidade de penetração destes no MTB, são necessárias. Uma nova série de moléculas, candidatas a inibidores da *MtHisD*, a serem sintetizadas, devem levar em consideração os resultados obtidos neste trabalho.

A rota de biossíntese da L-His em MTB ainda precisa ser melhor estudada, visto que uma grande parte da via ainda não foi caracterizada para este microrganismo. Entretanto dados da literatura ressaltam a aplicabilidade da biossíntese da L-His como alvo para o desenvolvimento de novos fármacos anti-TB (64). Além disso, a enzima *MtHisD*, que catalisa as duas últimas etapas desta via, está entre os 50 alvos mais importantes na busca de novos medicamentos para esta doença (89). As conclusões alcançadas com os experimentos aqui executados representam um importante avanço no entendimento do mecanismo da reação catalisada pela *MtHisD* e um passo significativo na busca por moléculas inibitórias da atividade desta enzima.

Referências

1. World Health Organization. **Global tuberculosis control**: WHO report 2014. Geneva, 2014.
2. Enarson, DA and Murray, JF. **Global epidemiology of tuberculosis**. In: **Tuberculosis**. Rom, WM and Garay, S; Eds. Little, Brow and Co., Boston, MA, p. 57-75, 1996.
3. Pieters, J. *Mycobacterium tuberculosis* and the macrophage: maintaining a balance. **Cell Host Microbe**. v.3, n.6, p.399-407, 2008.
4. Yew, WW; Leung, CC. Update in tuberculosis. **Am. J. Respir. Crit. Care Med.** v.177, n.5, p.479-485, 2008
5. Corbett, E; Watt, C; Walker, N; Maher, D; Williams, B; Ravaglione, M; et al. The growing burden of tuberculosis: global trends and interactions with the HIV epidemic. **Arch. Intern Med.** v.163, n.9, p.1009-1021, 2003.
6. Ruffino-Neto, A. Tuberculosis: the neglected calamity. **Ver. Soc. Brasil. Med. Trop.** v.35, p.51-58, 2002.
7. Brennan, PJ. Tuberculosis in the context of emerging and reemerging diseases. **FEMS Immunol. Med. Microbial.** v.18, p.263-269, 1997.
8. Fatkenheuer, G; Taelman, H; Lepage, P; Schwenk, A and Wenzel, R. The return of tuberculosis. **Diag. Microbial. Infect. Dis.** v.34, p.139-146, 1999.
9. World Health Organization. Global tuberculosis control : WHO report 2013. Geneva, 2013.
10. Ministério da Saúde. **Panorama da tuberculose no Brasil: indicadores epidemiológicos e operacionais**. Secretaria de Vigilância em Saúde, Departamento de Vigilância das Doenças Transmissíveis. Brasília, 2014.
11. Jamison, DT; Breman, JG; Measham, AR; Alleyne, G; Claeson, M; Evans, DB, et al. **Disease Control Priorities in Developing Countries**, 2nd edition, Disease Control Priorities Project. World Bank, Washington DC, p.1401, 2006.
12. Bloom, BR and Murray, CJL. Tuberculosis: commentary on a reemergent killer. **Science**. v.257, p.1055-1064, 1992.
13. Ramaswamy, S; Musser, JM. Molecular genetic basis of antimicrobial agent resistance in *Mycobacterium tuberculosis*: 1998 update. **Tuber Lung Dis.** v.79, n.1, p.3-29, 1998.

14. Elston, JW; Thaker, HK. Co-infection with human immunodeficiency virus and tuberculosis. **Indian J dermatol Venereol Leprol.** v.74, n. 3, p.194-199, 2008.
15. World Health Organization. **Treatment of Tuberculosis: guidelines for national programmes.** Geneva, 2003.
16. Koul, A; Arnoult, E; Guillemont, J; Andries, K. The challenge of new drug discovery for tuberculosis. **Nature.** v.469, p.483-490, 2011.
17. Storla, DG; Yimer, S; Bjune, GA. A systematic review of delay in the diagnosis and treatment of tuberculosis. **BMC Publ Health.** v.8, p.15, 2008.
18. Cole, ST; Brosch, R; Parkhill, J; Garnier, T; Churcher, C; Harris, D; et al. Deciphering the biology of *Mycobacterium tuberculosis* from the complete genome sequence. **Nature.** v.393, p.537-544, 1998.
19. Brennan, PJ and Nikaido, H. The envelope of mycobacteria. **Annu. Ver. Biochem.** v.64, p.29-63, 1995.
20. Warner, DF and Mizrahi, V. Tuberculosis chemotherapy: the influence of bacillary stress and damage response pathways on drug efficacy. **Clin Microbiol Rev.** v.19, n.3, p.558-570, 2006.
21. Maartens, G; Wilkinson, RJ. Tuberculosis. **Lancet.** v.370, p.2030-2043, 2007.
22. Hirsch-Moverman, Y; Daftary, A; Franks, J; Colson, PW. Adherence to treatment for latent tuberculosis infection: systematic review of studies in the US and Canada. **Int J Tuberc Lung Dis.** v.12, p.1235-1254, 2008.
23. Butcher, K; Biggs, B-A; Leder, K; Lemoh, C; O'Brien, D; Marshall, C. Understanding of latent tuberculosis, its treatment and treatment side effects in immigrant and refugee patients. **BMC Research Notes.** v.6, n.342, p.7-8, 2013.
24. Dutta, NK; Karakousis, PC. Latent Tuberculosis Infection: myths, models, and molecular mechanisms. **Microbiol Mol Biol Rev.** v.78, n.3, p.343-371, 2014.
25. Dooley, KE; Chaisson, RE. Tuberculosis and diabetes mellitus: convergence of two epidemics. **Lancet Infect. Dis.** v.9, p.737- 746, 2009.
26. Keane, J; Gershon, S; Wise, RP; Mirabile-Levens, E; Kasznica, J; Schwieterman, WD; Siegel, JN; Braun, MM. Tuberculosis associated with infliximab, a tumor necrosis factor alphaneutralizing agent. **N. Engl. J. Med.** v.345, p.1098-1104, 2001.
27. Parrish, NM; Dick, JD; Bishai, WR. Mechanisms of latency in *Mycobacterium tuberculosis*. **Trends Microbiol.** v.6, n.3, p.107-12, 1998.

28. American Thoracic Society and Centers for Disease Control and Prevention: Targeted tuberculin testing and treatment of latent tuberculosis infection. **Am J Resp Crit Care Med.** v.161, p.S221–S247, 2000.
29. Jasmer, RM; Nahid, P; Hopewell, PC. Latent tuberculosis infection. **N. Engl. J. Med.** v.347, p.1860-1866, 2002.
30. Cruz-Knight, W; Blake-Gumbs, L. Tuberculosis: an overview. **Prim. Care.** v.40, p.743-756, 2013.
31. Advisory Council for the Elimination of Tuberculosis (ACET). Tuberculosis elimination revisited: obstacles, opportunities, and a renewed commitment. **MMWR Recomm. Rep.** v.48, p.1-13, 1999.
32. World Health Organization. **Global tuberculosis control:** WHO report 2010. Geneva, 2010
33. Waksman, S. **The Conquest os Tuberculosis.** Hale, London,1965.
34. Zhang, Y and Young, D. Molecular mechanisms of isoniazid: a drug at the front line of tuberculosis control. **Trends Microbiol.** v.1, p.109-113, 1993.
35. Petrini, B and Hoffner, S. Drug-resistant and multidrug-resistant tubercle bacilli. **Int. J. Antimicrob. Agents.** v.13, p.93-97, 1999.
36. Telenti, A and Iseman, M. Drug-resistant tuberculosis: what do we do now? **Drugs.** v.59, p.171-179, 2000.
37. O'Brien, RJ, Nunn, PP. The need for new drugs against tuberculosis. Obstacles, opportunities, and next steps. **Am J Respir Crit Care Med.** v.163, n.5, p.10558, 2001.
38. Pasqualoto, KF & Ferreira, EI. An approach for the rational design of new antituberculosis agents. **Curr. Drug Targets.** v.2, p.427-437, 2001.
39. Dorman, SE & Chaisson, RE. From magic bullets back to the magic mountain: the rise of extensively drug-resistant tuberculosis. **Nat. Med.** v.13, p.295-298, 2007.
40. World Health Organization. XDR-TB - Extensive Drug Resistant TB. 2006. Disponível em: <http://who.int/mediacentre/news/notes/2006/np23/index.html>. Acesso em: 28 Maio 2015.
41. Wise, J. Southern Africa is moving swiftly to combat the threat of XDT-TB. **Bull World Health Organ.** v.84, n.12, p.924-925, 2006.

42. Velayati, A; Masjedi, M; Farnia, P; Tabarsi, P; Ghanavi, J; ZiaZarifi, A; et al. Emergence of new forms of totally drug-resistant tuberculosis bacilli. **CHEST**. Nov 16; v.136, p.420-425, 2009.
43. Velayati, A; Farnia, P; Masjedi, M; Ibrahim, T; Tabarsi, P; Haroun, R; et al. Totally drug-resistant tuberculosis strains: evidence of adaptation at the cellular level. **Eur. Resp. J.** Nov 01; v.34, n.5, p.1202-1203, 2009.
44. Andries, K; Verhasselt, P; Guillemont, J; Göhlmann, HWH; Neefs, J-M; Winkler, H; et al. A diarylquinoline drug active on the ATP synthase of *Mycobacterium tuberculosis*. **Science**. v.307, p.223-227, 2005.
45. De Jonge, MR; Koymans, LHM; Guillemont, JEG; Koul, A; Andries, K. A computational model of the inhibition of *Mycobacterium tuberculosis* ATPase by a new drug candidate R207910. **Proteins**. v.67, p.971-980, 2007.
46. Diacon, AH; Pym, A; Grobusch, M; Patientia, R; Rustomjee, R; Page-Shipp, L; et al. The diarylquinoline TMC207 for multidrug-resistant tuberculosis. **N. Engl. J. Med.** v.360, p.2397-2405, 2009.
47. US Food and Drugs Administration. Press Announcements - **FDA approves first drug to treat multi-drug resistant tuberculosis**. Disponível em: <http://www.fda.gov/newsevents/newsroom/pressannouncements/ucm333695.htm>. Acesso em: 25 Maio 2015.
48. Avorn J. Approval of a tuberculosis drug based on a paradoxal surrogate measure. **JAMA**. v.309, p.1349-1350, 2013.
49. Koul, A; Dendouga, N; Vergauwen, K; Molenberghs, B; Vranckx, L; Willebroords, R; et al. Diarylquinolines target subunit c of mycobacterial ATP synthase. **Nat. Chem. Biol.** v.3, p.323-324, 2007.
50. Robertson JG. Mechanistic basis of enzyme-targeted drugs. **Biochemistry**. v.44, n.15, p.5561-5571, 2005.
51. Alifano, P; Fani, R; Liò, P; Lazcano, A; Bazzicalupo, M; Carlomagno, MS; Bruni, CB. Histidine biosynthetic pathway and genes: structure, regulation, and evolution. **Microbiol. Rev.** v.60, p.44–69, 1996.
52. Ames, BN; Garry, B; Herzenberg, LA. The genetic control of the enzymes of histidine biosynthesis in *Salmonella typhimurium*. **J. Gen. Microbiol.** v.22, p.369–378, 1960.
53. Stepansky, A; Leustek, T. Histidine biosynthesis in plants. **Amino Acids**. v.30, p.127–142, 2006.
54. Javid-Majd, F; Yang, D; Ioerger, TR; Sacchettini, JC. The 1.25 Å resolution structure of phosphoribosyl-ATP pyrophosphohydrolase from

Mycobacterium tuberculosis. **Acta Crystallogr. D Biol. Crystallogr.** v.64, p.627–635, 2008.

55. D'Ordine, R.L; Linger, RS; Thai, CJ; Davisson, VJ. Catalytic zinc site and mechanism of the metalloenzyme PR-AMP cyclohydrolase. **Biochemistry**. v.51, p.5791–5803, 2012.
56. Sivaraman, J; Myers, RS; Boju, L; Sulea, T; Cygler, M; Jo Davisson, V; Schrag, JD. Crystal structure of *Methanobacterium thermoautotrophicum* phosphoribosyl-AMP cyclohydrolase Hisl. **Biochemistry**. v.44, p.10071–10080, 2005.
57. Målen, H; Pathak, S; Søfteland, T; de Souza, GA; Wiker, HG. Definition of novel cell envelope associated proteins in Triton X-114 extracts of *Mycobacterium tuberculosis* H37Rv. **BMC Microbiol.** v.10, p.132, 2010.
58. Smith, DW; Ames, BN. Phosphoribosyladenosine monophosphate, an intermediate in histidine biosynthesis. **J. Biol. Chem.** v.240, p.3056–3063, 1965.
59. Carlomagno, MS; Chiariotti, L; Alifano, P; Nappo, AG; Bruni, CB. Structure and function of the *Salmonella typhimurium* and *Escherichia coli* K-12 histidine operons. **J. Mol. Biol.** v.203, p.585–606, 1988.
60. Fujimori, K; Tada, S; Kanai, S; Ohta, D. Molecular cloning and characterization of the gene encoding N’-[5'-phosphoribosyl]-formimino]-5-aminoimidazole-4-carboxamide ribonucleotide (BBM II) isomerase from *Arabidopsis thaliana*. **Mol. Gen. Genet.** v.259, p.216–223, 1998.
61. Crane, DI; Gould, SJ. The *Pichia pastoris* HIS4 gene: nucleotide sequence, creation of a non-reverting his4 deletion mutant, and development of HIS4-based replicating and integrating plasmids. **Curr. Genet.** v.26, p.443–450, 1994.
62. Donahue, TF; Farabaugh, PJ; Fink, GR. The nucleotide sequence of the HIS4 region of yeast. **Gene**. v.18, p.47–59, 1982.
63. Legerton, TL; Yanofsky, C. Cloning and characterization of the multifunctional his-3 gene of *Neurospora crassa*. **Gene**. v.39, p.129–140, 1985.
64. Lunardi, J; Nunes JES; Bizarro, CV; Basso, LA; Santos, DS; Machado, P. Targeting the Histidine Pathway in *Mycobacterium tuberculosis*. **Current Topics in Medicinal Chemistry**. v.13, p.2866-2884, 2013.
65. Due, AV; Kuper, J; Geerlof, A; von Kries, JP; Wilmanns, M. Bisubstrate specificity in histidine/tryptophan biosynthesis isomerase from *Mycobacterium tuberculosis* by active site metamorphosis. **Proc. Natl. Acad. Sci. U.S.A.** v.108, p.3554–3559, 2011.

66. Barona-Gómez, F; Hodgson, DA. Occurrence of a putative ancient-like isomerase involved in histidine and tryptophan biosynthesis. **EMBO Rep.** v.4, p.296–300, 2003.
67. Beismann-Driemeyer, S; Sterner, R. Imidazole glycerol phosphate synthase from *Thermotoga maritima*. Quaternary structure, steady-state kinetics, and reaction mechanism of the bienzyme complex. **J. Biol. Chem.** v.276, p.20387–20396, 2001.
68. Klem, TJ; Chen, Y; Davisson, VJ. Subunit interactions and glutamine utilization by *Escherichia coli* imidazole glycerol phosphate synthase. **J. Bacteriol.** v.183, p.989–996, 2001.
69. Chittur, SV; Chen, Y; Davisson, VJ. Expression and purification of imidazole glycerol phosphate synthase from *Saccharomyces cerevisiae*. **Protein Expr. Purif.** v.18, p.366–377, 2000.
70. Brilli, M; Fani, R. Molecular evolution of *hisB* genes. **J. Mol. Evol.** v.58, p.225–237, 2004.
71. Hawkes, TR; Thomas, PG; Edwards, LS; Rayner, SJ; Wilkinson, KW; Rice, DW. Purification and characterization of the imidazoleglycerol-phosphate dehydratase of *Saccharomyces cerevisiae* from recombinant *Escherichia coli*. **Biochem. J.** v.306, n.2, p.385–397, 1995.
72. Parker, AR; Moore, TD; Edman, JC; Schwab, JM; Davisson, VJ. Cloning, sequence analysis and expression of the gene encoding imidazole glycerol phosphate dehydratase in *Cryptococcus neoformans*. **Gene.** v.145, p.135–138, 1994.
73. Mano, J; Hatano, M; Koizumi, S; Tada, S; Hashimoto, M; Scheidegger, A. Purification and properties of a monofunctional imidazoleglycerol-phosphate dehydratase from wheat. **Plant Physiol.** v.103, p.733–739, 1993.
74. Ames, BN; Mitchell, HK. The biosynthesis of histidine; imidazoleglycerol phosphate, imidazoleacetol phosphate, and histidinol phosphate. **J. Biol. Chem.** v.212, p.687–696, 1955.
75. Ames, BN. The biosynthesis of histidine; D-erythro-imidazoleglycerol phosphate dehydrase. **J. Biol. Chem.** v.228, p.131–143, 1957.
76. Ahangar, MS; Khandokar, Y; Nasir, N; Vyas, R; Biswal, BK. HisB from *Mycobacterium tuberculosis*: cloning, overexpression in *Mycobacterium smegmatis*, purification, crystallization and preliminary X-ray crystallographic analysis. **Acta Crystallogr. Sect. F Struct. Biol. Cryst. Commun.** v.67, p.1451–1456, 2011.
77. Fani, R; Brilli, M; Fondi, M; Lió, P. The role of gene fusions in the evolution of metabolic pathways: the histidine biosynthesis case. **BMC Evol. Biol.** v.7, n.2, S4, 2007.

78. Nasir, N; Vyas, R; Biswal, BK. Sample preparation, crystallization and structure solution of HisC from *Mycobacterium tuberculosis*. **Acta Crystallogr. Sect. F Struct. Biol. Cryst. Commun.** v.69, p.445–448, 2013.
79. Weigent, DA.; Nester, EW. Purification and properties of two aromatic aminotransferases in *Bacillus subtilis*. **J. Biol. Chem.** v.251, p.6974–6980, 1976.
80. Weigent, DA; Nester, EW. Regulation of histidinol phosphate aminotransferase synthesis by tryptophan in *Bacillus subtilis*. **J. Bacteriol.** v.128, p.202–211, 1976.
81. Adams, E. The enzymatic synthesis of histidine from histidinol. **J Biol Chem.** v.209, p.829-846, 1954.
82. Adams, E. L-Histidinal, a biosynthetic precursor of histidine. **J Biol Chem.** v.217, p.325-344, 1955.
83. Loper, JC; Adams, E. Purification and properties of histidinol dehydrogenase from *Salmonella typhimurium*. **J. Biol. Chem.** v.240, p.788–795, 1965.
84. Grubmeyer, CT; Chu, KW; Insinga, S. Kinetic mechanism of histidinol dehydrogenase: histidinol binding and exchange reactions. **Biochemistry**. v.26, p.3369–3373, 1987.
85. Barbosa, JARG; Sivaraman, J; Li, Y; Larocque, R; Matte, A; Schrag, JD; Cygler, M. Mechanism of action and NAD⁺-binding mode revealed by the crystal structure of L-histidinol dehydrogenase. **Proc. Natl. Acad. Sci. U.S.A.** v.99, p.1859–1864, 2002.
86. Parish, T. Starvation survival response of *Mycobacterium tuberculosis*. **J. Bacteriol.** v.185, p.6702–6706, 2003.
87. Sassetti, CM; Boyd, DH; Rubin, EJ. Genes required for mycobacterial growth defined by high density mutagenesis. **Mol. Microbiol.** v.48, p.77–84, 2003.
88. Parish, T; Stoker, NG. Mycobacteria: bugs and bugbears (two steps forward and one step back). **Mol. Biotechnol.** v.13, p.191–200, 1999.
89. Agüero, F; Al-Lazikani, B; Aslett, M; Berriman, M; Buckner, FS; Campbell, RK; et al. Genomic-scale prioritization of drug targets: the TDR Targets database. **Nat Rev Drug Discov.** v.7, p.900–907, 2008.
90. Köhler, S; Foulongne, V; Ouahrani-Bettache, S; Bourg, G; Teyssier, J; Ramuz, M.; Liautard, J.-P. The analysis of the intramacrophagic virulome of *Brucella suis* deciphers the environment encountered by the pathogen inside

- the macrophage host cell. **Proc. Natl. Acad. Sci. U.S.A.** v.99, p.15711–15716, 2002.
91. Fields, PI; Swanson, RV; Haidaris, CG; Heffron, F. Mutants of *Salmonella typhimurium* that cannot survive within the macrophage are avirulent. **Proc. Natl. Acad. Sci. U.S.A.** v.83, p.5189–5193, 1986.
92. Pilatz, S; Breitbach, K; Hein, N; Fehlhaber, B; Schulze, J; Brenneke, B; Eberl, L; Steinmetz, I. Identification of *Burkholderia pseudomallei* genes required for the intracellular life cycle and in vivo virulence. **Infect. Immun.** v.74, p.3576–3586, 2006.
93. Grubmeyer, C; Skiadopoulos, M; Senior, AE. L-histidinol dehydrogenase, a Zn²⁺-metalloenzyme. **Arch. Biochem. Biophys.**, v.272, p.311–317, 1989.
94. DeJesus, MA; Zhang, YJ; Sassetti, CM; Rubin, EJ; Sacchettini, JC; Ioerger, TR. Bayesian analysis of gene essentiality based on sequencing of transposon insertion libraries. **Bioinformatics**. v.29, p.695–703, 2013.
95. Nunes, JES; Ducati, RG; Breda, A; Rosado, LA; de Souza, BM; Palma, MS; Santos, DS; Basso, LA. Molecular, kinetic, thermodynamic, and structural analyses of *Mycobacterium tuberculosis* *hisD*-encoded metal-dependent dimeric histidinol dehydrogenase (EC 1.1.1.23). **Arch. Biochem. Biophys.** v.512, p.143–153, 2011.
96. Lopez, M; Köhler, S; Winum, J-Y. Zinc metalloenzymes as new targets against the bacterial pathogen Brucella. **J. Inorg. Biochem.** v.111, p.138–145, 2012.
97. Teng, H; Grubmeyer, C. Mutagenesis of histidinol dehydrogenase reveals roles for conserved histidine residue. **Biochemistry**. v.38, p.7363–7371, 1999.
98. Dancer, JE; Ford, MJ; Hamilton, K; Kilkelly, M; Lindell, SD; O'Mahony, M.J; Saville-Stones, EA. Synthesis of potent inhibitors of histidinol dehydrogenase. **Bioorg. Med. Chem. Lett.**, v.6, p.2131-2136, 1996.
99. Grubmeyer, CT; Insinga, S; Bhatia, M.; Moazami, N. *Salmonella typhimurium* histidinol dehydrogenase: complete reaction stereochemistry and active site mapping. **Biochemistry**. v.28, p.8174- 8180, 1989
100. Abdo, M-R; Joseph, P; Boigegrain, R-A; Lautard, J-P; Montero, J-L; Köhler, S; Winum, J-Y. *Brucella suis* histidinol dehydrogenase: synthesis and inhibition studies of a series of substituted benzylic ketones derived from histidine. **Bioorg. Med. Chem.** v.15, p.4427-4433. 2007
101. Abdo, M-R; Joseph, P; Boigegrain, R-A; Montero, J-L; Köhler, S; Winum, J-Y. *Brucella suis* histidinol dehydrogenase: synthesis and inhibition

- studies of substituted N-L-histidinylphenylsulfonyl hydrazide. **J Enzyme Inhib Med Chem.** v.23, n.3, p.357–361, 2008.
102. Abdo, M-R; Joseph, P; Mortier, J; Turtaut, F; Montero, J-L; Masereel, B; et al. Anti-virulence strategy against *Brucella suis*: synthesis, biological evaluation and molecular modeling of selective histidinol dehydrogenase inhibitors. **Org. Biomol. Chem. OBC.** v.9, p.3681, 2011.
103. Basso, LA; Blanchard, JS. Resistance to antitubercular drugs. **Adv Exp Med Biol.** v.456, p.115-144, 1998.
104. Ramaswamy, S; Musser, JM. Molecular genetic basis of antimicrobial agent resistance in *Mycobacterium tuberculosis*: 1998 update. **Tuber Lung Dis.** v.79, p.3-29, 1998.
105. Heifets, LB. Antimycobacterial drugs. **Semin Respir Infect.** v.9, p.84-103, 1994.
106. Dutt, AK, Stead, W. The treatment of tuberculosis. **Dis Mon.** v.43, p.247-274, 1994.
107. Hingley-Wilson, SM; Sambandamurthy, VK; Jacobs; WRJr. Survival perspectives from the world's most successful pathogen, *Mycobacterium tuberculosis*. **Nat Immunol.** v.4, p.949-955, 2003.
108. Gomez, JE; McKinney, JD. *M. tuberculosis* persistence, latency, and drug tolerance. **Tuberculosis.** v.84, p.29-44, 2004.
109. Morel, CM; Acharya, T; Broun, D; Dangi, A; Elias, C; Ganguly, NK; et al. Health innovation networks to help developing countries address neglected diseases. **Science.** v.309, 401-404, 2005.
110. Gorish, H; Holke, W. Binding of histidinal to histidinol dehydrogenase. **Eur J Biochem.** v.150, p.305-308, 1985.
111. Robertson, JG. Enzymes as a special class of therapeutic target: clinical drugs and modes of action. **Curr Opin Struct Biol.** v. 17, p. 674–679, 2007.
112. Grubmeyer, C; Teng, H. Mechanism of *Salmonella typhimurium* histidinol dehydrogenase: kinetic isotope effects and pH profiles. **Biochemistry.** v.38, p.7355-7362, 1999.
113. Vopel, T; Makhatadze, G. Enzyme activity in the crowded milieu. **Plos One.** v.7, p.e39418, 2012.
114. Palomino, J-C; Martin, A; Camacho, M; Guerra, H; Swings, J; Portaels, F. Resazurin Microtiter Assay Plate: simple and inexpensive method for detection of drug resistance in *Mycobacterium tuberculosis*. **Antimicrob Agents Chemother.** v.46, p.2720-2722, 2002.

Anexos

ANEXO A – Carta de submissão do
artigo científico do Capítulo 2 no
periódico *Journal of Biological
Chemistry*, 2015

ANEXO B – Artigo publicado
“Production of human annexin V by
fed-batch cultivation”

Anexo A

Carta de submissão do artigo
científico do Capítulo 2 no periódico
Journal of Biological Chemistry, 2015

De: jbc@asbmb.org [jbc@asbmb.org]
Enviado: quinta-feira, 11 de junho de 2015 21:01
Para: Pablo Machado
Assunto: JBC/2015/672022 Manuscript Submission

MS ID#: JBC/2015/672022
MS TITLE: Mycobacterium tuberculosis histidinol dehydrogenase: biochemical characterization and inhibition studies

Dear Dr. Machado:

This is an automatic message acknowledging your online submission
to The Journal of Biological Chemistry.

Thank you for your submission.

Sincerely,

Editorial Staff
The Journal of Biological Chemistry

Sent on: June 11, 2015

Anexo B

Production of human annexin V by fed-batch cultivation

Artigo científico publicado no
periódico *BMC Biotechnology*, v.14,
p.33, 2014.

RESEARCH ARTICLE

Open Access

Production of recombinant human annexin V by fed-batch cultivation

Laura S Marder^{1,2†}, Juleane Lunardi^{2,4†}, Gaby Renard⁴, Diana C Rostirolla^{1,3}, Guilherme O Petersen^{1,2,4}, José E S Nunes⁴, Ana Paula D de Souza⁵, Ana Christina de O Dias⁴, Jocelei M Chies⁴, Luiz A Basso^{1,2,3}, Diógenes S Santos^{1,2,3} and Cristiano V Bizarro^{1,2*}

Abstract

Background: Annexin V, a 35.8 kDa intracellular protein, is a Ca^{2+} -dependent phospholipid binding protein with high affinity to phosphatidylserine (PS), which is a well-known hallmark of apoptosis. Annexin V is a sensitive probe for PS exposure upon the cell membrane, and used for detection of apoptotic cells both *in vivo* and *in vitro*. Large-scale production of recombinant human annexin V is worth optimization, because of its wide use in nuclear medicine, radiolabeled with $^{99\text{m}}\text{Tc}$, for the evaluation of cancer chemotherapy treatments, and its use in identification of apoptotic cells in histologic studies. Here we describe the high-yield production of a tag-free version of human annexin V recombinant protein by linear fed-batch cultivation in a bioreactor.

Results: We cloned the human ANXA5 coding sequence into the pET-30a (+) expression vector and expressed rhANXA5 in batch and fed-batch cultures. Using *E. coli* BL21 (DE3) in a semi-defined medium at 37°C, pH 7 in fed-batch cultures, we obtained a 45-fold increase in biomass production, respective to shaker cultivations. We developed a single-step protocol for rhANXA5 purification using a strong anion-exchange column (MonoQ HR16/10). Using these procedures, we obtained 28.5 mg of homogeneous, nontagged and biologically functional human annexin V recombinant protein from 3 g wet weight of bacterial cells from bioreactor cultures. The identity and molecular mass of rhANXA5 was confirmed by mass spectrometry. Moreover, the purified rhANXA5 protein was functionally evaluated in a FITC-annexin V binding experiment and the results demonstrated that rhANXA5 detected apoptotic cells similarly to a commercial kit.

Conclusions: We describe a new fed-batch method to produce recombinant human annexin V in large scale, which may expand the commercial utilities for rhANXAV to applications such as *in vivo* imaging studies.

Keywords: Recombinant human annexin v, Fed-batch cultivation, Large-scale, Apoptosis detection

Background

Annexin V, formerly known as human placental anticoagulation protein, is a member of a family of calcium-dependent phospholipid binding proteins [1] that binds preferentially to phosphatidylserine (PS), a negatively charged phospholipid highly enriched in the inner leaflet of plasma membranes [2]. Annexin V shows minimal capacity to bind phospholipids that are constitutively present

in the outer leaflet of plasma membranes, such as phosphatidylcholine and sphingomyelin [1]. During the early stages of apoptosis, cells expose PS on the surface, which is specifically recognized by phagocytic cells [3]. The exposed PS residues can be bound selectively by annexin V with nanomolar to picomolar affinity [4,5]. Because of the role of apoptosis in the pathophysiology of many diseases, there is a wide range of current and potentially new applications for annexin V as an apoptotic marker in clinical diagnosis [6]. Staining cells simultaneously with annexin V labeled with the fluorochrome fluorescein isothiocyanate (FITC) and the non-vital dye propidium iodide (PI) allows the discrimination among intact cells ($\text{FITC}^-/\text{PI}^-$) early apoptotic cells ($\text{FITC}^+/\text{PI}^-$) and late

* Correspondence: cristiano.bizarro@pucrs.br

†Equal contributors

¹Centro de Pesquisas em Biologia Molecular e Funcional (CPBMF), Instituto Nacional de Ciéncia e Tuberculose (INCT-TB), Pontifícia Universidade Católica do Rio Grande do Sul (PUCRS), Av. Ipiranga 6681, 90619-900 Porto Alegre, Brazil

²Programa de Pós-Graduação em Biologia Celular e Molecular, PUCRS, Porto Alegre 90619-900, Brazil

Full list of author information is available at the end of the article

apoptotic or necrotic cells ($\text{FITC}^+/\text{PI}^+$) [7]. Moreover, recombinant human annexin V (rhANXA5) serves as an important *in vivo* diagnostic tool when labeled with different radionuclides, such as iodine-123 (^{123}I) and the metastable isotope technetium-99 ($^{99\text{m}}\text{Tc}$) providing a broad range of imaging applications in apoptosis research, as single-photon emission computed tomography and autoradiography to positron emission tomography [8]. In nuclear medicine, annexin V radiolabeled with $^{99\text{m}}\text{Tc}$ or ^{123}I is used to evaluate the efficacy of cancer therapy and disease progression or regression [9].

Because of its widespread use as a diagnostic tool, rhANXA5 is commercially produced in microorganisms such as *Escherichia coli* using recombinant DNA techniques [10-13]. To produce rhANXA5 in large scale in this study, we used *E. coli*, the most commonly used host for recombinant protein production [14]. In shake flask cultures, all components are added at the start of the cultivation, without the need to monitor or control any parameter such as pH or the level of dissolved oxygen, leading to slow growth and low recombinant protein production [15]. High cell-density culture techniques have been developed to improve productivity and to provide advantages such as reduced culture volume, enhanced downstream processing, reduced wastewater, lower production costs and reduced investment in equipment [14]. Fed-batch cultivation is an effective and simple method [16], allowing substantial concentrations of glucose, an inexpensive and readily usable carbon and energy source [17]. To our knowledge, there is currently no protocol available for a bioreactor-based, large-scale production of rhANXA5.

In this work, we describe a procedure for the production of 28.5 mg of homogeneous, nontagged rhANXA5 from 3 g wet weight of bacterial cells from bioreactor cultures. The identity and absence of host contaminants in purified rhANXA5 was confirmed by LC-MS/MS peptide mapping experiments. The molecular mass determination of intact rhANXA5 confirmed the integrity of the purified protein. Additionally, the produced rhANXA5 protein was shown to be functional in a bioassay for *in vitro* apoptosis/necrosis detection, in which it performed similarly to a commercially available kit.

Results and discussion

Cloning and expression of rhANXA5

The gene encoding human Annexin V, *ANXA5*, is located on human chromosome 4q27 locus and spans a region of DNA 29 kb in length containing 13 exons and 12 introns. *ANXA5* encodes a 35.8 kDa protein of 320 amino acid residues in length which is translated from a single mature transcript of approximately 1.6 kb [18]. The human *ANXA5* coding sequence was subcloned into the pET-30a (+) expression vector to generate the recombinant pET-30a (+)::ANXA5 plasmid. Both the sequence and the absence of

PCR-introduced mutations in the *ANXA5* coding sequence were confirmed by automated sequencing.

The BL21 (DE3) and C41 (DE3) *E. coli* strains were transformed with the pET-30a (+)::ANXA5 construct by electroporation. The expression profiles were tested in lysogeny broth (LB) and in our semi-defined (SD) medium. The best results of soluble recombinant protein production from shaker cultivation were obtained using the BL21 (DE3) strain in SD medium induced with 1 mM IPTG at 37°C (Additional file 1: Figures S1 and Figure S2).

Bioreactor cultivation

The best growth conditions found in shaker cultivations were applied to the bioreactor batch and fed-batch cultures. We employed our SD medium and a temperature of 37°C in all experiments.

Transformed BL21 (DE3) *E. coli* was grown from a master cell bank (MCB) under batch cultivation in 1 L of SD medium at 37°C monitoring glucose consumption. Within 4 h, glucose was depleted from media, indicating this was the right time to start feeding. We compared DO-stat, pH-stat and linear ascending feeding strategies in uninduced cultures. A biomass concentration of 26.01 g (DCW) L^{-1} was attained in an uninduced culture using the linear ascending feeding profile [17]. Lower values for biomass concentration were obtained using DO-stat (20.15 g (DCW) L^{-1}) or pH-stat (11.59 g (DCW) L^{-1}) feeding strategies. Therefore, we selected the linear ascending feeding strategy for further fed-batch cultivations.

After 4 h of batch cultivation without feeding, the biomass concentration reached 4.71 g (DCW) L^{-1} ($n = 4$, SD = 0.6). We induced rhANXA5 expression in fed-batch cultivations with linear ascending feeding by adding IPTG to a final concentration of 1 mM. From three independent fermentations, we obtained a mean value of 27.48 g (DCW) L^{-1} (SD = 1.96) for the biomass concentration and a total protein content of 4.8 g L^{-1} (Figure 1). In contrast, we obtained a biomass concentration of 0.615 g (DCW) L^{-1} in shaker cultivation ($\text{OD}_{600\text{nm}} = 1.84$) after 6 h of culture. This represents a 45-fold increase in biomass concentration.

In an independent bioreactor cultivation, we performed densitometric analysis of culture samples (in triplicate) to calculate the product yield (g (rhANXA5) L^{-1}), the productivity (g (rhANXA5) $\text{L}^{-1} \text{ h}^{-1}$) and the specific yield (g (rhANXA) g (DCW) $^{-1}$). rhANXA5 corresponded to 40.6% (mean value) of the total protein content ($n = 3$, SD = 0.03) (Additional file 1: Figure S4). Therefore, we obtained a product yield of 1.95 g (rhANXA5) L^{-1} of culture medium, a specific yield of 0.0715 g (rhANXA5) g (DCW) $^{-1}$ and a productivity of 0.065 g (rhANXA5) $\text{L}^{-1} \text{ h}^{-1}$, considering the entire fermentation period (30 h).

Moreover, we can consider the entire procedure, from bioreactor cultivation to protein purification, and calculate

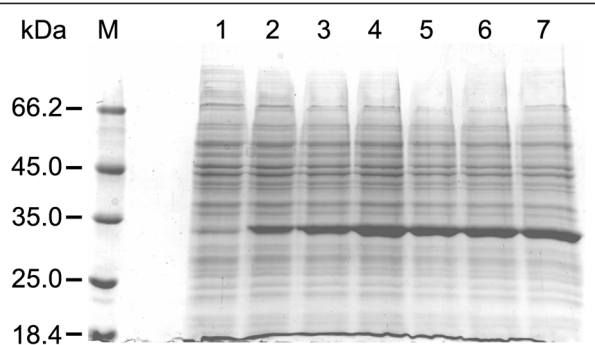


Figure 1 SDS-PAGE analysis of rhANXA5 expression in fed-batch cultivations. Recombinant *E. coli* BL21(DE3) cells were cultivated in semi-defined (SD) media for 30 h in fed-batch cultivations. Feeding started 4 h after the beginning of batch cultivation and rhANXA5 expression was induced after 18 h of cultivation by the addition of 1 mM IPTG to the cultures. M: Thermo Scientific™ Unstained Protein MW Marker; lane 1: sample collected immediately before IPTG induction (18 h culture); lanes 2–7: samples collected after IPTG induction from 20 h (lane 2), 22 h (lane 3), 24 h (lane 4), 26 h (lane 5), 28 h (lane 6), and 30 h (lane 7) cultures.

the yield and productivity of homogeneous rhANXA5. From four independent purifications, we obtained a mean value of 28.5 mg of purified rhANXA5 from 3 g wet weight of cells ($n = 4$, SD = 6.7). In terms of volumetric yield, we obtained (mean value) 0.983 g (purified rhANXA5) L^{-1} ($n = 4$, SD = 0.23). The productivity over the entire fermentation (30 h) was 0.0361 g (purified rhANXA5) $L^{-1} h^{-1}$ ($n = 4$, SD = 0.0084).

Purification

The overexpressed protein was purified by a single-step protocol consisting of a strong anion-exchange column (MonoQ HR16/10). Figure 2 shows the steps of rhANXA5 purification. The target protein eluted at approximately 190 mM of NaCl from a MonoQ HR 16/10 column (Additional file 1: Figure S3). The eluted protein was pooled and dialyzed against HEPES 100 mM NaCl pH 7.2, concentrated using an AMICON ultra-filtration membrane and stored at -80°C in 1 mL aliquots. This purification protocol yielded 28.5 mg of purified rhANXA5 from 3 g wet weight of cells ($n = 4$, SD = 6.7).

rhANXA5 identification by mass spectrometry

Homogeneous rhANXA5 samples were desalting and digested with trypsin, and the peptide mixtures were analyzed in LC-MS/MS peptide mapping experiments. A total of 320 spectra were identified with 29 different peptides derived from rhANXA5 protein. These peptides covered 80% of the rhANXA5 sequence.

Determination of rhANXA5 molecular mass

The spectra of intact rhANXA5 samples were recorded with a linear ion trap analyzer. Peaks spanning charge

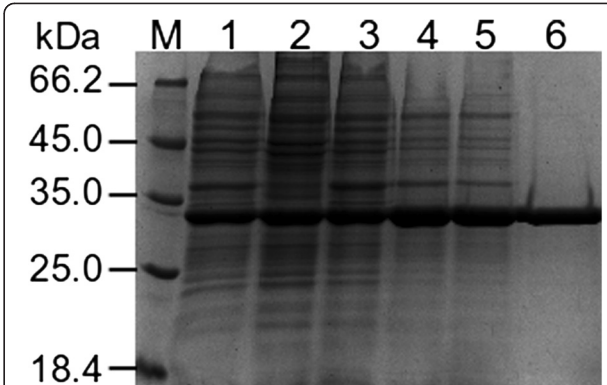


Figure 2 SDS-PAGE analysis of rhANXA5 purification steps. SDS-PAGE (12%) analysis of fractions from different steps of rhANXA5 purification. Each sample lane contains 8 µg of total protein. M corresponds to Thermo Scientific™ Unstained Protein MW Marker; lane 1: cells suspended in buffer A (50 mM Tris-HCl, pH 7.2, 10 mM CaCl₂) with no previous centrifugation step; lane 2: supernatant of cells in buffer A after sonication and centrifugation (for 20 min, 24,400 × g, 4°C); lane 3: cell pellet from the previous centrifugation suspended in buffer B (50 mM Tris-HCl, pH 7.2, 20 mM EDTA); lane 4: suspension from previous step dialyzed against 2 L of 20 mM Tris-HCl, pH 8.0 for 3 times, overnight in the first step, followed by two steps of dialysis 2 h each; lane 5: supernatant after centrifugation of dialyzed sample (for 30 min, 24,400 × g, 4°C); lane 6: homogeneous preparation of annexin V eluted from the Mono Q column.

states 18+ to 39+ were detected (Figure 3a) and the spectra deconvoluted. We obtained a value of 35,804 Da for the average molecular mass of rhANXA5 (Figure 3b), consistent with the post-translational removal of the N-terminal methionine (theoretical average molecular mass of 35,937 Da with methionine and 35,805 Da without methionine).

FITC-annexin V binding test

To test the functional activity of purified rhANXA5, we assayed its ability to detect cells undergoing apoptosis. We treated B16F10 cells with cisplatin to induce apoptosis and after 6 or 12 h, we stained treated cells simultaneously with the non-vital dye PI and with rhANXA5 labeled with the fluorochrome FITC. Double staining allows the discrimination between intact cells (FITC-/PI-), early apoptotic cells (FITC+/PI-) and late apoptotic or necrotic cells (FITC+/PI+) [7]. The ability of FITC-labeled rhANXA5 to detect apoptotic cells was compared with a commercial kit from BD. We performed dose curve experiments with different concentrations of cisplatin and stained treated cells for 6 h (Figure 4a) or 12 h (Figure 4b) after treatment. We obtained similar results using our home-made kit (QuattroG) or the commercial kit at different times after treatment (6 h or 12 h) and concentrations of cisplatin (20, 40, 80 and 160 µg/mL), indicating that purified rhANXA5 is functionally active. Dot plot representations

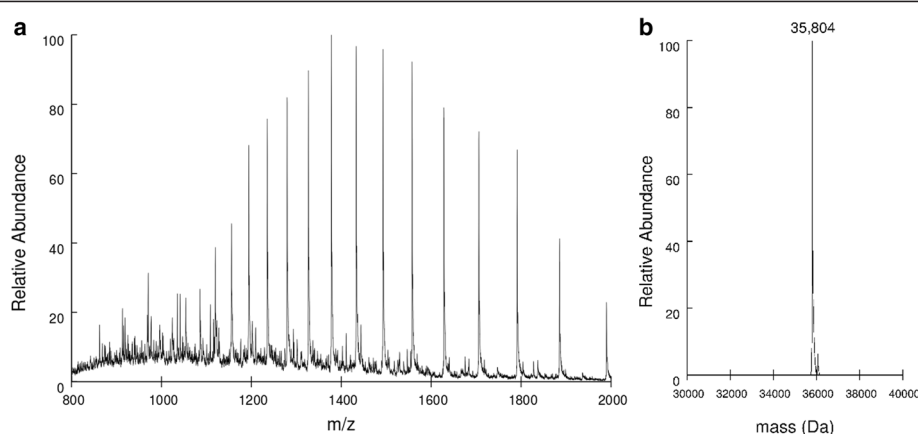


Figure 3 Determination of rhANXA5 molecular mass by mass spectrometry. **a)** ESI-FTMS spectra of rhANXA5 showing charge state distribution spanning from 18+ to 39+. **b)** Experimentally determined value of 35,804 Da for rhANXA5 average molecular mass after spectra deconvolution.

of flow cytometry experiments with cells stained 12 h after treatment clearly show differences in the distribution of FITC/PI cell populations between untreated cells (negative control), cells treated with 40 $\mu\text{g}/\text{mL}$ and cells treated with 160 $\mu\text{g}/\text{mL}$ of cisplatin (Figure 5).

Conclusions

Fed-batch cultivations represent an alternative to shaker cultivations, allowing control of process variables and improvement on biomass concentration and product yields [15]. A chimeric protein containing the C-terminus of hirudin fused to annexin V was previously expressed in large scale using fed-batch fermentation [19]. However, to the best of our knowledge, this is the first report of a scale up of rhANXA5 production.

Recombinant protein production methods must continuously be improved to meet commercial demands [14,20]. In this work, we produced 28.5 mg of purified recombinant human annexin V from 3 g wet weight of cells ($n = 4$, SD = 6.7) obtained in fed-batch cultures induced with IPTG. Moreover, this protocol generated a yield of homogeneous rhANXA5 (mean value) of 0.983 g (purified rhANXA5) L^{-1} ($n = 4$, SD = 0.23). The productivity over the entire fermentation (30 h) was 0.0361 g (purified rhANXA5) $\text{L}^{-1} \text{h}^{-1}$ ($n = 4$, SD = 0.0084).

rhANXA5 could be commercially distributed to several research groups and to radiopharmaceutical companies. The use of fluorescence-labeled annexin V to identify apoptotic cells is currently limited to histologic and cell-sorting studies performed *in vitro*. Its use for *in vivo* imaging studies is hampered mainly by cost issues. Hence, production in large scale may expand the commercial utilities for rhANXA5, reducing costs and allowing a greater access of the scientific and physician community to this product.

Methods

Strains and plasmids

The *E. coli* strains BL21(DE3) and C41(DE3) were purchased from Novagen® (EMD Biosciences, Inc., Madison, WI, USA) and Lucigen Corporation (Middleton, WI, USA), respectively. The PCR-Blunt® cloning vector was

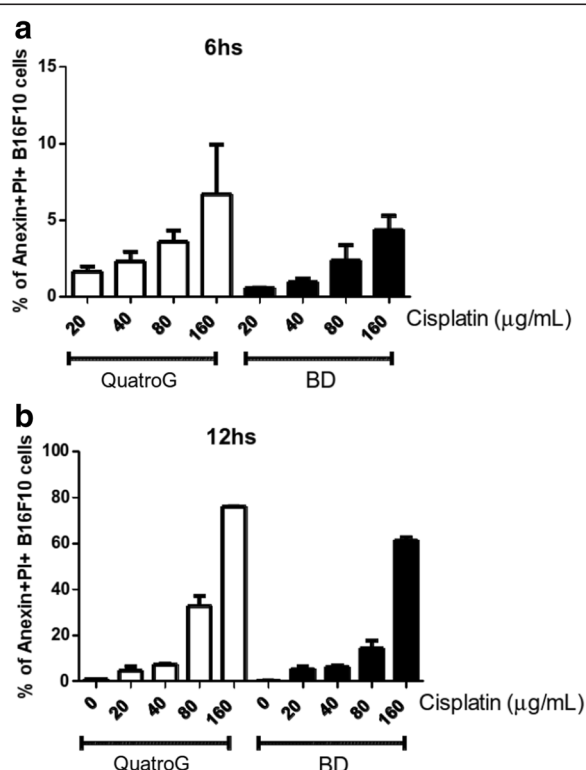


Figure 4 Analysis of apoptosis in B16F10 cells. Flow cytometric analysis of apoptotic cells stained with both FITC-labeled annexin V and PI using the BD Biosciences kit or a homemade kit (QuattroG) containing purified rhANXA5 conjugated with FITC. Apoptosis was induced by treating B16F10 cells with 20, 40, 80 or 160 $\mu\text{g}/\text{mL}$ of cisplatin and double staining was performed after 6 h **(a)** or 12 h **(b)**.

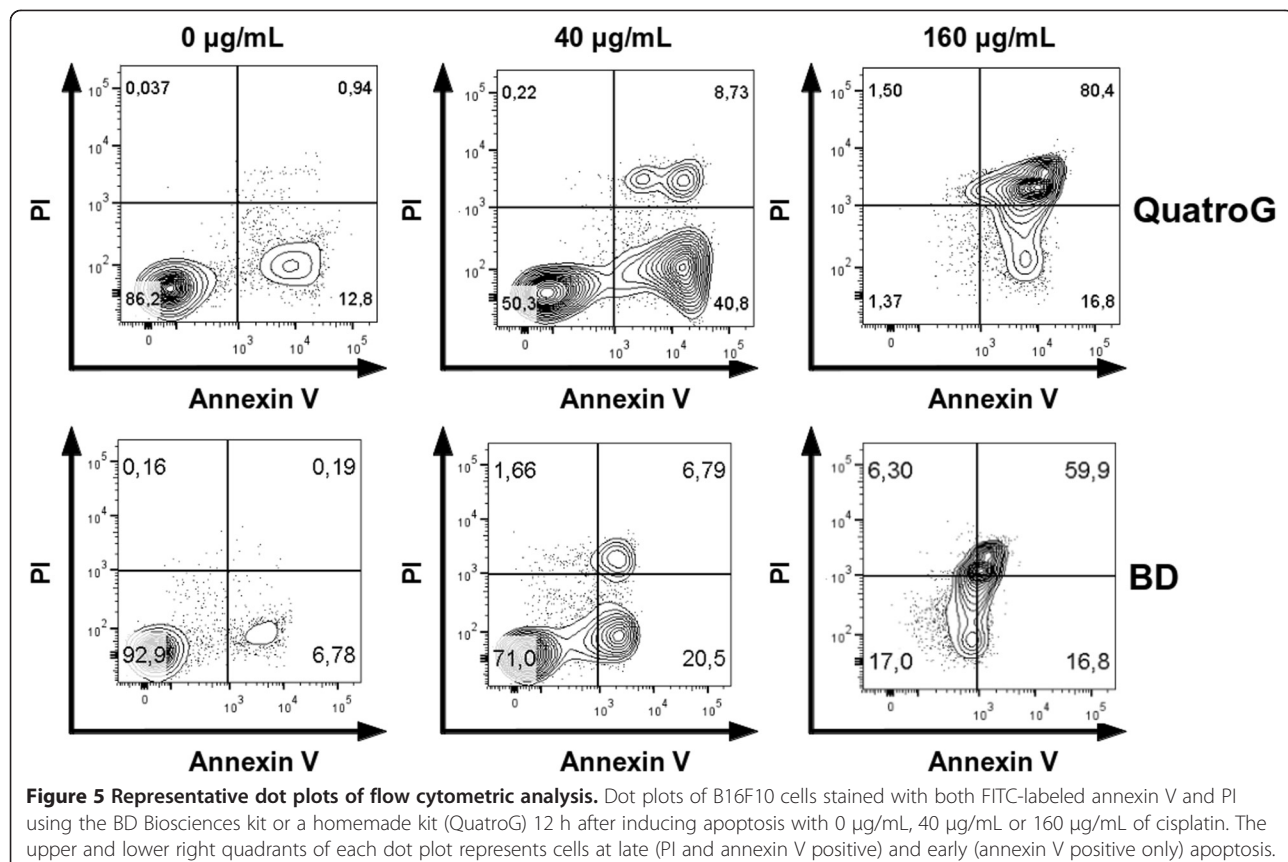


Figure 5 Representative dot plots of flow cytometric analysis. Dot plots of B16F10 cells stained with both FITC-labeled annexin V and PI using the BD Biosciences kit or a homemade kit (QuatroG) 12 h after inducing apoptosis with 0 μg/mL, 40 μg/mL or 160 μg/mL of cisplatin. The upper and lower right quadrants of each dot plot represents cells at late (PI and annexin V positive) and early (annexin V positive only) apoptosis.

purchased from Invitrogen® (Carlsbad, CA, USA) and the pET-30a (+) expression vector was from Novagen®.

Molecular cloning of rhANXA5

Oligonucleotides were designed based on the human ANXA5 coding sequence in the GenBank (accession number: NM_001154.3) National Institute of Health (NIH) genetic sequence database [18]. Specific primers were designed to contain *Nde*I (forward primer: 5' GCG CAT ATG GCA CAG GTT CTC AGA GGC ACT 3') and *Hind*III (reverse primer: 5' GCG AAG CTT TTA GTC ATC TTC TCC ACA GAG C 3') restriction sites (italics). The human ANXA5 gene sequence was PCR-amplified from a human blood cDNA sample.

The amplified ANXA5 coding sequence was cloned into the PCR-Blunt® vector, cleaved with *Nde*I and *Hind*III restriction endonucleases (New England BioLabs®, Ipswich, MA, USA) and subcloned into the pET-30a (+) expression vector, previously digested with the same restriction enzymes, to generate the pET-30a (+)::ANXA5 plasmid. The cloned ANXA5 sequence was confirmed by automated DNA sequencing.

Media preparation

Lysogeny broth (LB) (tryptone, 10 g L⁻¹; yeast extract, 5 g L⁻¹; NaCl, 10 g L⁻¹) was sterilized by autoclaving

(30 min at 121°C). LB medium was used for shake-flask cultivation and for inoculum development of bioreactor cultivations.

Semi-defined medium (SD) [21] was used for shake-flask cultivations as well as fed-batch bioreactor cultivations, as both initial batch and also feeding media (with varied glucose and MgSO₄ concentrations). SD medium contains 0.5 g L⁻¹ NaCl (a), 1 g L⁻¹ NH₄Cl (b), 20 g L⁻¹ yeast extract (c), 6 g L⁻¹ Na₂HPO₄ (d), 3 g L⁻¹ KH₂PO₄ (e), 1 μg L⁻¹ thiamine (f), 1 mM MgSO₄ (g), 0.1% trace solution (h), and 0.1 mM CaCl₂ (i). For both shake-flask and bioreactor fed-batch cultivations (initial batch culture), SD medium was supplemented with glucose to a final concentration of 5 g L⁻¹ (j). Components (a) to (e) were assembled and sterilized together by autoclaving (30 min at 121°C), while components (g) to (i) were sterilized separately by autoclaving and added under aseptic conditions. Thiamine solution (f) was filter-sterilized. Trace solution (h) contained 2.8 g L⁻¹ FeSO₄, 2 g L⁻¹ MnCl₂, 2 g L⁻¹ CaCl₂, 0.26 g L⁻¹ CuCl₂, and 0.3 g L⁻¹ ZnSO₄. For feeding medium in bioreactor cultivations, SD medium was supplemented with glucose (final concentration of 300 g L⁻¹) and MgSO₄ (40 mM). To prepare this feeding medium, we mixed equal parts of a 2x concentrated SD medium and a 600 g/L glucose stock solution, both sterilized separately. SD medium used in

bioreactor cultivations was also supplemented with 100 μL of Antifoam 204 (Sigma-Aldrich, São Paulo, SP, Brazil) per liter of culture. Both LB and SD media were supplemented aseptically with filter-sterilized kanamycin to a final concentration of 30 $\mu\text{g mL}^{-1}$.

Shake-flask cultivation

E. coli BL21(DE3) and C41(DE3) strains were transformed with the pET-30a (+) vector or the pET-30a (+)::ANXA5 recombinant plasmid by electroporation. Transformant colonies were selected on LB agar plates containing 30 $\mu\text{g mL}^{-1}$ kanamycin [22]. Isolated colonies were selected and grown overnight (at 37°C and 180 rpm) in 5 mL of LB supplemented with 30 $\mu\text{g mL}^{-1}$ kanamycin. To compare the expression profile with different strains (BL21(DE3) or C41(DE3)) or media (LB or SD medium), saturated cultures were inoculated in 50 mL of LB or SD medium for shake-flask cultivations and grown at 37°C and 180 rpm to an optical density ($\text{OD}_{600\text{nm}}$) of 0.4–0.6. At this growth stage, we induced rhANXA5 expression by adding isopropyl- β -D-thiogalactopyranoside (IPTG) to a final concentration of 1 mM. At 3, 6, 9 or 24 h after induction, cells were harvested by centrifugation (11,800 g) for 30 min at 4°C, and the pellet was stored at -20°C. The expression of the recombinant soluble protein was confirmed by 12% sodium dodecyl sulfate-polyacrylamide gel electrophoresis (SDS-PAGE) visualized by Coomassie® Brilliant Blue R-250 staining. For biomass measurements from shake-flask cultures, isolated colonies were selected and grown overnight (at 37°C and 180 rpm) in 10 mL of LB supplemented with 30 $\mu\text{g mL}^{-1}$ kanamycin and inoculated in 500 mL of SD medium. Inoculated cultures were grown (37°C and 180 rpm) to an optical density ($\text{OD}_{600\text{nm}}$) of 0.4–0.6, rhANXA5 expression was induced by the addition of IPTG to a final concentration of 1 mM, and cells were harvested after 6 h of IPTG induction.

Inoculum development for bioreactor cultivation

A master cell bank (MCB) of transformed *E. coli* BL21 (DE3) cells containing the pET-30a (+)::ANXA5 recombinant plasmid was prepared in 50% glycerol and stored at -80°C. For inoculum development, 150 μL of *E. coli* BL21(DE3) MCB cells (stored at -80°C) were grown overnight at 180 rpm and 37°C in 1 L flasks containing 250 mL of LB medium supplemented with 30 $\mu\text{g mL}^{-1}$ kanamycin. The final optical density (OD_{600}) for each pre-inoculum culture was determined spectrophotometrically. For each experiment, we calculated and collected the initial volume of pre-inoculum culture needed to start bioreactor cultivation with an initial OD_{600} of 0.1. Collected aliquots were diluted in LB medium to a final volume of 100 mL before inoculation in 900 mL of SD medium for bioreactor cultivation.

Bioreactor cultivation

Batch and fed-batch culture experiments were conducted in a BIOSTAT® B Plus bioreactor (Sartorius Stedim, Goettingen, Germany) with two 2 L stirred tanks, filled with 1 L of SD medium each, at 37°C, pH 7.0 and supplemented with kanamycin. For pH control, 12% (v/v) ammonium hydroxide and 10% (v/v) phosphoric acid were employed. The bioreactor was equipped with two Rushton turbines and with agitation, aeration, temperature and pH controllers. A polarographic electrode was used to measure the dissolved oxygen concentration (DOC) in the culture. The pO_2 , pH, stirrer speed, base and acid consumption and aeration rate were measured online and recorded by an external data acquisition and control system (Sartorius Stedim). Feeding was implemented using the bioreactor proprietary software micro-DCU system v. 0.63 (Sartorius Stedim) that allows controlling a peristaltic pump for feeding medium addition. The flow rate varied linearly from 0.066 mL min^{-1} (starting after 4 h of batch culture) to 0.594 mL min^{-1} after 26 h of feeding (30 h of bioreactor cultivation). In batch cultures, the DOC was maintained at 30% by cascading agitation (400–1000 rpm) with constant aeration rate (1 vvm), and the process was finished when the biomass reached stationary phase.

Fed-batch cultivations were started as batch cultures with feeding starting at 4 h of cultivation (approximately $\text{OD}_{600\text{nm}}$ 16.0) with SD as feeding medium (see subsection "Media preparation"). Different feeding strategies were tested. In DO-stat feeding fermentations, with DOC setpoint at 30%, the agitation rate was maintained at 800 rpm (after feeding initiation). In fed-batch fermentations with a linear ascending or pH-stat feeding, the DOC was maintained at 30% by cascading agitation (400–1000 rpm) with constant aeration rate (1 vvm).

For linear ascending feeding profile we used the following equation:

$$F = at + b$$

where F is the feeding rate (mL min^{-1}), t the cultivation time after initiation of the fed-batch culture (min) and, a and b are constants for the linear ascending feeding profile [23].

Analytical methods

Samples were withdrawn periodically for quantitative analysis along the cultivation. Cell growth was monitored by measuring the optical density at 600 nm ($\text{OD}_{600\text{nm}}$) in a spectrophotometer. One optical density unit was found to be equivalent to 0.3342 g L^{-1} of dry cell weight by gravimetric quantitation. Glucose concentration in the medium was measured with a glucose analyzer (model 2700 select, Yellow Springs Instruments, Yellow Springs, OH, USA). Acetate concentration was determined by high performance

liquid chromatography (Äkta Purifier, GE HealthCare®, São Paulo, Brazil) equipped with an Aminex HPX-87H column (Bio-Rad Laboratories, Hercules, CA, USA), using 0.005 M H₂SO₄ as mobile phase and a UV-detector. The protein expression was analyzed by 12% SDS-PAGE stained with Coomassie® Brilliant Blue R-250 staining. The annexin V protein produced was quantified using the Qubit® Protein Assay Kit (Invitrogen™, Life Technologies, São Paulo, SP, Brazil) and a Qubit® 2.0 Fluorometer (Invitrogen™).

Purification

ANXA5 recombinant protein was purified using a Fast Performance Liquid Chromatography (FPLC) ÄKTA Purifier System (GE HealthCare®). All chromatographic steps were carried out at 4°C. Sample elution was monitored by UV detection at 215, 254 and 280 nm and fractions were analyzed by 12% SDS-PAGE. According to a previous report [24], frozen cells (3 g wet weight) were suspended in 30 mL of buffer A (50 mM Tris HCl, 10 mM CaCl₂ pH 7.2) and incubated with 1 mM of phenylmethanesulfonylfluoride for 30 min at 4°C. The cells were disrupted by sonication (eight pulses of 10") and centrifuged at 38,900 g for 30 min. The supernatant was discarded and the pellet was completely dissolved in 30 mL of buffer B (50 mM Tris HCl, 20 mM EDTA pH 7.2), stirred for 30 min at 4°C, and clarified by centrifugation at 38,900 g for 30 min at 4°C. The supernatant was dialyzed against 20 mM Tris HCl pH 8.0 (3 × 2 L, 3 h each). Residual precipitate was removed by centrifugation (38,900 g for 20 min) and the supernatant was loaded on a MonoQ HR 16/10 anion exchange column (GE Healthcare) previously equilibrated with 20 mM Tris HCl pH 8.0. Protein was eluted with 25% linear gradient of 20 mM Tris HCl, 1 M NaCl pH 8.0 at 1 mL min⁻¹ flow rate. Homogeneous rhANXA5 was eluted at approximately 190 mM NaCl. Fractions containing homogeneous rhANXA5 were pooled, dialyzed against 20 mM N-2-hydroxyethylpiperazine-N'-2-ethanesulfonic Acid (HEPES), 100 mM NaCl pH 7.2 and concentrated using an AMICON (Millipore Corporation, Bedford, MA, USA) ultra-filtration membrane (MWCO = 10 kDa), and stored at -80°C. Protein concentration was determined with Qubit® Protein Assay Kit using a Qubit® 2.0 Fluorometer.

rhANXA5 identification by mass spectrometry

rhANXA5 preparations (1 nmol) were desalted and subjected to proteolytic degradation using trypsin. The resulting peptides were separated by chromatography using 15 cm capillary columns (150 µm i.d., Kinetex C18 core-shell particles, Phenomenex, Inc., Torrance, CA, USA) and a nanoLC Ultra 1D plus equipment (Eksigent, Redwood City, CA, USA). Separated peptides were analyzed using an LTQ-Orbitrap hybrid mass spectrometer

(Thermo Fisher Scientific Inc, Waltham, MA, USA). The chromatographic method used a step gradient from mobile phase A (0.1% formic acid in water) to mobile phase B (0.1% formic acid in acetonitrile): 0–2% B over 5 min; 2–10% B over 3 min; 10–60% B over 60 min; 60–80% B over 2 min; 80% B isocratic for 10 min; 80–2% B over 2 min; and 2% B isocratic for 8 min. We performed MS/MS fragmentation using collision-induced dissociation (CID) with an activation Q of 0.250, an activation time of 30.0 ms, and an isolation width of 1.0 Da. Using the Proteome Discoverer software (v. 1.3), we compared experimentally obtained MS and MS2 spectra with the *in silico* trypsin digestion of the human proteome. We allowed a precursor tolerance of 10 ppm, a fragment tolerance of 0.8 Da, static carbamidomethylation on cysteines, and oxidation on methionine residues. We restricted our analysis to matches with an Xcorr score > 2.0 for doubly charged ions and Xcorr score > 2.5 for triply charged ions.

Determination of rhANXA5 molecular mass

Purified rhANXA5 samples were desalted, reconstituted in acetonitrile 50%/MilliQ-water 49%/formic acid 1% and directly injected using a 500 µL syringe (Hamilton Company, Reno, NV, USA) in a static mode into an IonMax electrospray ion source. The electrospray source parameters were as follows: positive ion mode, 4.5 kV of applied voltage to the electrospray source, 5 arbitrary units (range 0–100) of sheath gas flow, 45.6 V of capillary voltage, 250°C of capillary temperature, and 238.8 V of tube lens voltage. Full spectra (600–2000 m/z range) were collected on a Thermo Orbitrap Discovery XL in profile mode using the linear ion trap analyzer (ITMS mode). The average spectrum was processed with the software MagTran [25] for charge state deconvolution.

FITC-annexin V binding test

To confirm the ability of rhANXA5 to detect cells undergoing apoptosis, we labeled rhANXA5 with the FluoroTag™ FITC Conjugation Kit (Sigma-Aldrich®). Our home-made kit also contained PI solution (Sigma-Aldrich®) and a 10 × binding buffer (0.1 M HEPES-NaOH pH 7.4, 1.4 M NaCl, 25 mM CaCl₂). B16F10 melanoma cells (4X10⁴), a kind gift from Dr. Peter Henson (National Jewish Center for Immunology, Denver, CO, USA) were cultured in Dulbecco's Modified Eagle's Medium (DMEM) supplemented with 10% fetal bovine serum (FBS), gentamicin 80 mg L⁻¹ (Novaferma, Anápolis, Brazil), and Fungisone 5 mg L⁻¹ (Bristol Myers Squibb, New York, NY, USA). To induce apoptosis, the cells were treated with cisplatin (Libbs, Embu, SP, Brazil) at different concentrations (0, 40, 80 and 160 µg/mL) and after 6 or 12 h, the cells were stained with our home-made kit or with a commercial kit from BD Biosciences (FITC Annexin Apoptosis Detection Kit II, BD Biosciences, San Diego, CA, USA).

Cells were stained at a concentration of 10^5 cells mL $^{-1}$ in 100 μ L of 10X Binding Buffer using 5 μ L of PI and 5 μ L of rhANXA5 conjugated with FITC (home-made kit) or 5 μ L of annexin-FITC from FITC Annexin Apoptosis Detection Kit II. All data were collected in a FACSCanto II flow cytometer (BD Bioscience) and analyzed using FlowJo software (Tree Stat, San Carlos, CA, USA).

Availability of supporting data

Supporting data are included in an additional file.

Additional file

Additional file 1: Figure S1. SDS-PAGE analysis (12%) of samples from shaker cultivations of *Escherichia coli* BL21(DE3) and C41(DE3) strains in lysogeny broth (LB) and in our semi-defined (SD) media. M - Thermo Scientific™ Unstained Protein MW Marker; Lanes 1 and 5 - pET-30a(+) (empty vector) without IPTG induction; lanes 2 and 6 - pET-30a (+)::ANXA5 without IPTG induction; lanes 3 and 7 - pET-30a (+) (empty vector) after 6h of IPTG induction; lane 4 - pET-30a(+)::ANXA5 after 3h of IPTG induction; lane 8 - pET-30a (+)::ANXA5 after 6 h of IPTG induction. **a)** C41(DE3) and LB. Overexpression of pET-30a (+)::ANXA5 in *E. coli* C41(DE3) strain using LB media. **b)** BL21(DE3) and LB. Overexpression of pET-30a (+)::ANXA5 in *E. coli* BL21(DE3) strain using LB media. **c)** C41(DE3) and SD. Overexpression of pET-30a (+)::ANXA5 in *E. coli* C41(DE3) strain using SD media. **d)** BL21(DE3) and SD. Overexpression of pET-30a (+)::ANXA5 in *E. coli* BL21(DE3) strain using SD media. **Figure S2.** Densitometric analysis of lanes 4 and 8 from Figure S1d. **Figure S3.** rhANXA5 purification in MonoQ HR16/10 column. **(a)** Eluted fractions from MonoQ HR16/10 were analysed by SDS-PAGE (12%). M corresponds to Unstained Protein MW Marker (Fermentas); Lane 1 corresponds to crude extract; Lanes 2–12 corresponds to MonoQ HR16/10 elution fractions. **(b)** Chromatogram of eluted fractions. rhANXA5 was eluted in fractions 118 to 125 (inlet). **Figure S4.** SDS-PAGE densitometric analysis of rhANXA5 expression in fed-batch cultivations. M: Thermo Scientific™ Unstained Protein MW Marker; Lanes 1–3: samples collected at 30 h of culture (triplicate). rhANXA5 corresponded to (1) 45.3%, (2) 38.6% and (3) 37.9% of total protein content.

Abbreviations

DOC: Dissolved oxygen concentration; FITC: Fluorescein isothiocyanate; HEPES: Hydroxyethylpiperazine-N'-2-ethanesulfonic acid; LB: Lysogeny broth; MCB: Master cell bank; PI: Propidium iodide; PS: Phosphatidylserine; rhANXA5: Recombinant human annexin V; TB: Terrific broth.

Competing interests

The authors declare that they have no competing interests.

Authors' contributions

LSM carried out part of the experiments and contributed to the manuscript writing. JL carried out part of the experiments and contributed to the manuscript writing. GR helped in fermentation and protein purification. DCR helped in cloning, amplification and purification. GOP generated the FITC-rhANXA5. JESN assisted in the production of rhANXA5 in the bioreactor. APDS conducted the FITC-annexin V binding experiments. ACOD helped in cloning and expression. CVB performed the identification and molecular mass determination of rhANXA5 by mass spectrometry and contributed to the manuscript writing. JMC and LAB assisted in most of the experiments and DSS devised the experiments. All authors read and approved the final manuscript.

Acknowledgements

Financial support for this work was provided by the National Institute of Science and Technology on Tuberculosis (Decit/SCIE/MS-MCT-CNPq-FNDCT-CAPES) and Millennium Initiative Program (CNPq), Brazil to DS and LB. DS (CNPq, 304051/1975-06) and LB (CNPq, 5201182/99-5) are research career

awardees of the National Council for Scientific and Technological Development of Brazil.

Author details

¹Centro de Pesquisas em Biologia Molecular e Funcional (CPBMF), Instituto Nacional de Ciéncia e Tuberculose (INCT-TB), Pontifícia Universidade Católica do Rio Grande do Sul (PUCRS), Av. Ipiranga 6681, 90619-900 Porto Alegre, Brazil.

²Programa de Pós-Graduação em Biologia Celular e Molecular, PUCRS, Porto Alegre 90619-900, Brazil. ³Programa de Pós-Graduação em Medicina e Ciéncias da Saúde, PUCRS, Porto Alegre 90619-900, Brazil. ⁴Quatro G Pesquisa & Desenvolvimento, LTDA, Porto Alegre 90619-900, Brazil. ⁵Instituto de Pesquisas Biomédicas (IPB), Laboratório de Imunologia Molecular, PUCRS, Porto Alegre 90619-900, Brazil.

Received: 5 August 2013 Accepted: 11 April 2014

Published: 27 April 2014

References

1. Crompton MR, Moss SE, Crompton MJ: Diversity in the Lipocortin/Calpastin Family. *Cell* 1988, **55**:1–3.
2. Schick PK, Kurica KB, Chacko GK: Location of phosphatidylethanolamine and phosphatidylserine in the human platelet plasma membrane. *J Clin Invest* 1976, **57**:1221–1226.
3. Fadok VA, Voelker DR, Campbell PA, Cohen JJ, Bratton DL, Henson PM: Exposure of phosphatidylserine on the surface of apoptotic lymphocytes triggers specific recognition and removal by macrophages. *J Immunol* 1992, **148**(7):2207–2216.
4. Tait JF, Gibson D, Fujikawa K: Phospholipid binding properties of human placental anticoagulant protein-I, a member of the lipocortin family. *J Biol Chem* 1989, **264**(14):7944–7949.
5. Andree HA, Reutelingsperger CP, Hauptmann R, Hemker HC, Hermens ET, Willems GM: Binding of vascular anticoagulant alpha (VAC alpha) to planar phospholipid bilayers. *J Biol Chem* 1990, **265**(9):4923–4928.
6. Blankenberg FG, Tait JF, Strauss HW: Apoptotic cell death: its implications for imaging in the next millennium. *Eur J Nucl Med* 2000, **27**(3):359–367.
7. Vermes I, Haanen C, Steffens-Nakken H, Reutelingsperger C: A novel assay for apoptosis Flow cytometric detection of phosphatidylserine expression on early apoptotic cells using fluorescein labeled Annexin V. *J Immunol Methods* 1995, **18**:39–51.
8. Lahorte CM, Vanderheyden JL, Steinmetz N, Van de Wiele C, Dierckx RA, Slegers G: Apoptosis-detecting radioligands: current state of the art and future perspectives. *Eur J Nucl Med Mol Imaging* 2004, **31**:887–919.
9. Yang DJ, Azhdarinia A, Wu P, Yu DF, Tansey W, Kalimi SK, Kim EE, Podoloff DA: In Vivo and In Vitro Measurement of Apoptosis in Breast Cancer Cells Using ^{99m}Tc-EC-Annexin V. *Cancer Biother Radiopharm* 2001, **16**:73–83.
10. Brumatti G, Sheridan C, Martin SJ: Expression and purification of recombinant annexin V for the detection of membrane alterations on apoptotic cells. *Methods* 2008, **44**:235–240.
11. Logue SE, Elgendi M, Martin SJ: Expression, purification and use of recombinant annexin V for the detection of apoptotic cells. *Nat Protoc* 2009, **4**:1383–1395.
12. Coxon KM, Duggan J, Cordeiro MF, Moss SE: Purification of annexin V and its use in the detection of apoptotic cells. *Methods Mol Biol* 2011, **731**:293–308.
13. Wang F, He XW, Yan HL, Huang JJ, Zhang Y, Jiang L, Gao YJ, Sun SH: Non-fusion expression in *Escherichia coli*: Single-step purification of recombinant human annexin A5 for detection of apoptosis. *Protein Expr Purif* 2006, **45**:80–87.
14. Lee SY: High cell-density culture of *Escherichia coli*. *Trends Biotechnol* 1996, **14**:98–105.
15. Krause M, Ukkonen K, Haataja T, Ruottinen M, Glumoff T, Neubauer A, Neubauer P, Vasala A: A novel fed-batch based cultivation method provides high cell-density and improves yield of soluble recombinant protein in shaken cultures. *Microb Cell Fact* 2010, **9**:1–11.
16. Kim BS, Lee SC, Lee SY, Chang YK, Chang HN: High cell density fed-batch cultivation of *Escherichia coli* using exponential feeding combined with pH-stat. *Bioprocess Biosyst Eng* 2004, **26**:147–150.
17. Luli GW, Strohl WR: Comparison of growth, acetate production, and acetate inhibition of *Escherichia coli* strains in batch and fed-batch fermentations. *Appl Environ Microbiol* 1990, **56**:1004–1011.

18. The National Center for Biotechnology Information (NCBI) - ANXA5 annexin A5 (*Homo sapiens* human). [<http://www.ncbi.nlm.nih.gov/gene/308>].
19. Yuan H, Yang X, Hua Z-C: Optimization of expression of an Annexin V-Hirudin chimeric protein in *Escherichia coli*. *Microbial Res* 2004, 159:147–156.
20. Choi JH, Keum KC, Lee SY: Production of recombinant proteins by high cell density culture of *Escherichia coli*. *Chemical Engineering Science* 2006, 61:876–885.
21. Roth G, Nunes JES, Rosado LA, Bizarro CV, Volpato G, Nunes CP, Renard G, Basso LA, Santos DS, Chies JM: Recombinant *Erwinia carotovora* I-asparaginase II production in *Escherichia coli* fed-batch cultures. *Braz J Chem Eng* 2013, 30(2):245–256.
22. Sambrook J, Russell DW: *Molecular Cloning: A Laboratory Manual*. 3rd edition. New York: CSHL Press; 2001:159–174.
23. Ayub MAZ: Fed-batch bioreactor process with recombinant *Saccharomyces cerevisiae* growing on cheese whey. *Braz J Chem Eng* 2006, 23(4):435–442.
24. Wood BL, Gibson DF, Tait JF: Increased erythrocyte phosphatidylserine exposure in sickle cell disease: flow-cytometric measurement and clinical associations. *Blood* 1996, 88:1873–1880.
25. Zhang Z, Marshall AG: A universal algorithm for fast and automated charge state deconvolution of electrospray mass-to-charge ratio spectra. *J Am Chem Soc Mass Spectrom* 1998, 9:225–233.

doi:10.1186/1472-6750-14-33

Cite this article as: Marder et al.: Production of recombinant human annexin V by fed-batch cultivation. *BMC Biotechnology* 2014 14:33.

Submit your next manuscript to BioMed Central and take full advantage of:

- Convenient online submission
- Thorough peer review
- No space constraints or color figure charges
- Immediate publication on acceptance
- Inclusion in PubMed, CAS, Scopus and Google Scholar
- Research which is freely available for redistribution

Submit your manuscript at
www.biomedcentral.com/submit

